OXYGEN TRANSFER IN LAYERS
OF HEMOGLOBIN SOLUTION

PROEFSCHRIFT

DOOR

JOZEF AUGUSTINUS ELISABETH SPAAN

GEBOREN TE BREDA

DIT PROEFSCHRIFT IS GOEDGEKEURD

DOOR DE PROMOTOREN

Prof.Dr. P.C. Veenstra

en

Prof.Dr. F. Kreuzer

To all who contributed
to my personal and
scientific development

CONTENTS

List of symbols

$A = 1 + D^{\star}\dfrac{d\psi}{d\phi}$ constant used in the polygonal approximation

A_1, A_2 value of A holding in region I and II, respectively, in the polygonal approximation

$A_i^{\mathscr{e}}$ constants in Adair equation with $i = 1,2,3$ or 4

b concentration of hemoglobin in tetrameric form (mol/1)

$B = 1 + H\dfrac{d\psi}{d\phi}$ constant used in the polygonal approximation

B_1, B_2 value of B holding in region I and II, respectively, in the polygonal approximation

C concentration of physically dissolved oxygen (mol/1)

C_i boundary value of C for P_i

$C^{\mathscr{e}}$ concentration of physically dissolved oxygen in equilibrium with S according to the saturation curve; is being used in models considering reaction velocity (mol/1)

C_i initial concentration of physically dissolved oxygen

d layer thickness (cm or μm)

d_m minimum thickness of hemoglobin layer allowing assumption of chemical equilibrium (cm or μm)

$D^{\star} = H\dfrac{D_H}{D_C}$ oxygen diffusion ratio

D_C diffusion coefficient of oxygen (cm^2/s)

D_{eff} effective diffusion coefficient of oxygen in flowing blood (cm^2/s)

D_H diffusion coefficient of hemoglobin in tetrameric form (cm^2/s)

D_X diffusion coefficient of species X (cm^2/s)

E integration constant used in the polygonal approximation

E_1, E_2 value of E holding in region I and II, respectively, in the polygonal approximation

$f_1 = t_1^{\star}/t_1^{\star,0}$ factor describing the influence of the dimensionless saturation curve on t_n, defined by eq. 3.24

9

f_2	proportionality factor between $t_1^{*,\delta}$ and H, fig. 3.7
f_1^r	overall forward reaction rate constant
f_2^r	overall back reaction rate constant
J_{HbO_2}	flux of chemically bound oxygen $(mol/cm^2/s)$
J_{O_2}	flux of physically dissolved oxygen $(mol/cm^2/s)$
$g(\lambda)$	light sensitivity curve of the light sensor
h	oxygen binding capacity (mol/l)
$H = \dfrac{(S_1 - S_i)h}{C_1 - C_i}$	oxygen concentration ratio
$\lvert Hb \rvert$	concentration of monomeric hemoglobin when applied in chapters 1 and 2 (mol/l); concentration of tetrameric hemoglobin when applied in chapters 3 to 6 (g% = gram Hb per 100 cc solution)
Hb_4	hemoglobin in tetrameric form
$H_{i,j}$	concentration of hemoglobin species where i indicates the number of O_2 molecules bound to hemoglobin and j distinguishes the various forms of oxyhemoglobin with the same number of oxygen molecules
i	current generated by the light-sensor
I	intensity of light after passing through the hemoglob layer (actually light attenuation, hence dimensionless)
$1(t)$	intensity of light as a function of time
I_a	apparatus constant; appears in log I_a
I_o	intensity of light after passing through the hemoglob layer when $\bar{\psi} = 0$
$I_o(\lambda)$	intensity distribution function of LED
k	backward reaction rate constant
k'	forward reaction rate constant
k	dimensionless number describing influence of reaction velocity on oxygen transfer process when $D_H = 0$ (analogous to Damköhler and Thiele number)

k_f	reaction rate constant (1/mol/s)
K^e	equilibrium constant in Hüfner's or Hill's model for oxygen-hemoglobin reaction
K_i^e	equilibrium constant in Adair's model for oxygen-hemoglobin reaction with i = 1,2,3 or 4
K	integration constant used in the polygonal approximation
K_1, K_2	values of K holding in region I and II, respectively, in the polygonal approximation
P_1	boundary value of PO_2 (mm Hg)
P_{50}	value of PO_2 where S = 0.5 (mm Hg)
PCO_2	carbon dioxide partial pressure (mm Hg)
PO_2	oxygen partial pressure (mm Hg)
P_X	partial pressure of a gas X (mm Hg)
Q	fraction of oxygen that can be maximally dissolved per unit surface area when h = 0
Q_d	Q calculated according to the finite layer model
Q_∞	Q calculated according to the half-infinite layer model
R_C	rate of production of oxygen by chemical reaction (mol/1/s)
R_S	rate of increase of oxygen saturation by chemical reaction (1/s)
$R_{H_{i,j}}$	rate of production of $H_{i,j}$ (mol/1/s)
R_X	rate of production of species X by chemical reaction (mol/1/s)
S	oxygen saturation of hemoglobin
$\bar{S}$	average oxygen saturation of hemoglobin layer
S_1	final oxygen saturation
$\bar{S}_d$	average oxygen saturation calculated according to the finite layer model
S_i	initial oxygen saturation
S_∞	oxygen saturation in the half-infinite diffusion model
S_{Hi}	fraction of hemiglobin or methemoglobin
t	time (s)

t_1	oxygenation time of a hemoglobin layer; time when $\bar{\psi}_\infty = 1$ (s)
t_d	oxygenation time of a hemoglobin layer assuming chemical equilibrium (s)
t_r	oxygenation time of a hemoglobin layer due to chemical reaction alone (s)
$t_{r,d}$	oxygenation time of a hemoglobin layer when both reaction velocity and diffusion are taken into account (s)
$t_n = t/d^2$	normalized time (s/cm^2)
$t_{n,1} = t_1/d^2$	normalized oxygenation time (s/cm^2)
$t_{1/2}$	time to reach one half saturation
$t_{1/3}$	time to reach one third saturation
$t^* = t\,D_C/d^2$	dimensionless time
t_1^*	dimensionless oxygenation time; equals t^* when $\bar{\psi}_\infty = 1$
$t_1^{*,0}$	t_1^* when calculated for $\phi_{50} = 0$
$\vec{v}$	velocity vector
x	space coordinate used in the diffusion models (cm)
x_{50}	place in layer of hemoglobin solution where $S = 0.5$
$x^* = x/d$	dimensionless space coordinate
x_1	parameter to be estimated
x_2	parameter to be estimated (cm/s$^{\frac{1}{2}}$)
x_f	distance of advancing front from gas-liquid interface
X	arbitrary species
$[X]$	concentration of species X (mol/l)
y	arbitrarily chosen variable
$Z_1 = h/\alpha D_C$	first basic parameter to be estimated from the experimental $t_{n,1}$ versus $1/P_1$ curve (mm Hg s/cm^2)
$Z_2 = h\,D_H/\alpha D_C$	second basic parameter to be estimated from the experimental $t_{n,1}$ versus $1/P_1$ curve (mm Hg)
α	solubility of oxygen in hemoglobin solutions (mol/l/mm Hg)
α^X	solubility of species X (mol/l/mm Hg)
α_B	solubility of oxygen in blood (mol/l/mm Hg)

12

α_{H_2O}	solubility of oxygen in water (mol/l/mm Hg)
α_{Hb}	solubility of oxygen in hemoglobin solutions (mol/l/mm Hg)
ε	extinction coefficient (1/cm/g%)
ε_o	extinction of hemoglobin solution in deoxygenated state (Hi may be present) (1/cm/g%)
ε_1	extinction of hemoglobin solution in oxygenated state (Hi may be present)(1/cm/g%)
ε^*	adapted extinction coefficient used in order to correct for finite bandwidth of LED (1/mol/cm)
ε_{HbO_2}	extinction of oxyhemoglobin (1/cm/g%)
ε_{Hb}	extinction of deoxyhemoglobin (1/cm/g%)
ε_{Hi}	extinction of methemoglobin (1/cm/g%)
$\eta = \dfrac{x}{\sqrt{D_C\ t}}$	independent dimensionless variable used in the half-infinite layer diffusion model
η_C	value of η where $\phi = \phi_c$ and $\psi = \psi_c$ in the polygonal approximation
η_{50}	value of η where $S = 0.5$
μ	tangent of wedge angle
$\xi = R_C t$	reaction velocity function in the half-infinite layer model (mol/l)
$\phi = \dfrac{C-C_i}{C_1-C_i}$	dimensionless oxygen concentration
ϕ_c	abcsissa value of intercept point of polygonal approximation of the saturation curve
ϕ_d	as ϕ but calculated according the finite layer model
$\phi_{50} = \dfrac{P_{50}}{P_1}$	dimensionless half-saturation oxygen pressure characterizing the position of the dimensionless saturation curve
ϕ_∞	as ϕ but calculated according to the half-infinite oxygenation model
$\psi = \dfrac{S-S_i}{S_1-S_i}$	dimensionless oxygen saturation
$\bar{\psi}$	space-average dimensionless oxygen saturation of a hemoglobin layer with finite thickness

ψ_c	ordinate value of intercept point of polygonal approximation of the saturation curve
ψ_d	as ψ but calculated according to the finite layer model
ψ_∞	as ψ but calculated according to the half-infinite layer model
MW	molecular weight
LED	light-emitting diode
SDC	Standard Dissociation Curve of human whole blood
STPD	Standard conditions of Temperature (0°C), Pressure (760 mm Hg), humidity (Dry)

CHAPTER 1

INTRODUCTION

1.1 Short historical review of investigations of oxygen transport by blood

Starting in the past century, the mechanism of oxygen transport by the blood has received wide attention of scientists in several fields, e.g. physiology, biochemistry, physical chemistry, mathematics,and in the past 15 years also in engineering.

Paul Bert (1833-1886) was the first to show that physiological effects of gases depend on their partial pressures, and he published an oxygen dissociation curve of hemoglobin as early as 1872. Hüfner in 1894 reported a value of 1.34 cc O_2 (STPD) as the oxygen binding capacity of one gram of hemoglobin. Knowledge concerning the reaction ratesof association and dissociation reactions of hemoglobin with oxygen is important for the understanding of oxygen exchange in lungs and tissues. Hartridge and Roughton (1923) were the first to investigate this matter and reported reaction times in the order of milliseconds.

At Cambridge theoretical studies were performed by Roughton (1932,1952) and Nicholson and Roughton (1951) on the rate of free penetration of oxygen and carbon monoxide into thin layers of hemoglobin solution with or without bounding membranes. At Fribourg (Müller 1945, Laszt 1945, Kreuzer 1950, Pircher 1951) experiments were performed to investigate the rate of penetration of oxygen into layers (50 to 1000 µm thick) of hemoglobin solutions and red blood cell suspensions, using a photometric technique. The work of Perutz (1969) has been of great importance concerning the knowledge of the stereochemical structure of the hemoglobin molecule and its changes after reaction with ligands. Many other scientists have made significant contributions to our present knowledge of oxygen transfer by hemoglobin in blood. A complete survey, however, would go far beyond the scope of the present thesis.

Engineers became interested in oxygen transport by blood since they were involved in the development of artificial oxygenators, after this technique had been shown to be successful in open heart surgery. Gibbon (1959) was the first to apply such a device clinically. The physiologists were primarily interested in the gas exchange of a single red blood cell; the engineers, however, considered the oxygen uptake by whole blood, being a flowing suspension of red cells. Buckles (1966) was one of the first to study this topic systematically.

In order to understand the influence of the heterogeneous character of the blood on the diffusion process, the situation of stationary mass transfer through non-moving layers of blood has received much attention in the literature. The most complete study was published by Stroeve (1973) who considered both reaction velocity and facilitation of diffusion by hemoglobin within the red cell.

Almost all theoretical models applied to oxygen transfer in flowing blood, assume a homogeneous character of the blood with respect to the diffusion of oxygen and the distribution of hemoglobin. They also neglect the facilitation of oxygen transfer by hemoglobin diffusion. An exception is the microscopic-macroscopic model developed by Garred (1975). If a "homogeneous" model is used to describe oxygen transfer in blood an effective diffusion coefficient (D_{eff}) is used as an overall quantity to describe the oxygenation process. It also accounts for the deviation between results of different model calculations. Keiler (1971) showed D_{eff} to be dependent on shearing in Couette flow. This dependence of D_{eff} on shearing has been confirmed by several investigations, although large differences exist between the results of several authors. For example it has been shown by Oomens et al. (1976) that D_{eff} increases fivefold when increasing the shear rate from zero to 15000 sec^{-1} whereas Overcash (1972) reported a similar increase at a shear rate of only 100 sec^{-1}.

It is obvious that a correct description of the oxygen transfer process in a single red cell as well as in flowing blood is related to the values of the physical quantities involved. With regard to the diffusion coefficient of oxygen in plasma and in the red cell interior ther exists sufficient agreement in the literature. This agreement, however, is far from satisfactory regarding data of reaction kinetics and the diffusion coefficient of hemoglobin . These topics will be considered more closely in the present thesis.

1.2 Purpose and scope of the present investigation

The present study deals with the nonsteady-state uptake of oxygen by completely deoxygenated layers of hemoglobin solution spread on a glass plate. At its free boundary the layer of hemoglobin solution is exposed to a gas atmosphere which initially does not contain any oxygen. Then a sudden change in oxygen partial pressure from zero to a certain value P_1 at the free boundary of the layer is induced. The course of the

subsequent oxygenation (determined colorimetrically) is compared to predictions from the diffusion-reaction equation based on Fick's law for the diffusion of both oxygen and hemoglobin and on the assumption of chemical equilibrium between oxygen and hemoglobin. This comparison is performed over a wide range of hemoglobin concentrations and P_1 values.

The transfer equations as such are classical and may be found in several publications. Up to now, however, no serious parameter analysis has been presented as needed for the interpretation of the experiments mentioned above (see chapter 3).

The basic ideas in performing the present experiments are the same as those developed by the Fribourg group in the fifties. The reasons for carrying out new experiments were thought to be:

1) the Fribourg experiments were performed at only two values of P_1 (700 mm Hg and 140 mm Hg);

2) the experimental results show too much scattering (approximately 30%) to serve as a basis for a sophisticated parameter analysis according to the theoretical model presented in this thesis;

3) the evaluation of experiments at high hemoglobin concentrations needs certain corrections as will be explained below.

The experimental principle, designed by the Fribourg group, however, proved to be very valuable. It permits to observe the penetration of oxygen into a hemoglobin solution continuously without any disturbance of the diffusion process. In principle the method is subject to small experimental errors as compared with other diffusion experiments. This statement will be discussed in more detail in chapter 6.

Our investigations result in quantitative information which is important for the understanding of the oxygen uptake and release by the red cell in the context outlined in section 1.1. However, the value of the results obtained reaches further than merely to the behavior of the red cell. At very low concentrations hemoglobin may be used as an indicator for the study of the penetration of O_2, CO and NO into different liquids (e.g. Kreuzer 1950, Pircher 1951, and section 3.4). Moreover, the results of the present study may be of practical interest since hemoglobin solutions are being used as a transfusion fluid or as a perfusate for isolated organs. From comparative oxygen transfer studies using blood or a hemoglobin solution respectively, information may be obtained concerning the influence of the heterogeneous character

of the blood on the oxygen exchange in organs and in artificial
oxygenators.

CHAPTER 2

FUNDAMENTALS OF OXYGEN TRANSFER IN HEMOGLOBIN SOLUTIONS AND BLOOD

2.1 Physiological importance of hemoglobin

The macromolecule hemoglobin (MW=64,500) is present in the red cells at a high concentration (approx.35 g%),whereas the red cells occupy 45% of the total blood volume. Hemoglobin plays a key role in the gas transport and buffering system of mammalians as it reversibly reacts with O_2, CO_2, H^+, and 2,3-DPG. The respective equilibrium relationships are interdependent such that optimal levels of PO_2, PCO_2 and pH in the blood are maintained.

The oxygen binding capacity h (mol/l) of blood or hemoglobin solutions is defined as the maximal amount of oxygen bound by hemoglobin.

The oxygen saturation S is defined as the ratio of the concentration of bound oxygen and the oxygen binding capacity. The concentration of free oxygen in blood or hemoglobin solution is determined by the oxygen partial pressure PO_2. The concentration of a dissolved gas X and its partial pressure P_X are related by Henry's law

$$\left[X \right] = \alpha^X P_X \tag{2.1}$$

where α^X = solubility coefficient in mol/l/mm Hg.

At equilibrium there is a certain relationship between saturation and PO_2 known as the "oxygen saturation curve" or "oxygen dissociation curve". This curve is sigmoid and its position is affected mainly by temperature, pH, PCO_2 and 2,3-DPG concentration. Saturation curves in several conditions are shown in fig.2.1.The curve at $T = 37^{\circ}C$ and pH = 7.4 is known as the standard human whole blood oxyhemoglobin dissociation curve ("SDC"). At an arterial PO_2 of 100 mm Hg the fractional saturation is close to one.

Arterial blood with a hemoglobin concentration of 16g% contains approx. 10 mmol O_2/l but only 0.15 mmol/l is physically dissolved. In resting normal man the venous saturation is about 0.7. The PO_2 difference is the driving force in the exchange of oxygen between alveolar air and blood as well as between blood and tissues. Therefore shape and position of the curve are important factors in the O_2 supply of the body (see e.g. Turek et al. 1973).

The total CO_2 concentration in venous blood is 25 mmol/l, 86% of which is present as bicarbonate (HCO_3^-). Bicarbonate concentration, pH and $[CO_2]$ are related by the equilibrium equation (Henderson-Hasselbalch equation) belonging to the following reactions:
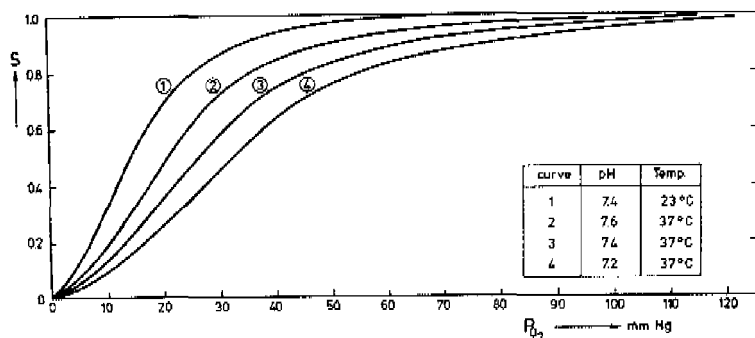
*Fig. 2.1. Saturation curves (fractional oxygen saturation S as a
function of oxygen partial pressure PO_2) of normal human whole blood
($PCO_2 = 40$ mm Hg) at several values of pH and temperature. Curve 3
is known as the Standard Dissociation Curve of whole blood (SDC).
Both decreasing temperature and increasing pH shift the standard
curve to the left.*

$$CO_2 + H_2O \rightleftharpoons H_2CO_3 \rightleftharpoons H^+ + HCO_3^- \tag{2.2}$$
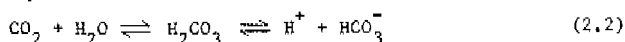
These reactions occur predominantly within the red cells where they are
greatly accelerated (factor 500) by the enzyme carbonic anhydrase
(Roughton 1964). Reaction 2.2 is shifted to the right when CO_2 is
transferred from the tissues to the blood, and to the left in the lungs.
The venous PCO_2 equals approx. 46 mm Hg and the arterial PCO_2 is 40 mm
Hg.

The affinity of hemoglobin for CO_2 depends on the oxygen saturation
and the pH. The role of carbamate formation in CO_2 transport of resting
man in terms of the difference in total CO_2 content between arterial
and venous blood (Haldane effect) amounts to 33%.

Hemoglobin behaves as a weak acid, but deoxyhemoglobin is a still
weaker acid and therefore a better buffer than oxyhemoglobin. Thus
the H^+ produced in the blood when CO_2 is exchanged in the tissues is
largely buffered by hemoglobin. Because of this mechanism the pH between
arterial and venous blood does not differ by more than 0.05 pH units in
normal situation.

The total 2,3-DPG concentration in the red cell does not change
during the respiratory cycle, but it may change under abnormal
physiological circumstances, e.g. low hematocrit, high altitude, or
altered pH. Sometimes 2,3-DPG concentration may change within a few

20

hours (de Leeuw 1971). After a few days of storage no more 2,3-DPG is present in the blood.

2.2 Structure and stability of hemoglobin

In the red cell and in concentrated hemoglobin solutions the hemoglobin molecule is a tetramer consisting of four tetrahedrally arranged subunits which are identical in pairs and are referred to as α and β chains. The tetramer of hemoglobin (Hb_4) approaches a spheroid with dimensions of 76 Å, 55 Å and 50 Å. Each subunit (Hb) is a combination of a protein chain named globin and the pigment heme, a flat molecule with a Fe^{2+} ion in its center. Each protein is folded in such a way that a kind of basket is formed around the heme (heme pocket). The iron is linked to four nitrogen atoms of the heme and with one nitrogen atom of a histidine in the globin chain. Within the pocket there remains an empty space for oxygen to be attached to the iron. Originally it was assumed that on binding with oxygen the iron remained ferrous and therefore the O_2-binding process is called oxygenation rather than oxidation. More recently, however, it has been suggested that at "oxygenation" of a heme the iron ion changes to the ferric state (e.g. Koster 1975). Linkage of the O_2 to the iron causes changes in the orbitals of two of its valency electrons which results in a shrinkage of 13% of the iron radius and as a consequence in a changed position of the iron relative to the heme and the globin (Perutz 1971). This displacement of the iron induces alterations in the structure of the respective globin as well as in one or more other subunits. These interactions between subunits accompanying oxygenation of hemes may enhance the oxygenation of other hemes. Reactions of hemoglobin with CO_2, H^+ and 2,3-DPG also elicit alterations in chemical bonds and interactions between subunits and are in turn influenced by the degree of oxygenation. Therefore these reactions influence the equilibrium between hemoglobin and oxygen and consequently the position and shape of the oxygen saturation curve.

Besides the reaction of the heme with oxygen the heme is also able to combine with CO and NO. The affinity of the heme for CO is many times higher than that for O_2. Therefore even a low percentage of CO in the air makes the hemoglobin useless as an oxygen carrier.

The iron within the heme can be oxidized to the ferric state. In this condition the heme is no longer capable of reacting with oxygen. Oxidized

hemoglobin is known as hemiglobin or methemoglobin and can react with some ions, e.g. F^-, NO_2^-, N_3^- and CN^-. In normal blood only a small percentage of heme exists in a form different from Hb or HbO_2 but in hemoglobin solutions, depending on their age and way of storing, a relatively high amount of hemiglobin may be present.

Hemoglobin does not always appear in tetrameric form. In solutions of human hemoglobin the tetrameric form is stable when $[Hb]$ exceeds 0.25 mmol(heme)/l (in the red cell : 21 mmol/l Hb). At lower Hb concentrations dimers (Hb_2) as well as monomers are present (Schachman 1966, Barnikol 1969). Oxyhemoglobin is less stable in terms of tetrameric configuration than deoxyhemoglobin. The stability is pH dependent and an optimum is found at a pH of 9 for oxyhemoglobin and at a pH of 7.4 for deoxyhemoglobin (Briehl 1965, 1970). The ionic strength of the solution is also important, high values favoring dissociation of the tertramer(Kellett 1971).

2.3 Models of the hemoglobin-oxygen reaction

Experimental and theoretical evidence on the detailed structure, stability and reaction mechanisms of hemoglobin is of recent date although the oxygen saturation curve was discovered already a century ago (Bert 1872). Subsequently many workers have tried to describe this curve mathematically and by means of models to elucidate the physico-chemical character of the reaction of hemoglobin with oxygen. None of these models appeared to be completely satisfactory although most of them are based on some hypothesis to be partly confirmed later to hold in a special case. Some equations are still being used in describing the saturation curve.

The first model suggested was that of Hüfner (1890). He did not assume any interaction between hemes, so

$$Hb + O_2 \rightleftharpoons HbO_2 \qquad (2.3)$$

This results in the following relationship between S and $[O_2]$ according to the law of mass action

$$S = \frac{K'[O_2]}{1 + K'[O_2]} \qquad (2.4)$$

with $K' =$ equilibrium constant. This equation 2.4 represents a hyperbolic saturation curve. It holds for myoglobin, a related molecule with only one heme, which is found in muscular tissue.

From the reaction scheme given by eq. 2.5 and the related equilibrium eqs. 2.6.a and 2.6.b Hill (1910) tried to deduce the number of subunits aggregated in the hemoglobin molecule

$$Hb_n + n\ O_2 \rightleftharpoons Hb_n(O_2)_n \tag{2.5}$$

resulting in

$$S = \frac{K^e\ P^n}{1 + K^e\ P^n} \tag{2.6.a}$$

and

$$\frac{1}{n}\ \log\ \frac{S}{1-S} = \log P - \log P_{50} \tag{2.6.b}$$

where $K^e = 1/P_{50}^n$,

$P_{50} = PO_2$ where $S = 0.5$, and

n = a whole number .

Hill's model appeared to be incorrect because the saturation curve could not be described by one constant value of n. However, eq. 2.6 holds fairly well in the middle range of the saturation curve $(0.3 < S < 0.9)$ where n is constant and has a value between 2.5 and 3. Because of its simplicity the Hill equation is still used in describing individual saturation curves in the range of physiological importance. The Hill equation is also used to determine the P_{50} of the saturation curve, a value commonly used in physiology to indicate the position of the saturation curve.

Haldane suggested in 1912 that, in certain cases, deoxygenated hemoglobin has a greater tendency to aggregate into polymers than has oxygenated hemoglobin and that its reaction with oxygen only occurs when the protein is in the monomeric form. The sigmoid curve was explained by the differing equilibria of hemoglobin and oxyhemoglobin with their respective polymers. Although for human hemoglobin in the red cell Haldane's model cannot be correct, it holds in the case of lamprey hemoglobin (Briehl 1964) and more or less in dilute solutions of human hemoglobin.

In 1925 Adair established that the mammalian hemoglobin molecule is tetrameric containing four iron atoms which led him to propose his well known intermediate compound hypothesis, according to which oxygen or other ligands react in four successive steps:

$$
\begin{array}{ll}
Hb_4 + O_2 \rightleftharpoons Hb_4O_2 & K_1^e \\
Hb_4O_2 + O_2 \rightleftharpoons Hb_4O_4 & K_2^e \\
Hb_4O_4 + O_2 \rightleftharpoons Hb_4O_6 & K_3^e \\
Hb_4O_6 + O_2 \rightleftharpoons Hb_4O_8 & K_4^e
\end{array}
\tag{2.7}
$$
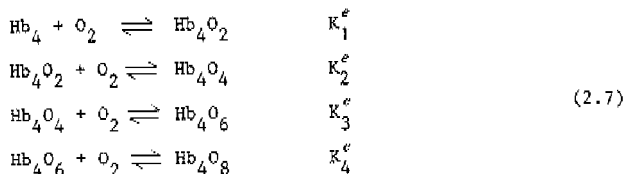
whence

$$
S = \frac{1/4 \sum\limits_{i=1}^{4} i \, A_i^e \, PO_2^i}{1 + \sum\limits_{i=1}^{4} A_i^e \, PO_2^i}
\tag{2.8}
$$

where $A_1^e = K_1^e$; $A_2^e = A_1^e K_2^e$; $A_3^e = A_2^e K_3^e$; $A_4^e = A_3^e K_4^e$.
If the hemes were equivalent and independent, the ratios of $K_1^e : K_2^e : K_3^e : K_4^e$ should be $1 : 3/8 : 1/6 : 1/16$ according to purely statistical behavior. A hyperbola would result as was the case with eqs. 2.4 and 2.5 if $n=1$. The sigmoid shape is explained by interaction of the hemes. Application of the Hill equation to very precise data of Roughton (1972) for $S < 0.02$ shows $n=1$, and hence in this range Hb_4 reacts with only one O_2 molecule at a time. Fitting of the SDC to the Adair scheme (see below) leads to the supposition that $Hb_4(O_2)_3$ is present only in very small amount. Values for K_1^e, K_2^e, K_3^e, K_4^e giving a good fit to the experimental curve of the SDC from Roughton (1972) are:

values of K^e	K_i^e/K_1^e	values of A^e
$K_1^e = 2.18 \ 10^{-2}$	1	$A_1^e = 2.18 \ 10^{-2} \ mm \ Hg^{-1}$
$K_2^e = 4.20 \ 10^{-2}$	1.9	$A_2^e = 9.12 \ 10^{-4} \ mm \ Hg^{-2}$
$K_3^e = 4.10 \ 10^{-3}$	0.19	$A_3^e = 3.75 \ 10^{-6} \ mm \ Hg^{-3}$
$K_4^e = 6.60 \ 10^{-1}$	30	$A_4^e = 2.47 \ 10^{-6} \ mm \ Hg^{-4}$

The Adair model and Haldane's suggestion formed the basis for other models trying to arrive at equations describing the saturation curve

using less than four constants. Pauling (1935) and Thompson (1968)
assumed a certain interaction between hemes. Monod et al. (1965) assumed
that Hb_4 as a whole exists in two different conformations with
distinguishable affinities for oxygen but no interaction between hemes.
Koshland et al. (1966) assumed that every heme changes its conformation
before it is able to bind oxygen and tried several possibilities of heme-
heme interaction. Forbes and Roughton (1931) and later Margaria (1963)
concluded that the first 3   reactions in the Adair scheme are independent,
and only in the last stage the reaction is enhanced by a factor of 125.
Although these conclusions are not in agreement with the present accepted
values of $K_1^c - K_4^c$, the resulting equation is often used in the literature
for its simplicity.

The models of the authors cited and of some others show fair
agreement with saturation curves measured in hemoglobin solutions from
different mammals; however, a good fit does not necessarily confirm an
individual model. Koshland et al. (1966) concluded already that if several
models are describing the saturation curve, further information will be
necessary to obtain a unique mechanism. Roughton (1972) concluded from his
comparative calculations that the models of Pauling, Monod and Koshland
are not applicable to the data of human whole blood and that the Adair
equation still provides the most appropriate approach to describe the
saturation curve. Roughton recognized the fact that this approach is of
an empirical nature and does not lead to a deeper understanding of the
problem in terms of molecular biology.

2.4 Transfer equations of physically dissolved and chemically bound oxygen

Diffusion processes are commonly described by one or a set of
differential equation(s) holding in every point of the medium where
transfer occurs. Many solutions of this (these) equation(s) are possible
but boundary values for the particular problem determine the specific
solution.

When oxygen passes through hemoglobin solutions it will react with
hemoglobin to form oxyhemoglobin. Assuming the mass density of the
solution to remain constant during oxygenation, the transfer of all
species involved in the reaction can be described by (e.g. Bird et
al. 1966)

$$\frac{\partial [X]}{\partial t} = - \vec{v} \cdot \text{grad } [X] + \text{div } (D_X \text{ grad } [X]) + R_X \qquad (2.9) \qquad)^*$$

where $[X]$ = concentration of a certain species X,

R_X = rate of production of species X by chemical reaction,

D_X = diffusion coefficient of X, and

$\vec{v}$ = velocity of fluid .

In the present thesis it is assumed that in all situations the oxyhemoglobin molecule remains in tetrameric form.

Equation 2.9 holds for oxygen of concentration C and for all hemoglobin species with concentration $H_{i,j}$ where $i = 0,1,2,3$ or 4 indicates the number of O_2 molecules bound to hemoglobin and j distinguishes the various forms of oxyhemoglobin with the same number of oxygen molecules. Taking into account all different forms of hemoglobin, there is a relationship between R_C and the various $R_{H_{i,j}}$, where R_C and $R_{H_{i,j}}$ are the rates of production by chemical reaction of C and $H_{i,j}$ respectively

$$R_C + \sum_{i=1}^{4} i \sum_{j} R_{H_{i,j}} = 0 \qquad (2.10)$$

For all possible forms of hemoglobin

$$\sum_{i=0}^{4} \sum_{j} R_{H_{i,j}} = 0 \qquad (2.11)$$

We also assume that the diffusion coefficient is the same for all (see section 6.5.5) hemoglobin species. When defining $b = \sum_i \sum_j H_{i,j}$ as the total hemoglobin concentration (tetrameric) we now can derive a differential equation for b as a function of time and place. Adding all equations describing $H_{i,j}$ and using eq. 2.9 we get

$$\frac{\partial b}{\partial t} = - \vec{v} \cdot \text{grad } b + \text{div } (D_H \text{ grad } b) \qquad (2.12)$$

Because of eq. 2.11 there is no reaction term left. Eq. 2.12 shows that in a system where O_2 and hemoglobin species are moving and the

---

$)^*$ we shall refer to an equation of type 2.9 for species X as eq $\{X\}$

assumptions mentioned apply, the local hemoglobin concentration is only affected by gradients of b.

Only situations are considered here where b is a uniform concentration at the start. In this case, if there is no change in boundary values of b, no gradients of b will occur and b has a constant value throughout the whole process. The conclusion that b is constant is required for the derivation of eq. 2.14 below. However, this conclusion is generally valid and thus applies to any specific problem (e.g. Kutchai 1971a, Kreuzer and Hoofd 1970, Zilversmit 1965).

The fractional oxygen saturation of hemoglobin is defined as

$$S = (\sum_{i=0}^{4} i \sum_{j} H_{i,j})/(4\ b) \tag{2.13}$$

We can readily see that the summation

$$\frac{1}{4b} \sum_{i=1}^{4} i \sum_{j} eq\ \{H_{i,j}\} \tag{2.14}$$

leads to

$$\frac{\partial S}{\partial t} = - \vec{v}. \text{ grad } S + \text{div } (D_H \text{ grad } S) + R_S \tag{2.15}$$

where

$$R_S = \sum_{i=1}^{4} i \sum_{j} R_{H_{i,j}} = - R_C/4b \tag{2.16}$$

Thus the saturation may be expressed by a transfer equation as if S were a transported species itself. Eq $\{C\}$ and eq $\{4\ b\ S\}$ can be added to give

$$\frac{\partial}{\partial t} (C+4bS) = - \vec{v} \text{ grad } (C+4bS) + \text{div } (\text{grad}(D_C C+4b\ D_H S)) \tag{2.17}$$

In addition to the transfer equations of physically dissolved and chemically bound oxygen we need equations for R_C and R_S depending on C

and S. The formulation of these equations depends on the assumed reaction scheme for hemoglobin and oxygen. The assumption of near-equilibrium means that the saturation curve may be used as a second relationship required in addition to eq. 2.17. We may quantitatively understand the meaning of this assumption from the following considerations. Generally we may state according to basic theory of reaction kinetics (Laidler 1965) that

$$- R_C = f_1^r \ C - f_2^r \tag{2.18}$$

where f_1^r is a function of all terms $H_{i,j}$ of hemoglobin combining with one or more molecules of oxygen (forward reaction) and f_2^r is a function of all terms of $H_{i,j}$ slowing down the overall rate (back reaction). It should be noted that f_1^r and f_2^r are always positive. Defining C^e as the concentration of oxygen where $R_C = 0$ (equilibrium) we get for finite reaction velocity

$$R_C = (C^e - C) \ f_1^r \tag{2.19}$$

Relationship 2.18 holds when only one O_2 molecule is involved in each reaction step. If there are more molecules involved per step then eq. 2.18 will be a polynome whilst eq. 2.19 still holds as a first-order approximation. The assumption of near-equilibrium means that $C^e - C$ is small compared to C^e (see also section 3.6).

CHAPTER 3

THEORETICAL MODELS OF OXYGEN TRANSFER IN THIN LAYERS OF HEMOGLOBIN
SOLUTION

3.1 Equations and boundary conditions for oxygen transfer in layers of hemoglobin solution

3.1.1 Layers with finite thickness

A flat thin layer of hemoglobin solution is at one side ($x=0$) in
contact with a gaseous atmosphere and at the other side ($x=d$) with a
gas-impermeable wall. At $t < 0$ the layer is in equilibrium with the gas
containing oxygen at a partial pressure P_i. The oxygen concentration all
over the layer equals C_i according to Henry's law and the oxygen
saturation equals S_i as required by the saturation curve. At time $x=0$
the gaseous atmosphere is changed abruptly to a PO_2 value of P_1. Oxygen
will diffuse into the hemoglobin layer and react with hemoglobin to
produce oxyhemoglobin. Because of symmetry net mass transfer will occur
in only one direction (x) and the transfer eq. 2.17 reduces to:

$$\frac{\partial}{\partial t} (C+hS) = D_C \frac{\partial^2 C}{\partial x^2} + h\, D_H \frac{\partial^2 S}{\partial x^2} \qquad (3.1)$$

where h = oxygen binding capacity of hemoglobin.
As has been mentioned in chapter 2 and as will be discussed in section 6
of this chapter, the assumption of near—equilibrium is valid and hence
the saturation curve can be used as a second relationship between S en C.
When the layer has a finite thickness the boundary conditions are

$$t < 0, \; 0 \leqslant x \leqslant d \quad ; \quad C = C_i \text{ hence } S = S_i \qquad (3.2)$$

$$t \geqslant 0, \; x = 0 \qquad ; \quad C = C_1 \text{ hence } S = S_1 \qquad (3.3)$$

$$t \geqslant 0, \; x = d \qquad ; \quad \partial C/\partial x = 0 \qquad (3.4)$$

Commonly dimensionless variables are introduced

$$x^* = x/d \qquad (3.5)$$

$$t^* = t\, D_C/d^2 \qquad (3.6)$$

$$\phi = (C-C_i)/(C_1-C_i) \qquad (3.7)$$

$$\psi = (S-S_i)/(S_1-S_i) \qquad (3.8)$$

Substituting eqs. 3.5 and 3.6 into eq. 3.1 yields the dimensionless parameters

$$H = (S_1 - S_i) \ h/(C_1 - C_i) \tag{3.9}$$

$$D^* = H \ D_H/D_C \tag{3.10}$$

and eq. 3.1 can be rewritten to be

$$\frac{\partial}{\partial t^*} (\phi + H\psi) = \frac{\partial^2 \phi}{\partial x^{*2}} + D^* \frac{\partial^2 \psi}{\partial x^{*2}} \tag{3.11}$$

with the boundary conditions

$$\left. \begin{array}{lll} t^* < 0 \ , \ 0 \leqslant x^* \leqslant 1 & ; & \phi = \psi = 0 \\[2mm] t^* \geqslant 0 \ , \ x^* = 0 & ; & \phi = \psi = 1 \\[2mm] t^* \geqslant 0 \ , \ x^* = 1 & ; & \partial\phi/\partial x^* = 0 \end{array} \right\} \tag{3.11,a}$$

H will be called "oxygen concentration ratio" as it represents the ratio of oxygen bound to hemoglobin and physically dissolved. D^* will be called "oxygen flux ratio" as it represents at steady state the ratio of carrier-mediated oxygen flux and free oxygen flux.

Solutions $\phi(x^*, t^*)$ and $\psi(x^*, t^*)$ depend on:
1) the dimensionless saturation curve or the relationship between ψ and ϕ,
2) the oxygen concentration ratio,
3) the oxygen flux ratio.

3.1.2 Layers with half-infinite thickness

When the layer is assumed to extend into infinity the boundary condition 3.4 has to be modified to

$$x \to \infty \ ; \ C \to C_i \tag{3.12}$$

Now eq. 3.4 can be transformed into an equation with only one independent variable when replacing eqs. 3.5 and 3.6 by

$$\eta = \frac{x}{\sqrt{D_C t}} \tag{3.13}$$

In the analysis of mass and heat transfer problems this transformation is well known. Then eq. 3.1 changes by introducing the operators

$$\frac{\partial}{\partial t} = -\frac{1}{2} \frac{\eta}{t} \frac{d}{d\eta} \quad ; \quad \frac{\partial}{\partial x^2} = \frac{1}{D_C t} \frac{d^2}{d\eta^2} \tag{3.14}$$

and applying eqs. 3.7 to 3.10 into

$$-\frac{1}{2} \eta \frac{d}{d\eta} (\phi + H\psi) = \frac{d^2 \phi}{d\eta^2} + D^* \frac{d^2 \psi}{d\eta^2} \tag{3.15}$$

The boundary conditions now become

$$\begin{array}{ll}
\eta = 0 \quad ; \quad \phi = \psi = 1 \\
\\
\eta \to \infty \quad ; \quad \phi \text{ and } \psi \to 0
\end{array} \tag{3.15.a}$$

The solutions of the equations applying to the finite slab can be compared with those holding for the half-infinite slab for $x \leqslant d$. In dimensionless form this comparison can be done by writing

$$\eta = \frac{x^*}{\sqrt{t^*}} \tag{3.16}$$

where x^* and t^* are the dimensionless place and time, respectively, corresponding to the finite slab problem.

The solutions $\phi(\eta)$ and $\psi(\eta)$ are dependent on the same parameters as the solutions of the finite slab problem (see 3.1.1). In order to distinguish between the solutions of the finite slab problem and the half-infinite slab problem these solutions will be referred to as ϕ_d, ψ_d and ϕ_∞, ψ_∞ respectively.

3.2 Solutions of the transfer equations without chemical reaction

When H=0, eqs. 3.11 and 3.15 reduce to transfer equations without chemical reaction. Both equations can be solved by applying methods

described in most textbooks on mass and heat transfer (e.g. Bird et al. 1966). For the finite layer the following solution is found

$$\phi_d = 1 - 2 \sum_{j=0}^{\infty} \frac{(-1)^j}{(j+\frac{1}{2})\pi} e^{-((j+\frac{1}{2})\pi t^*)'} \cos(j+\frac{1}{2})\pi(1-x^*)$$

and for the half-infinite layer

(3.17)

$$\phi_\infty = 1 - erf(\frac{1}{2}\eta)$$

(3.18)

where error function $erf(y) = \frac{2}{\sqrt{\pi}} \int_0^y e^{-x^2} dx$.
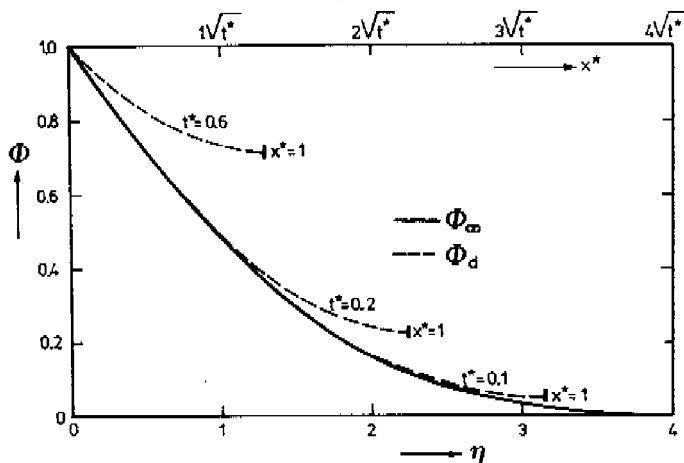
Fig. 3.1. Oxygen concentration profiles within a half-infinite slab (solid line) and a finite slab (broken lines) in the absence of chemical reaction as a result of an instantaneous increase in oxygen partial pressure at the gas-liquid interface ($x^* = \eta = 0$). Solid line: dimensionless oxygen concentration ($\phi = \phi_\infty$) as a function of $\eta(= x^*/t^*)$ for a half-infinite slab.

Broken lines: dimensionless oxygen concentration ($\phi = \phi_d$) as a function of $x^* (= x/d)$ at several values of $t^* (= tD_c/d^2)$ for a finite slab. At each value of t^* the scale value of x^* is different and equals $\eta\sqrt{t^*}$. In this way comparison between concentration profiles, calculated according to the finite slab model and the half-infinite slab model, is possible. For values of $t^* \leq 0.1$, ϕ_d and ϕ_∞ coincide. When t^* increases the deviation between the two models increases.

In fig. 3.1 both solutions are compared. The quantity ϕ_∞ asymptotically approaches zero when increasing η. In order to represent the solutions of the finite slab problem at several values of t^* the ordinate is attenuated by a factor $\sqrt{t^*}$ for each solution. It is clear from this figure that ϕ_d and ϕ_∞ coincide until the value of ϕ_d at $x^* = 1$ differs significantly from zero. In a popular way one may say that up to this moment the concentration profile does not "know" whether it exists in a finite or half-infinite slab.

The fraction of oxygen that can be dissolved maximally per unit surface area in a layer of thickness d equals $(C_1-C_i)d$. The fraction Q that has been dissolved in the dimensionless lapse of time t^* amounts to

$$Q(t^*) = Q_d(t^*) = \int_0^1 \phi_d(x^*, t^*)dx^* \qquad (3.19)$$

If we assume that up to Q=1 the oxygen flux into the layer of finite thickness equals the flux into the half-infinite layer we get

$$Q < 1 \; ; \quad Q(t^*) = Q_\infty(t^*) = \int_0^\infty \phi_\infty(\frac{x^*}{\sqrt{t^*}})dx^* = 2\sqrt{\frac{t^*}{\pi}} \qquad (3.20)$$
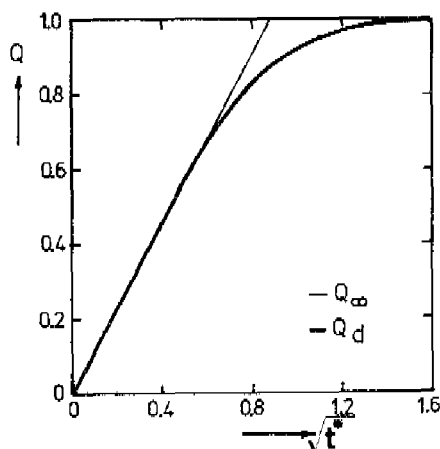
Fig. 3.2. Fractional increase of dissolved oxygen Q (eq. 3.19) as a function of dimensionless time t^* ($Q = 0$ at $t^* = 0$, $Q = 1$ at $t^* = \infty$) according to both the finite slab ($Q = Q_d$) and the half-infinite slab ($Q = Q_\infty$) model.

In fig. 3.2 the quantities Q_d and Q_∞ are compared. Both curves coincide up to $Q \approx 0.5$. When increasing the (dimensionless) time, Q_∞ reaches $Q=1$ abruptly whereas Q_d approaches $Q = 1$ asymptotically.

3.3 Solutions of the transfer equations including the oxygen-hemoglobin reaction

3.3.1 Methods of solution

When O_2 combines with hemoglobin the transfer equations can only be solved analytically but for simplifying the saturation curve. Examples for simplifications from the literature will be given in Chapter 6.

Eqs. 3.12 and 3.15 have to be solved numerically (by computer). Solutions of the finite layer problem are obtained by an adapted finite difference scheme of Crank-Nicholson (e.g. Lapidus 1962). This method calculates ϕ and ψ at n+1 equidistant points at time intervals of Δt^*. In the program used here the value of Δt^* changes with t^*. The difference scheme used is convergent in the second order. A detailed description is given in Appendix A.
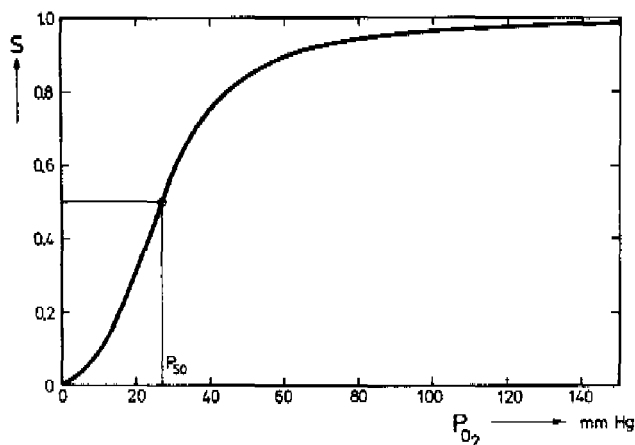
Fig. 3.3. Oxygen saturation curve according to the Adair equation (eq. 2.8) as used in all the calculations. Values of the Adair constants used are: $K_1^\beta = 0.0216$, $K_2^\beta = 0.0425$, $K_3^\beta = 0.00558$, $K_4^\beta = 0.477$ 1/mm Hg. $P_{50} = 26.74$ mm Hg. Dimensionless saturation curves (ψ versus ϕ) are obtained from this curve through eqs. 3.7 and 3.8 and are characterized by the value of $\phi_{50} = P_{50}/P_1$ (fig. 3.10).

Eq. 3.15 has been solved by a fourth-order Runge-Kutta integration procedure[*]. In order to use this procedure, eq. 3.15 was modified to

$$\frac{d^2\phi}{d\eta^2} = \frac{-1}{(1+D^* \frac{d\psi}{d\phi})} \frac{d\phi}{d\eta} \left\{ \frac{1}{2} \eta(1+H \frac{d\psi}{d\phi}) + D^* \frac{d^2\psi}{d\phi^2} \frac{d\phi}{d\eta} \right\} \qquad (3.21)$$

The Runge-Kutta method requires two different boundary conditions at $\eta=0$, i.e. $\phi_{\eta=0}$ and $(d\phi/d\eta)_{\eta=0}$. The latter replaces the physical condition $\phi \to 0$ when $\eta \to \infty$. Hence a parameter estimation program has been developed in order to determine the particular value of $(dC/d\eta)_{\eta=0}$ satisfying the physical boundary conditions. A detailed description of the numerical procedure is given in Appendix B. The dimensionless saturation curves used in all the calculations have been derived from the saturation curve given in fig. 3.3. In the computer program the saturation and the first and second derivatives of the saturation curve were calculated according to the Adair equation using the constants given in fig. 3.3 and taking $P_i=0$.

3.3.2 <u>Concentration profiles within the finite and half-infinite slab</u>

Profiles ψ and ϕ within the half-infinite slab are presented in fig. 3.4. For the sake of simplicity the dimensionless parameter analysis partly has been abandoned here because of the fact that some physical parameters (e.g. P_1) are related to more than one dimensionless parameter (e.g. H, D^* and the dimensionless saturation curve). In fig. 3.4 the dependence of the profiles on P_1 and the ratio D_H/D_C is shown.

If hemoglobin is not mobile (curves 1 and 2) the saturation profile in general shows quite a steep course. This may be understood from the dimensionless saturation curve which is shifted to the left and so becomes steeper if P_1 is increased (see fig. 3.10). Obviously the oxygenation front has moved further into the layer at the high P_1 value. The profiles of ϕ at $D_H = 0$ are virtually linear within the oxygenated part of the layer whereafter they flatten rapidly. If the hemoglobin is assumed to diffuse, all profiles become smooth. In relative terms the influence of carrier facilitation is stronger at lower values of P_1 than at the higher ones.

[*] THE Library Procedure Computer Centre
Eindhoven University of Technology
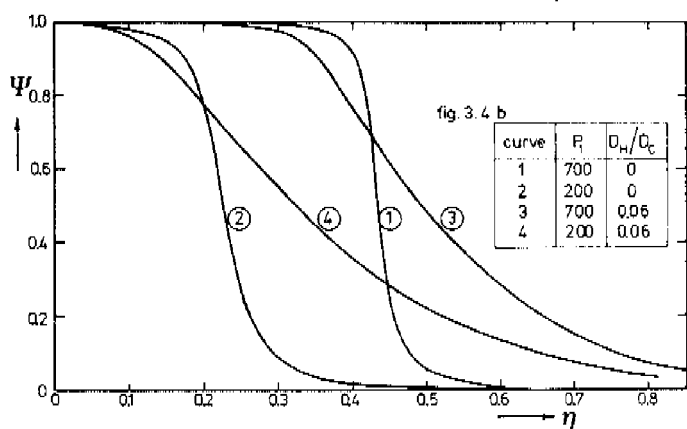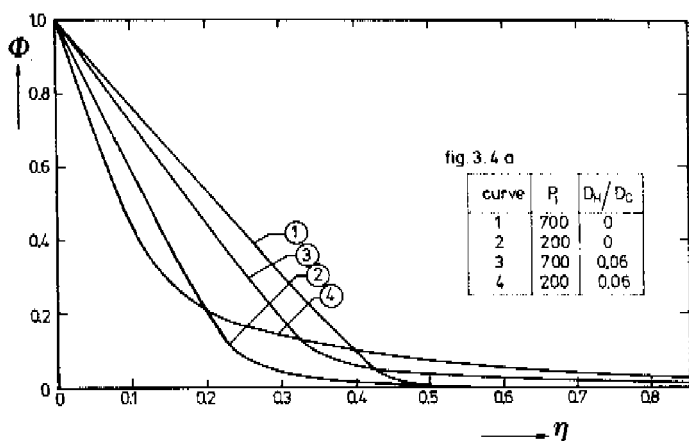
Fig. 3.4(a,b). Oxygen concentration and oxygen saturation profiles within a half-infinite slab of hemoglobin solution (oxygen binding capacity $h = 1.073$ mol/l ($[Hb] = 17.3$ g%), $P_i = 0$, $\alpha = 1.53 \ 10^{-6}$ mol/l/mm Hg); a) dimensionless oxygen concentration ϕ as a function of η ($= x^*/\sqrt{t^*}$); b) dimensionless oxygen saturation of hemoglobin ψ as a function of η. The curves are calculated for different values of P_1 and D_H/D_C ratio; curves: 1) $P_1 = 700$ mm Hg, $D_H/D_C = 0$; 2) $P_1 = 200$ mm Hg, $D_H/D_C = 0$; 3) $P_1 = 700$ mm Hg, $D_H/D_C = 0.06$; 4) $P_1 = 200$ mm Hg $D_H/D_C = 0.06$. Both the concentration profiles and the saturation profiles tend to be smoother at low values of P_1 as well as at high values of D_H/D_C.
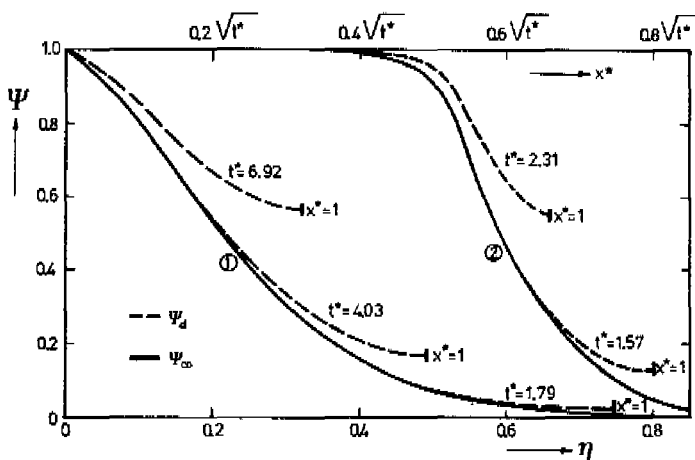
*Fig. 3.5. Comparison of the saturation profiles within a layer of
hemoglobin solution as calculated from the half-infinite slab model
(solid line) and the finite slab model (broken lines). Oxygen binding
capacity h = 6.2 10^{-3} mol/l ([Hb] = 10 g%), D_H/D_C = 0.0281, α = 1.33 10^{-8}
mol/l/mm Hg; 1) P_1 = 717 mm Hg; 2) P_1 = 65.2 mm Hg. The steeper the
oxygenation profile, the more abruptly the oxygenation process of a
finite slab will be completed.*

Fig. 3.5 compares the saturation profiles within both a layer of
finite thickness and a layer of half-infinite thickness analogous to
fig. 3.1. It is clear that the steeper the oxygenation profile, the
more abruptly the oxygenation process of a finite slab will be
completed (see also fig. 3.6 below).

3.3.3 Oxygenation of the layer with finite thickness as a function of time

The quantity of main interest within the scope of the present work is
the increase of the average oxygen saturation in a finite layer of
hemoglobin. The average dimensionless oxygen saturation is defined by

$$\bar{\psi}_d\ (t^*) = \frac{1}{d} \int_0^d \psi(x,t^*)dx = \int_0^1 \psi(x^*,t^*)dx^* \qquad (3.22)$$

In analogy to section 3.1.3, $\bar{\psi}_\infty(t^*)$ is defined as the average saturation of the layer with finite thickness, but calculated by means of the half-infinite layer model

$$\bar{\psi}_\infty \, (t^*) \; = \; \int_0^\infty \psi_\infty \; (\frac{x^*}{\sqrt{t^*}}) \; dx^* \; = \; \sqrt{t^*} \left\{ \int_0^\infty \psi_\infty(\eta) \; d\eta \right\} \tag{3.23}$$

$\bar{\psi}_\infty$ can only be ≤ 1 according to definition. The integral in brackets is independent of time. Hence according to the half-infinite model and independent of the saturation curve used, the average saturation has to increase proportionally to the square root of time. However, this conclusion only holds as far as $\bar{\psi}_\infty$ equals $\bar{\psi}_d$.
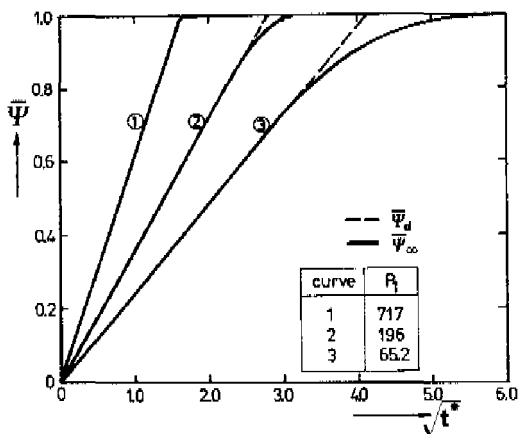
Fig. 3.6. Oxygenation of a finite slab as a function of t^* (solid lines) and the deviation from the half-infinite slab model (broken lines). Oxygen binding capacity $h = 6.22 \ 10^{-3} \ mol/l \ ([Hb] = 10 \ g\%)$, $D_H/D_C = 0.0281$, $\alpha = 1.51 \ 10^{-6} \ mol/l/mm \ Hg; \ 1) \ P_1 = 717 \ mm \ Hg$, 2) $P_1 = 196 \ mm \ Hg$, 3) $P_1 = 65.2 \ mm \ Hg$. Curves 1 and 3 of this figure correspond to curves 1 and 2 of fig. 3.5.

The oxygenation increases of the finite and half-infinite slab model are compared in fig. 3.6. As may be seen from fig. 3.6, the range of coincidence of $\bar{\psi}_d$ and $\bar{\psi}_\infty$ is considerable and tends to increase as P_1 is higher. This range of coincidence is controlled by the same conditions

that make the saturation profile steeper. This is understandable because
the steeper the saturation profile, the longer the profile "is not aware
of the dimension of the layer". Obviously it is permitted to apply the
half-infinite slab solution throughout a large part of the saturation
process in layers with finite thickness. The solution in the range of
$\bar{\psi}_d = \bar{\psi}_\infty$ can now be represented by a single figure, being the value of t^*
when $\bar{\psi}_\infty = 1$. For this the notation t_1^* is introduced which will be referred
to as the dimensionless oxygenation time.

3.4 Parametric analysis

3.4.1 Dependence of dimensionless oxygenation time on oxygen concentration ratio and oxygen flux ratio with a step-like saturation curve

According to the experimental procedure chosen (see chapter 4) P_i has
been taken to be zero for this analysis. On the basis of the saturation
curve given in fig. 3.3 and according to common practice in physiology,
ϕ_{50}, being the value of the ratio P_{50}/P_1, is chosen as a quantity to
characterize the dimensionless saturation curve.

If ϕ_{50} approaches to zero the dimensionless saturation curve assumes a
step-like shape. For this shape t_1^* can be calculated by means of a
moving boundary model as will be shown in section 3.5. The dimensionless
time calculated for $\phi_{50} = 0$ will be denoted by $t_1^{*,0}$. This quantity has been
calculated for H varying between 0 and 500 and D^* varying between 0 and
7. Numerical results are listed in tables 3.1 and 3.2. Concerning the
choice of the values of H and D^* refer to section 3.4.3 below.

Fig. 3.7 shows $t_1^{*,0}$ as a function of H for several values of D^*.
The relationship between $t_1^{*,0}$ and H at constant D^* appears to be linear
(data from tables 3.1 and 3.2). The intercept with the vertical axis is
close to zero, and D^* determines the slope of the curves to be denoted by f_2.

Fig. 3.8 presents the slope f_2 as a function of D^*. The curve of f_2
versus D^* approaches to a hyperbolic shape as indicated by the broken
line. The sensitivity of f_2 as a function of D^* is much higher at lower
values of D^* than at higher values. From this behavior the facilitation may
be derived as will be described later.
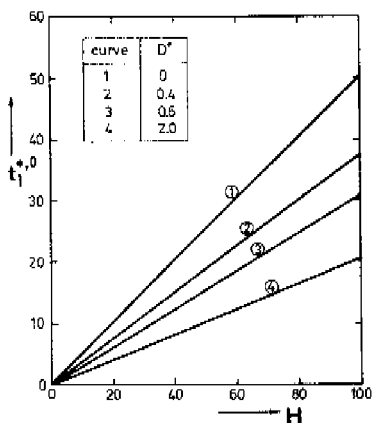
Fig. 3.7. Dimensionless oxygenation time using a step-like saturation curve (= $t_1^{*,0}$) as a function of the oxygen concentration ratio (H) for four different values of the oxygen diffusion ratio (D^*).
1) $D^* = 0$, 2) $D^* = 0.4$, 3) $D^* = 0.6$, 4) $D^* = 2.0$. The intercepts of the curve with the ordinate are close to zero. Data are taken from tables 3.1 and 3.2.
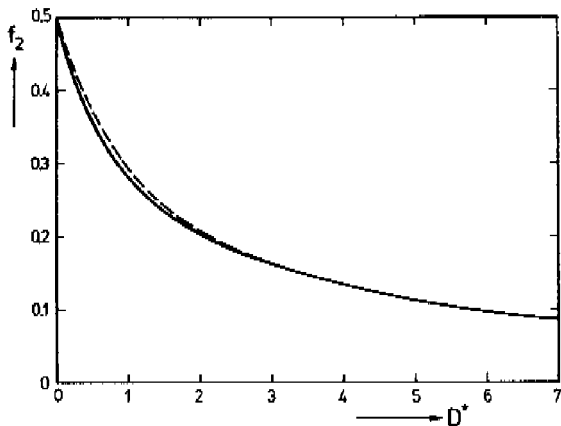
Fig. 3.8. The tangent f_2 of the relationship between the dimensionless oxygenation time, using a step-like saturation curve ($t_1^{*,0}$), and oxygen concentration ratio (H) as a function of oxygen diffusion ratio $D^* (= H D_H/D_C)$ (solid line). The f_2 versus D^* curve has a hyperbolic shape and can be approximated (broken line) by $f_2 = 0.739/(D^* + 1.477)$. In fact f_2 shows the sensitivity of the oxygenation process for the diffusivity of hemoglobin.

3.4.2 The influence of the dimensionless saturation curve on the dimensionless oxygenation time

For the arbitrarily chosen situation of $H = 100$ the influence of ϕ_{50} on the ratio $t_1^*/t_1^{*,0}$ has been studied for both $D^* = 0$ and $D^* = 3$. The results are given in fig. 3.9. At a fixed value of D^*, this ratio first increases and subsequently decreases with increasing ϕ_{50}. This behavior is due to the shape of the saturation curve which shows a concave and a convex part. A curve is defined to be concave when both the first and second derivative are positive. A curve is defined to be convex when the first derivative is positive but the second derivative is negative. At small values of ϕ_{50} the convex part dominates the influence of the curve whereas at increasing values of ϕ_{50} the concave part becomes more important.

curve	H	D
1	100	0
2	100	3
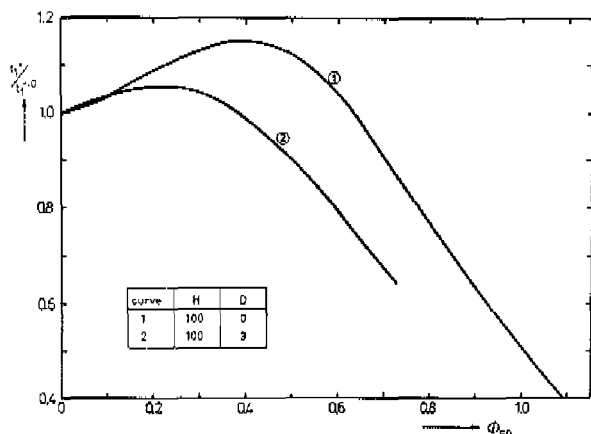
Fig. 3.9. The ratio $t_1^*/t_1^{*,0}$ as a function of ϕ_{50}; $t_1^{*,0}$ is the dimensionless oxygenation time applying a step-shaped saturation curve; $\phi_{50} = P_{50}/P_1$ characterizes the dimensionless saturation curve. 1) $H = 100$, $D^* = 0$; 2) $H = 100$, $D^* = 3$. Initially the dimensionless oxygenation time t_1^* increases and next decreases with increasing ϕ_{50}. This behavior is due to the shape of the saturation curve showing a concave and a convex part.

Fig. 3.9 is important with regard to the choice of the P_1 values to be applied in the experiments. As will be explained in section 3.5 and as has been shown in fig. 3.4 the influence of the carrier facilitation

becomes more pronounced at low than at high P_1 values. However, three important objections may be advanced against low P_1 values:

1) The real oxygenation times to be measured experimentally increases with decreasing P_1, and hence the degree of possible experimental error increases with decreasing P_1;

2) As is clear from fig. 3.6 the range of coincidence of $\bar{\psi}_d$ and $\bar{\psi}_\infty$, hence the range where $\bar{\psi}$ changes with $\sqrt{t^*}$, decreases with decreasing P_1; this relationship is of particular importance to check the experimentall[y] determined oxygenation course for errors;

3) Within the parts of the curves of fig. 3.9 having a positive slope, knowledge of the position of the real saturation curve is less important than within the parts having a negative slope.
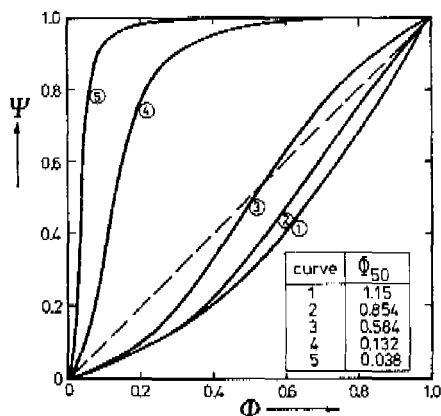
Fig. 3.10. Dimensionless saturation curves (ψ versus ϕ; $P_i = 0$, $\psi = S/S_1$, $\phi = P/P_1$) at several values of ϕ_{50} (P_{50}/P_1). Every dimensionless saturation curve is obtained from the standard saturation curve given in fig. 3.3 and the boundary values P_1 and S_1. 1) $\phi_{50} = 1.15$; 2) $\phi_{50} = 0.854$; 3) $\phi_{50} = 0.589$; 4) $\phi_{50} = 0.132$; 5) $\phi_{50} = 0.0378$. In calculating t_1^* using curves 4 and 5 the convex part of the curve dominates whereas when using curves 1,2 and 3 the concave part becomes dominant (see fig. 3.9). The broken line represents an approximation of curve 3 (see section 3.5.2).

The latter point is also illustrated by fig. 3.10 giving dimensionless saturation curves for several values of ϕ_{50}. The small difference in

shape between curves 1 and 2 results in a large difference between
the respective t_1^* values (H=100, D^*=0) curve 1) $t_1^* = 16.4$, curve 2) $t_1^* = 34.2$).
Consequently it was decided to experimentally study only the region
where the oxygenation time increases with increasing ϕ_{50}.

3.4.3 Completion of the dimensionless parametric analysis

The three parameters influencing t_1^* are H, D^* and ϕ_{50}. Since the
relations are non-linear the limiting values of these parameters have to
be defined. Two sets of limiting values are relevant:
1) H varies between 5 and 175, D^* varies between 0 and 2, and ϕ_{50}
   varies between 0.019 and 0.203 (table 3.1).
2) H varies between 100 and 500, D^* varies between 1 and 7, and ϕ_{50}
   varies between 0.019 and 0.377 (table 3.2).
These boundary values of the dimensionless parameters are chosen in such
a way that all those physical parameters are covered which belong to
hemoglobin concentrations between 7.7 10^{-4} mol/l (5 g%) and 5.4 10^{-3} mol/l
(30 g%). The minimum value of P_{50} equals 12.5 mm Hg and P_1 values vary
between 32 and 720 mm Hg in table 3.2 and between 62.5 and 720 mm Hg
in table 3.1.

Table 3.2 shows that the oxygen concentration ratio hardly influences
the dependency of $t_1^*/t_1^{*,o}$ on ϕ_{50}. The maximum in this relationship
decreases and shifts to smaller values of ϕ_{50} with increasing D^* as is
also seen in fig. 3.9.

Table 3.1 presents results restricted to a narrower region of boundary
values than applied in table 3.2. Table 3.1 may be divided into regions
where the dependency of the ratio $t_1^*/t_1^{*,o}$ on ϕ_{50} is identical within 0.5
percent. These regions are: $H \geqslant 25$, $D^* \geqslant 0.2$; $H = 5$, $D^* \geqslant 0.4$;
$H \geqslant 25$, $D^* = 0$. The relationships of $t_1^*/t_1^{*,o}$ with ϕ_{50} in these regions
are summarized in fig. 3.11. It is evident from this figure that for
$\phi_{50} \to 0$ the computer solutions converge to the solutions obtained by the
moving boundary model using a step-like saturation curve.

H	Φ_{50}	D^* ⟋ $\begin{array}{c}t_1^{*,0}\\ t_1^*/t_1^{*,0}\end{array}$	0.0	0.2	0.4	0.6
5		$t_1^{*,0}$	2.6625	2.2222	1.9411	1.753
	0.01910	$t_1^*/t_1^{*,0}$	1.002	1.015	1.015	1.018
	0.03820		1.005	1.020	1.025	1.028
	0.05348		1.019	1.038	1.047	1.049
	0.08913		1.041	1.072	1.081	1.083
	0.1337		1.078	1.110	1.124	1.129
	0.2026		1.136	1.174	1.183	1.185
25		$t_1^{*,0}$	12.666	10.715	9.4306	8.4724
	0.01910	$t_1^*/t_1^{*,0}$	1.001	1.012	1.013	1.013
	0.03820		1.003	1.014	1.017	1.022
	0.05348		1.015	1.027	1.033	1.035
	0.08913		1.030	1.052	1.057	1.058
	0.1337		1.054	1.080	1.085	1.087
	0.2026		1.096	1.121	1.122	1.120
50		$t_1^{*,0}$	25.166	21.328	18.790	16.898
	0.01910	$t_1^*/t_1^{*,0}$	1.004	1.010	1.010	1.013
	0.03820		1.006	1.017	1.019	1.020
	0.05348		1.014	1.028	1.029	1.031
	0.08913		1.031	1.047	1.052	1.053
	0.1337		1.054	1.076	1.081	1.080
	0.2026		1.092	1.112	1.114	1.111
75		$t_1^{*,0}$	37.666	31.941	28.149	25.312
	0.01910	$t_1^*/t_1^{*,0}$	1.004	1.008	1.012	1.010
	0.03820		1.006	1.014	1.017	1.013
	0.05348		1.014	1.028	1.029	1.032
	0.08913		1.028	1.049	1.051	1.054
	0.1337		1.053	1.075	1.080	1.080
	0.2026		1.089	1.110	1.112	1.110
100		$t_1^{*,0}$	50.167	42.553	37.509	33.732
	0.01910	$t_1^*/t_1^{*,0}$	1.004	1.008	1.010	1.013
	0.03820		1.006	1.016	1.020	1.013
	0.05348		1.011	1.028	1.031	1.032
	0.08913		1.027	1.048	1.051	1.054
	0.1337		1.051	1.074	1.079	1.079
	0.2026		1.091	1.111	1.110	1.107
175		$t_1^{*,0}$	87.667			58.990
	0.01910	$t_1^*/t_1^{*,0}$	1.003			1.023
	0.03820		1.006			1.023
	0.05348		1.014			1.029
	0.08913		1.030			1.051
	0.1337		1.050			1.073
	0.2026		1.088			1.107

0.8	1.2	1.6	2.0
1.5742			
1.019			
1.027			
1.049			
1.087			
1.128			
1.184			
7.7157	6.5783	5.7527	5.1205
1.011	1.011	1.012	1.009
1.021	1.022	1.023	1.020
1.033	1.031	1.030	1.030
1.056	1.052	1.051	1.045
1.084	1.075	1.071	1.066
1.117	1.108	1.096	1.086
15.391			
1.012			
1.019			
1.031			
1.052			
1.079			
1.106			
23.066	19.684	17.223	15.336
1.012	1.012	1.011	1.008
1.019	1.021	1.021	1.017
1.030	1.029	1.027	1.027
1.051	1.047	1.043	1.042
1.078	1.068	1.063	1.057
1.104	1.092	1.082	1.073
30.741			
1.013			
1.019			
1.032			
1.053			
1.077			
1.102			
	45.894	40.163	35.768
	1.012	1.007	1.008
	1.023	1.020	1.017
	1.030	1.026	1.025
	1.047	1.042	1.053
	1.067	1.059	1.053
	1.089	1.080	1.071

Tables 3.1 (p.p. 44-45) and 3.2 (p.46). For several combinations of values of oxygen concentration ratio H and oxygen diffusion ratio D^*, the dimensionless oxygenation time t_1^* is given as a function of $\phi_{50}(=P_{50}/P_1)$, being the quantity chosen to characterize the dimensionless saturation curve. The calculations were performed according to the half-infinite layer model and are accurate within $\pm$ 0.3% (section 3.3.3). The results are given in terms of the ratio $t_1^*/t_1^{*,0}$, where $t_1^{*,0}$ stands for the dimensionless oxygenation time in case of a step-shaped saturation curve ($\phi_{50}=0$). The values of $t_1^{*,0}$ were calculated using a moving boundary model (section 3.5) and are listed in the table.

Table 3.1. All experiments were performed in conditions where the parameters H, D^* and ϕ_{50} range as listed. The values of $t_1^*/t_1^{*,0}$ for ϕ_{50} < 0.1337 may be approximated within 1% by the polygonal approximation as described in section 3.5.

H	ϕ_{50}	D^*	1	3	5	7
		$t_1^{*,0}$	28.292	16.105	11.360	8.7914
	0.0191	$t_1^*/t_1^{*,0}$	1.012	1.007	1.007	1.005
	0.1337		1.071	1.044	1.029	<u>1.022</u>
100	0.2010		1.096	<u>1.053</u>	<u>1.033</u>	1.017
	0.2674		<u>1.111</u>	1.050	1.022	1.003
	0.3766		1.101	1.010	0.973	0.949
		$t_1^{*,0}$	63.616	36.229	25.556	19.779
	0.0191	$t_1^*/t_1^{*,0}$	1.012	1.009	1.007	1.006
	0.1337		1.069	1.042	1.028	<u>1.019</u>
225	0.2010		1.094	<u>1.050</u>	<u>1.030</u>	1.015
	0.2674		<u>1.108</u>	1.048	1.017	1.000
	0.3766		1.097	1.007	1.967	0.944
		$t_1^{*,0}$	78.941	56.353	39.753	30.767
	0.0191	$t_1^*/t_1^{*,0}$	1.012	1.006	1.007	1.003
	0.1337		1.069	1.045	<u>1.030</u>	<u>1.020</u>
350	0.2010		1.093	<u>1.051</u>	1.028	1.016
	0.2674		<u>1.106</u>	1.045	1.015	1.001
	0.3766		1.095	1.005	0.965	0.943
		$t_1^{*,0}$	141.33	80.502	56.709	43.952
	0.0191	$t_1^*/t_1^{*,0}$	1.009	1.008	1.004	1.004
	0.1337		1.069	1.043	<u>1.029</u>	<u>1.018</u>
500	0.2010		1.092	<u>1.049</u>	1.029	1.017
	0.2674		<u>1.106</u>	1.046	1.015	1.999
	0.3766		1.093	0.996	0.964	0.943

Table 3.2. The range of the values of the parameters H, D^* and ϕ_{50} was chosen in order to estimate approximately the maximum of the relationship between $t_1^*/t_1^{*,0}$ and ϕ_{50} (see also fig. 3.9) as a function of H and D^*. The different maximum values thus obtained are underlined in the table. Obviously the value of ϕ_{50} where the maximum value of $t_1^*/t_1^{*,0}$ appears, as well as the numerical value of this maximum , merely depend on D^*.
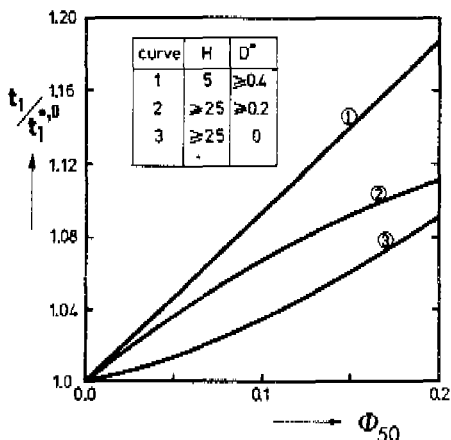
Fig. 3.11. The ratio $t_1^*/t_1^{*,O}(=f_1)$, being the ratio of dimensionless oxygenation time t_1^* and the dimensionless oxygenation time at a step-shaped saturation curve $t_1^{*,O}$ as a function of ϕ_{50}. The curves shown hold approximately within ± 0.01 for the following range of parameter values: 1) $H = 5$, $D^* \geq 0.4$; 2) $H \geq 25$, $D^* > 0.2$; 3) $H \geq 25$, $D^* = 0$. This figure is analogous to fig. 3.9 where, however, only one value of H and two values of D^*, but a much wider range of ϕ_{50} values are considered.

3.4.4 The dependency of real oxygenation time on physical parameters

The course of the real oxygenation is not explicitly evident from the dimensionless parametric analysis applied so far. The value of P_{50} determining the position of the real saturation curve (S versus P) is (linearly) related to ϕ_{50} only; the same holds for D_H with respect to D^*. Hence the influence of these physical parameters on oxygenation versus time can be demonstrated directly from the dimensionless parametric analysis. However, the other physical parameters involved are related to more than one dimensionless parameter. The oxygen binding capacity h occurs in both H and D^*; the boundary condition P_1 in H, D^* and ϕ_{50}; the diffusion coefficient of oxygen D_C in t^* and D^*; the solubility α in H and D^*.

From the results of the parametric analysis the relationship between real oxygenation time t_1 and the physical parameters can now be explicited. Thus we get

$$\frac{t_1}{d^2} = f_1 \left(\frac{P_{50}}{P_1}, \frac{hS_1}{\alpha P_1}, \frac{hS_1 D_H}{\alpha D_C} \frac{i}{P_1} \right) \quad f_2 \left(\frac{hS_1 D_H}{\alpha D_C} \frac{1}{P_1} \right) \frac{hS_1}{\alpha D_C} \frac{1}{P_1}$$

$$(3.24)$$

where f_1 is a function of ϕ_{50}, H and D^* as given in fig. 3.11, and f_2 is a function of D^* alone as was shown in fig. 3.8.
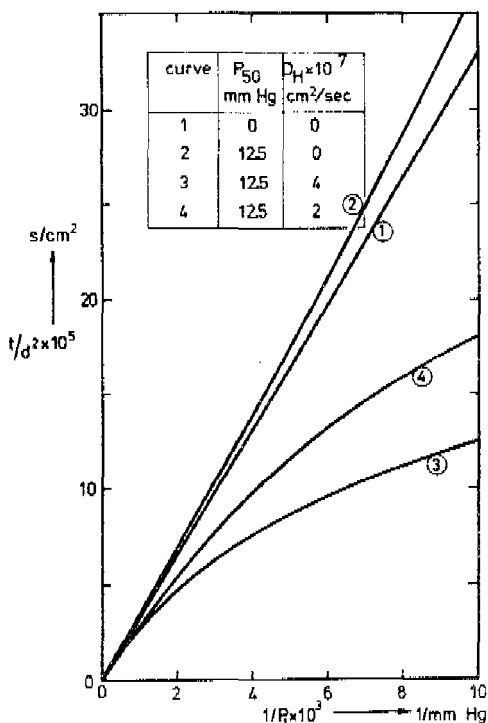
Fig. 3.12. *The ratio of real oxygenation time and the square of layer thickness as a function of the reciprocal value of the boundary condition P_1, and the influence of both saturation curve and diffusion of oxyhemoglobin on this relationship. $h = 1.24 \ 10^{-3}$ mol/l ([Hb] = 20%), $\alpha = 1.53 \ 10^{-6}$ mol/l/mm Hg, $D_C = 1.8 \ 10^{-5}$ cm^2/s, $P_{50} = 12.5$ mm Hg. 1) no influence of saturation curve ($\phi_{50} = 0$) and $D_H = 0$; 2) influence of saturation curve and $D_H = 0$; 3) influence of saturation curve and $D_H = 4 \ 10^{-7}$ cm^2/s; 4) as curve 3 but $D_H = 2 \ 10^{-7}$ cm^2/s.*

The small deviation of the intercept of the plot of $t_1^{*,0}$ versus H from the origin has been neglected (fig. 3.7). In fact, however, P_1 is the only parameter that can be varied experimentally without influencing other physical parameters.

It is clear from eq. 3.24 that the experimental study of the relationship between t_1/d^2 and $1/P_1$ of a certain hemoglobin solution can provide quantitative information on the physical parameters involved. In this regard the following conclusions may be drawn from eq. 3.24 as demonstrated in fig. 3.12 (except conclusion 1):

1) Apart from the quantity f_1 the solubility α and the diffusion coefficient D_C are only relevant as a product, being the permeability. However, f_1 as such has only a minor influence on t_1 (fig. 3.11), and moreover the influence of α on f_1 through H is very small. Consequently the permeability αD_C should be considered as the physical parameter to be determined from the oxygenation experiments rather than D_C.

2) If a) no influence of the saturation curve on the oxygenation process exists,

    b) the hemoglobin molecules are immobile, and

    c) P_1 is varied such that S_1 remains unity,

then the relationship between t_1/d^2 and $1/P_1$ will be linear (curve 1 in fig. 3.12).

3) The influence of the saturation curve, while still assuming $D_H = 0$, leads to a concave shape of the t_1/d^2 versus $1/P_1$ curve (curve 2 in fig. 3.12).

4) The carrier facilitation as a result of the diffusion of hemoglobin leads to a convex shape of the t_1/d^2 versus $1/P_1$ curve (curves 3 and 4 in fig. 3.12).

From eq. 3.24 it may be concluded that, in case S_1 is known from P_1, two groups of parameters can be estimated from an experimental curve like 3 or 4 in fig. 3.12

$$Z_1 = \frac{h}{\alpha D_C} \quad \text{and} \quad Z_2 = \frac{h}{\alpha D_C} D_H \qquad (3.24.a)$$

The information concerning Z_1 is contained in the scale value of the vertical axis, the information concerning Z_2 is contained in the curvature of the graph. It is important to note that the ratio of both expressions results in a value of D_H independent of both h and αD_C.

49

According to eq. 3.24 the value of $h/\alpha D_C$ can be estimated from the slope of the curve at the origin because in the neighbourhood of this point $f_1 \to 1$ and $f_2 \to 0.5$. Using figs. 3.7, 3.8 and 3.11, the value D_H can be estimated from experimental points at higher values of $1/P_1$ (see also chapter 5).

3.5 The "polygonal approximation"

3.5.1 Definition and equations

When aiming only at an estimate of the values of physical constants, in general sophisticated theoretical models are not efficient with regard to computer time. From this point of view the polygonal approximation of the saturation curve, as presented by Curl and Schultz (1973), has been chosen here although the authors have not offered a complete evaluation of their approximation method. Moreover, the parameters chosen seem unnecessarily complex. For this reason and considering its importance for parametric estimation this approximation will now be reviewed briefly. For a detailed description see Appendix C.

In the polygonal approximation the saturation curve is represented by two straight lines. The first line originates from the point ($\psi=\phi=0$) and intercepts the second line originating from the point ($\psi=\phi=1$) at ($\psi=\psi_c$, $\phi=\phi_c$). According to the half-infinite layer model ψ and ϕ are explicit functions of η. Hence there will exist a value η_c where $\psi = \psi_c$ and $\phi = \phi_c$. So the half-infinite layer may be divided into two regions, $0 \leqslant \eta \leqslant \eta_c$ and $\eta_c \leqslant \eta$ respectively. In both regions the second derivative $d^2\psi/d\phi^2=0$, thus according to eq. 3.21 the following differential equation holds

$$A \frac{d^2\phi}{d\eta^2} - \frac{1}{2} \eta \ B \ \frac{d\phi}{d\eta} = 0 \tag{3.25}$$

where

$$A = 1+D^* \frac{d\psi}{d\phi} \quad ; \quad B = 1+H \frac{d\psi}{d\phi} \tag{3.26}$$

The parameters A and B have different values in each different region, and hence for $0 \leqslant \eta \leqslant \eta_c$ referred to as region I , $A = A_1$ and $B = B_2$, for $\eta_c \leqslant \eta$ referred to as region II, $A = A_2$ and $B = B_2$.

The general solution of eq. (3.25) is

$$\phi = E \ \mathrm{erf} \ (\frac{\eta}{2}\sqrt{\frac{B}{A}}) + K \tag{3.27}$$

E and K are integration constants the values of which are to be determined from the boundary conditions. For region I these conditions are

$$\eta = 0 \quad ; \quad \phi = 1 \; , \quad \eta = \eta_c \quad ; \quad \phi = \phi_c$$

so

$$K_1 = 1 \quad , \qquad E_1 = (\phi_c - 1)/\mathrm{erf}\left(\frac{\eta_c}{2}\sqrt{\frac{B_1}{A_1}}\right) \qquad (3.28)$$

For region II the boundary conditions are

$$\eta \to \infty \quad ; \quad \phi \to 0 \quad , \qquad \eta = \eta_c \quad ; \quad \phi = \phi_c$$

$$(3.29)$$

so

$$E_2 = -K_2 \quad , \qquad E_2 = \frac{\phi_c}{\mathrm{erf}\left(\frac{\eta_c}{2}\sqrt{\frac{B_2}{A_2}}\right) - 1}$$

Since η_c is still unknown one more equation is needed. This equation follows from the condition that the total oxygen fluxes at the interface between regions I and II as calculated from the conditions in the different regions should be equal. Hence we get

$$A_1 \left(\frac{d\phi}{d\eta}\right)_{\eta = \eta_c}, \text{ region I} \quad = \quad A_2 \left(\frac{d\phi}{d\eta}\right)_{\eta = \eta_c}, \text{ region II} \qquad (3.30)$$

This relationship leads to the following implicit equation for η_c

$$\frac{\phi_c}{1-\phi_c}\sqrt{\left(\frac{A_2}{A_1}\frac{B_2}{B_1}\right)} = \exp\left(\left(-\frac{\eta_c^2}{4}\left(\frac{B_2}{A_2} - \frac{B_1}{A_1}\right)\right)\right) \frac{1 - \mathrm{erf}\left(\frac{\eta_c}{2}\sqrt{\frac{B_2}{A_2}}\right)}{\mathrm{erf}\left(\frac{\eta_c}{2}\sqrt{\frac{B_1}{A_1}}\right)}$$

$$(3.31)$$

Thus ϕ and ψ are known for all values of η and next the quantity $\vec{\psi}$ may be found by integration of ψ (see Appendix C).

3.5.2 Evaluation of the polygonal approximation

The polygonal approximation belongs to the so-called class of moving boundary models to be discussed in more detail in chapter 5.

In the case of section 3.5.1 the results of the polygonal model depend on the choice of the approximation of the saturation curve. Curl and Schultz suggested as a reasonable procedure to qualitatively minimize the area between the saturation curve and the straight line segments. However, this suggestion appears to be far too optimistic as is clearly demonstrated by the straight line approximation of curve 3 in fig. 3.10. The computer solution for this curve 3 yields $t_1^* = 12.7$ ($H = 100$, $D^* = 3$) whereas the straight line approximation yields in this case $t_1^* = 19.8$.

In selecting an approximation of the saturation curve apparently first the influence of the saturation curve on the oxygenation process has to be known. Considering fig. 3.9 (t_1^* versus ϕ_{50}), probably the saturation curve has to be approximated by more than two lines (which is mathematically possible) in the region where t_1^* decreases with increasing ϕ_{50}. However, for reasons explained in section 3.4.2, the ϕ_{50} values of interest for the experiments have been chosen such that the concave part of the saturation curve dominates. For this region of ϕ_{50} the polygonal approximation of the saturation curve has been chosen such that ψ_c always equals 1. Then for a particular dimensionless saturation curve characterized by its value at ϕ_{50} (= 0.1337) and arbitrarily chosen values of H(=100) and D^*(=0.6), the value for ϕ_c(=0.2945) was estimated such that the quantity t_1^* calculated according to the Runge-Kutta numerical integration method equals the value calculated from the polygonal approximation.

To evaluate the applicability of the polygonal approximation the same parameter analysis has been performed as used in table 3.1. A change of the value of ϕ_{50} was replaced by a proportional change of ϕ_c. The numerical agreement of both parameter analyses is within 1% over a wide range of parameter values for ϕ_{50} and D^*. This range is included in table 3.1. Hence, the polygonal approximation may be applied successfully for the interpretation of the experimental results.

3.6 Estimation of the influence of finite reaction velocity on the oxygenation process of a non-moving layer

3.6.1 Literature dealing with theoretical models including reaction velocity

In view of the gas exchange of the red cell the mathematics of oxygen and carbon monoxide absorption by thin layers of hemoglobin including reaction velocity, as well as the related problem of oxygen uptake by carboxyhemoglobin (HbCO) have received much attention by Roughton (1932), Nicholson and Roughton (1951), and Klug, Kreuzer and Roughton (1956). The reactions were assumed to be of first order, characterized by a forward reaction velocity constant k' and a backward reaction velocity constant k. Approximate solutions were obtained mostly by neglecting the back reaction. Sometimes the diffusion of hemoglobin and/or the influence of membranes bounding the layers were considered. For a comprehensive survey of the results of these studies the reader is referred to Roughton (1959).

Mochizuki and Fukuoka (1958) considered the oxygen uptake by the red cell surrounded by a plasma layer. Their model was one-dimensional too. The reaction scheme used was of first order, but k was varied and made to depend on saturation and k' in such a way that at equilibrium the first-order reaction equation resulted in a sigmoid shape. Hemoglobin diffusion was neglected. All methods discussed so far are of a combined analytical-numerical nature and appear to be quite complex.

Moll (1968) presented computer solutions for the oxygen uptake by layers of hemoglobin solution of finite thickness obtained by a finite-difference method. The objective of his study was to predict the rate of oxygen uptake and release by the red cell. The reaction velocity was taken into account in the same way as Mochizuki and Fukuoka (1958) had done. The results were presented only in terms of a change of average saturation as a function of time. A limited number of cases relevant to our problem were considered, i.e. (half) layer thicknesses of 0.8 μm and 1.8 μm, only one value of $[Hb]$ (33 g%), D_C and k', two values of D_H (0 and 4.5 10^{-8} cm^2/s), and two values of P_l (40 and 100 mm Hg) though the lower value of P_l was considered only in connection with the layer of 1.8 μm. Moll showed for the layer thickness of 0.8 μm that until the initial saturation increase is 35% the diffusion of hemoglobin has no influence, indicating that in the first stage of oxygenation a sufficient gradient of saturation is not yet present. For the case

of the 1.6 μm layer this limit is seen at 10% initial saturation increase.

Kutchai (1970) presented numerical results using a first-order reaction model but accepted the consequence of a hyperbolic saturation curve. He studied only one hemoglobin concentration (33 g%) and one value of P_1 (100 mm Hg) while, however, including a wider range of layer thicknesses (0.25 μm to 10 μm) as well the influence of D_H, D_C and k'. He also studied the effect of the diffusion of hemoglobin on half-saturation time ($t_{1/2}$ = time where $S = 0.5$) as a function of layer thickness. There is no reduction in $t_{1/2}$ for the layer of 0.125 μm but with increasing layer thicknesses the facilitating effect increases to become constant with layers thicker than 2.5 μm. According to the chemical equilibrium model the reduction in oxygenation time by carrier facilitation should be independent of layer thickness. Hence one might conclude that 2.5 μm is the minimum layer thickness that allows applying the chemical equilibrium model. As has been shown before in this chapter, the chemical equilibrium model results in a linear relationship between ψ and $\sqrt{t}$ over a wide range of ψ. In order to test this relationship from Kutchai's results it was tried to fit, by means of the method of least squares, the data of his table 2 with ψ between 0.2 and 0.95 to the model curve; $\psi = pt^q$ (see also chapter 6). This curve fitting appeared to be satisfactory for $d = 1.8$ μm, although the time for $\psi = 0.108$ appears to be too large as also shown by Garred (1975). The value of q had to be 0.5 but was actually found for various layer thicknesses to be:
$d = 1.8$ μm, $q = 0.502 \pm 0.005$; $d = 2.5$ μm, $q = 0.485$ μm ± 0.006; $d = 5$ μm, $q = 0.469 \pm 0.0013$; $d = 10$ μm, $q = 0.464 \pm 0.014$ (values of $q \pm$ S.D.). So in fact the numerical procedure of Kutchai leads to questionable results at larger layer thicknesses.

Garred (1975) compared Moll's results with a chemical equilibrium model and showed that the time needed to obtain a saturation of 10% calculated with the model including reaction velocity (2 ms) is five times higher than when calculated with the equilibrium model (0.4 ms). At a saturation of 90% this time difference is only 10% (41 ms versus 37 ms). Garred (1975) also repeated the calculations of Kutchai with a different numerical technique, and compared his results with those obtained when assuming chemical equilibrium. From a comparison of both

models he showed that for the parametric values the time for reaching
a degree of oxygenation calculated with the transfer model including
reaction velocity (= $t_{r,d}$) equals the sum of the time obtained from the
reaction velocity equation (= t_r) and the time resulting from the
equilibrium transfer model (= t_d). He also concluded to a limit of 2.5 μm
layer thickness above which chemical equilibrium may safely be applied
under these conditions. The results of Garred with the finite reaction
velocity model, however, differ significantly from Kutchai's results
concerning the time for a 10% initial saturation increase.

Thus a sufficiently complete parametric analysis with models
including reaction velocity is lacking. However, from the papers
cited it is likely that for a given hemoglobin solution with a certain
boundary value P_1 a layer thickness d_m can be defined in such a way
that for $d > d_m$ the finite slab model with chemical equilibrium results
in the same temporal course of oxygenation as does a model which accounts
for reaction velocity (see section 3.6.5 below). The remainder of this
section will be concerned with elucidating the applicability of the
equilibrium assumption and defining a relationship between d_m and h, P_1,
D_C and and reaction velocity constants for the models used here.

There exist three marked differences between the transfer models
including chemical reaction and those assuming equilibrium. The first
two differences (sections 3.6.2 and 3.6.3) refer to the boundary
conditions and the third one (section 3.6.4) deals with the reaction
throughout the whole layer.

3.6.2 Delay time in the boundary saturation

Finite reaction velocity means that for $x = 0$ and $t = 0$, $P = P_1$ and
$S = 0$ rather than $S = S_1$ for chemical equilibrium. Even if chemical
equilibrium would be possible at the gas-fluid interface (see section
3.6.3) some time would be required for S_1 to be reached. It is relatively
easy to estimate the delay time in the boundary condition for S. The
simplified reaction velocity equation of Moll and Garred will be adopted.
The rate of uptake of oxygen (R_C) by hemoglobin is assumed to be

$$- R_C = k_f \ h \ (C-C^e)(1-S) \qquad (3.32)$$

where k_f = reaction velocity constant, 1/mol/s

    h = oxygen binding capacity of hemoglobin, mol/l

    The relationship between S and C^e is represented by the equilibrium
saturation curve.

From eqs. 2.15 and 2.16, when neglecting diffusion and convection, it follows

$$- R_C = R_S \, h = \frac{dS}{dt} \, h \qquad (3.33)$$

and hence $C = C_1$ at $x = 0$,

$$\frac{dS}{dt} = k_f \ (C_1 - C^e)(1-S) \qquad (3.34)$$

Numerical solutions of 3.34 can easily be obtained by writing 3.34 in an integral form

$$\int_0^S \frac{1}{(C_1 - C^e)(1-S)} \ dS = k_f \ t \qquad (3.35)$$

curve	P_1
1	700
2	300
3	150
4	100
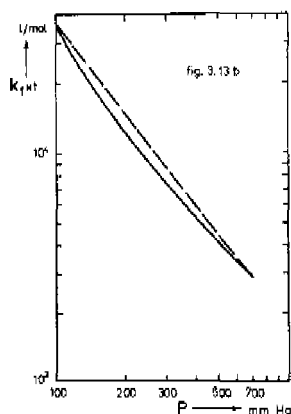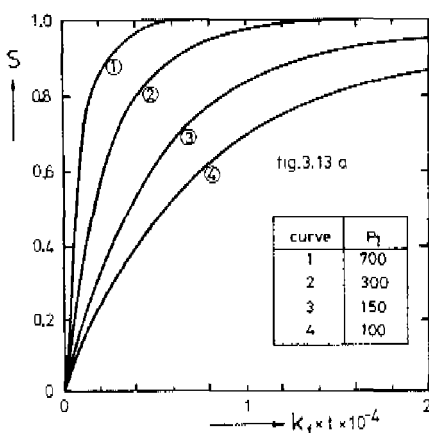
Fig. 3.13a. Saturation increase at the gas-hemoglobin solution interface as a function of $k_f t$ where k_f is the forward reaction velocity constant. The value of k_f is assumed to be 3.5 10^6 l/mol/s. Hence in case $P_1 = 700$ mm Hg the boundary condition S_1 at the gas-liquid interface has a delay time in the order of 1 ms.

Fig. 3.13b. The solid curve shows the value of $k_f t$ needed for the saturation to reach an arbitrary value of 0.941 as a function of P_1. The broken line is an arbitrarily chosen upper limit of the solid curve.

Results are shown in fig. 3.13a with P_i as a parameter. Obviously the velocity of the reaction is proportional to k_f, independent of the oxygen binding capacity h, and increases when P_i increases. Fig. 3.13b shows the dependency of $(k_f\ t)_{0.94}$ on P_i, the value of $k_f t$ for $S = 94\%$ (arbitrarily chosen). Using a value of $3.5\ 10^6$ 1/mol/s for k_f according to Garred we find small values (between 1 and 10 ms) for the delay time of the boundary saturation.

3.6.3 Contradictions between chemical equilibrium assumption and physical boundary conditions

Since application of the equilibrium model implies that not only S and C are uniquely related but also their gradients, the equilibrium model results in a flux of hemoglobin-bound oxygen away from the boundary which is physically impossible. From a purely mathematical point of view the ratio of the flux of chemically bound oxygen and the flux of physically dissolved oxygen can be written as

$$\frac{J_{HbO_2}}{J_{O_2}} = \frac{h\,D_H\,\frac{dS}{dx}}{D_C\,\frac{dC}{dx}} = \frac{h\,D_H}{D_C}\ \frac{dS}{dC} \tag{3.36}$$

At the high PO_2 values used in the present analysis ($P_i \geqslant 150$ mm Hg) dS/dC is small and the ratio J_{HbO_2}/J_{O_2} is less than 2.5%.

From a physical point of view this reasoning is not very sound. In fact, there will probably exist a thin boundary layer at the gas-liquid interface where the saturation profile will deviate from the one calculated by the chemical equilibrium model in order to satisfy the condition of $dS/dx = 0$ at $x = 0$. In case of steady-state oxygen diffusion through a stagnant layer of hemoglobin solution, such thin boundary layers have been described both theoretically (Kutchai 1970, Kreuzer and Hoofd 1970) and experimentally (Weigelt 1976). However, up to now saturation profiles in case of transient oxygen uptake have not been published.

3.6.4 Reaction throughout the whole layer

The models including finite chemical reaction velocity maintain a finite value of $(C-C^e)$ as has been discussed in section 2.4. Thus the actual saturation curve (S vs P) pertaining within the hemoglobin layer

will be a function of place (x) and time (t), but it is always shifted to the right of the equilibrium curve. The assumption of chemical equilibrium means here that the shift of the "saturation curve" is so small that it does not affect the overall result of oxygen uptake time. An indication of the value of $(C-C^e)$ may be found from eq. 3.32 when R_C is known. In the case of equilibrium R_C follows from

$$R_C = \frac{\partial C}{\partial t} - D_C \frac{\partial^2 C}{\partial x^2} \tag{3.37}$$

For a half-infinite layer this results in

$$\xi(\eta) \equiv R_C t = -\frac{1}{2} \eta \frac{dC}{d\eta} - \frac{d^2 C}{d\eta^2} \tag{3.38}$$

Eq. 3.38 shows the product $R_C t$ to be a function of η only. Combination of eqs. 3.38 and 3.32 results in

$$\Delta C = C - C^e = \frac{\xi(\eta)}{(1-S)} \quad \frac{1}{k_f \cdot h \cdot t} \tag{3.39}$$

Fig. 3.14 shows $\xi(\eta)/(1-S)$ as a function of η for two values of h and two values of C_1. The curves show a peak at a value of η where the oxygen saturation is about 70%. Now ΔC will be considered at $S = 0.5$, defining $\Delta C = \Delta C_{50}$ and $\eta = \eta_{50}$. The place where this particular shift occurs is given by

$$x_{50} = \eta_{50} \sqrt{D_C t} \tag{3.40}$$

and thus

$$\Delta C_{50} = (C-C^e)_{50} = \frac{\xi(\eta_{50})\eta^2_{50}}{0.5} \quad \frac{D_C}{k_f h x^2_{50}} \tag{3.41}$$

The function $\xi(\eta_{50})\eta^2_{50}$ was calculated for a parameter range of h, P_1 and D^* ($2.8 \ 10^{-3} < h < 1.7 \ 10^{-2}$; $150 < P_1 < 700$ mm Hg; $0 < D^* < 0.6$). The influence of D^* appears to be small (12% when D^* is between 0 and 0.6). For this reason in the following $D^* = 0$. The influence of h on $\xi(\eta_{50})\eta^2_{50}$ is also small (5% difference when h ranges between $6 \ 10^{-3}$ mol/l and $1.68 \ 10^{-}$ mol/l). Therefore only the factor C_1 appears to be important.
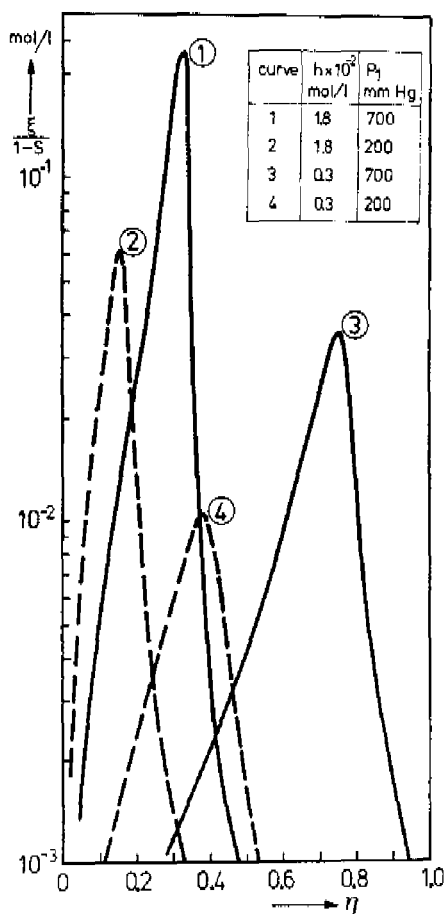
Fig. 3.14. Rate of oxygen uptake (R_C) by hemoglobin scaled by the factor $t/(1-S)$, $(\xi = R_C \ t)$, in a half-infinite layer of hemoglobin solution as calculated by the model assuming chemical equilibrium. The maximum rate of oxygen uptake occurs at approximately $S = 0.7$. 1) $h = 1.8 \ 10^{-2} \ mol/l$, $P_1 = 700 \ mm \ Hg$; 2) $h = 1.8 \ 10^{-2} \ mol/l$, $P_1 = 200 \ mm \ Hg$; 3) $h = 3 \ 10^{-3} \ mol/l$, $P_1 = 700 \ mm \ Hg$; 4) $h = 3 \ 10^{-3} \ mol/l$, $P_1 = 200 \ mm \ Hg$.

Eq. 3.41 now becomes

$$\Delta C_{50} = 1.5 \ 10^4 \ \frac{D_C}{x_{50}^2} \ \frac{(C_1)^2}{k_f \ h}$$

(3.42)

If we interpret the influence of reaction velocity as a shift of the local saturation curve at place x, eq. 3.42 provides a quantification of the "near-equilibrium condition" of the oxygenation process.

3.6.5 Minimal layer thickness allowing chemical equilibrium assumption

Eq. 3.42 is a scaling formula for the half-infinite equilibrium model but does not give explicit information on the influence of finite reaction velocity on t_1^*. A scaling number for this may be obtained, in case hemoglobin is not mobile, by substituting eq. 3.32 into eq. 3.37 and making the resulting equation dimensionless with regard to time and place according to eqs. 3.5 and 3.6. This results in a dimensionless number k^* (analogous to Damköhler (1937) and Thiele number (1939))

$$k^* = \frac{k_f \ h \ d^2}{D_C}$$

(3.43)

This number presents a relationship between layer thickness d, reaction velocity constant, oxygen binding capacity, and diffusion coefficient of oxygen. For identical values of C_1 and k^* eq. 3.37 provides identical results and hence in this situation d_m, the minimal layer thickness allowing the chemical equilibrium assumption, can be defined by k^*. However, a mathematical expression is needed for d_m in which P_1 and D_H are incorporated too.

In order to obtain such an expression, it is obvious to use the ratio t_r/t_d ($\approx t_r/t_{r,d}$ at small ratios, t_r = oxygenation time due to chemical reaction, t_d = oxygenation time assuming chemical equilibrium, $t_{r,d}$ = oxygenation time when both reaction velocity and diffusion are taken into account). According to the broken line of fig. 3.13b and eq. 3.24 we obtain

$$\frac{t_r}{t_d} \approx \frac{1.5 \ 10^7}{P_1^{1.3} \ k_f} \ \frac{\alpha D_C \ P_1}{f_1 f_2 h_1 d^2}$$

(3.44)

From Garred's calculations one may deduce a value of 0.03 for the ratio t_r/t_d to be small enough to obtain identical results from the models with and without assumption of chemical equilibrium, at least for the parameter values used by him (P_1 = 100 mm Hg, [Hb] = 33 g%). Hence eq. 3.44 may be rewritten in order to calculate d_m

$$d_m = \sqrt{\frac{5 \cdot 10^8}{P_1^{0.31} k_f} \quad \frac{\alpha D_C}{f_1 f_2 h S_1}}\qquad(3.45)$$

Obviously the significance of this equation depends on the assumption that t_r/t_d = 0.03 is small enough to apply when using boundary conditions and hemoglobin concentrations different from those used by Garred. However, when substituting the most unfavourable parameter values with respect to the experimental conditions chosen (h = 10^{-3} mol/l, D_C = 2 10^{-5} cm^2/s, f_1 = 1, f_2 = 2, α = 1.51 10^{-6} mol/l/mm Hg, S_1 = 1, P_1 = 100 mm Hg, k_f = 3.5 10^6 1/mol/s) d_m shows the value of 23 μm which is below the minimum value of 50 μm as applied in the experiments.

3.7 Discussion of the models of oxygen transfer in non-moving layers of hemoglobin solutions

The parametric analysis given in section 3.4 applies to a situation where chemical equilibrium may be assumed throughout the whole hemoglobin layer. Three dimensionless parameters could be defined:

1) Oxygen concentration ratio H, being the ratio of binding capacity and dissolving capacity of a hemoglobin solution under the boundary conditions present;

2) Oxygen flux ratio D^*, being the ratio between the diffusion fluxes of bound and dissolved oxygen;

3) ϕ_{50}, the ratio P_{50}/P_1, characterizing the dimensionless saturation curve.

This dimensionless analysis has proved to be very useful. In the first place the number of parameters could be reduced to a minimum, making it relatively easy to compare the results of the three models:

1) finite layer thickness,

2) half-infinite layer thickness, and

3) polygonal approximation of model 2.

By comparing the half-infinite and finite layer model, the oxygenation process could be described by a single number(t_1^*), thus simplifying the presentation of numerical results. Yet the study of a system controlled by three parameters can be very complex. Fortunately the influence of ϕ_{50} appeared to be minor and, even better, it proved to be uniform over a wide range of values of H and D^*($H \geqslant 25$, $D^* \geqslant 0.2$). Moreover $t_1^{*,o}$ appeared to be a linear function of H for all values of D^* studied (at $\phi_{50} = 0$). Thus the influence of D^* on $t_1^{*,o}$ could be expressed by the slope of the $t_1^{*,o}$ versus H curves. As a result of this the complete parametric analysis in terms of $t_1^{*,o}$ can be represented by three simple diagrams (figs. 3.7, 3.8 and 3.11). From the analysis of the influence of the dimensionless saturation curve on oxygenation time a lower limit of P_1 relative to P_{50} could be defined such that accurate knowledge concerning the position and shape of the saturation curve is not required. The analysis of the relationship between oxygenation time and physical parameters resulted in some important conclusions:

1) The oxygen permeability αD_C rather than the diffusion coefficient D_C is the physical parameter to be determined;
2) Accurate knowledge of oxygen solubility is not required in order to estimate other parameters from the experimental results;
3) The diffusion coefficient of hemoglobin can be estimated without knowing the oxygen binding capacity of the solution.

The present thesis does not aim at studying the influence of reaction velocity on the oxygen uptake of layers of hemoglobin in a fundamental manner. Partly based on the parametric analysis of the chemical equilibrium model some ideas have been developed as to how to visualize the influence of finite reaction velocity. However, for sufficiently large values of x the concept of explaining the deviation from chemical equilibrium by a local shift of the saturation curve is probably correct. The number ΔC_{50} then appears to be a real scaling factor. However, it describes only local phenomena and does not give information on the behavior of an integral phenomenon such as the course of oxygenation as a function of time. Yet, based on the work of Garred (1975), a minimum layer thickness allowing chemical equilibrium could be defined. Using the most unfavorable parameter values this minimum thickness amounts to 23 μm which is safely below the minimum thickness used in the present experiments.

CHAPTER 4

EXPERIMENTAL METHOD FOR INVESTIGATION OF THE NONSTATIONARY OXYGENATION
PROCESS

4.1 Experimental principles and set-up

4.1.1 Optical method for measuring both change in oxygenation and layer thickness

According to the physical model developed in section 3.1 a layer of
deoxygenated hemoglobin solution (thickness between 50 and 300 μm) is
spread over a leveled glass plate. This layer is abruptly contacted with
a gaseous atmosphere having a known oxygen partial pressure P_1.

The oxygen saturation of the layer increases with time up to its
maximally possible value (depending on P_1). This process of oxygenation
is measured by recording the change in absorption of light at a wavelength
of 670 nm (bandwidth 40 nm) from a parallel beam of light transmitted
perpendicularly through the layer.

According to the law of Lambert-Beer the intensity of the light beam
as detected by the light sensor is

$$\log I = \log I_a - (\varepsilon_o (1-\bar{S}) + \varepsilon_1 \bar{S})bd \qquad (4.1)$$

I   = intensity of the light after passing the layer   )*
ε_o = extinction of deoxygenated hemoglobin solution
ε_1 = extinction of oxygenated hemoglobin solution
$\bar{S}$ = average oxygen saturation of the layer
bd   = product of hemoglobin concentration and layer thickness
$\log I_a$ = apparatus constant
The value of $\log I_a$ depends on the intensity of the light emitted by
the light source, reflection of light at the optical interfaces, and
absorption or scattering of light by species other than oxyhemoglobin
or deoxyhemoglobin molecules. In case the optical path and the physical
constants of the media remain constant $\log I_a$ will also be constant.

Before oxygen is supplied to the layer obviously $\bar{\psi} = 0$ ($S = S_i$), and
after completing the oxygenation process the situation is characterized
by $\bar{\psi} = 1$ ($S = S_1$). Hence according to eq. 4.1

)* actually I is the attenuation of light, hence dimensionless.

$$\log I_i = \log I_a - (\varepsilon_o(1-S_1) + \varepsilon_1 S_1)bd \qquad (4.2)$$

$$\log I_o = \log I_a - (\varepsilon_o(1-S_i) + \varepsilon_1 S_i)bd \qquad (4.3)$$

where I_1 = intensity of light at $\psi = 1$.

I_o = intensity of light at $\psi = 0$.

From eqs. 5.1 to 5.3 the oxygen saturation during the oxygenation process is obtained from the relationship

$$\bar{\psi}(t) = \frac{\log (I(t)/I_o)}{\log (I_1/I_o)} \qquad (4.4)$$

where $I(t)$ = intensity of light at time t.

From eqs. 4.2 and 4.3 a relationship is found from which the layer thickness can be calculated, assuming no geometrical changes to occur during the oxygenation process

$$d = \frac{\log (I_1/I_o)}{(\varepsilon_o b - \varepsilon_1 b)(S_1-S_i)} \qquad (4.5)$$

The apparatus constant does not appear in eqs. 4.4 and 4.5. When using monochromatic light the extinction coefficients of the various forms of hemoglobin are well known (e.g. van Assendelft 1970). However, in the present investigation the light is far from being monochromatic and moreover hemoglobin solutions usually contain some inactive species such as methemoglobin. Hence both ε_o and ε_1 may differ significantly from the extinctions of pure deoxy- and oxyhemoglobin at $\lambda = 670$ nm. Consequently the absorption coefficients $\varepsilon_o b$ and $\varepsilon_1 b$ have to be measured separately in order to be able to determine the layer thickness.

4.1.2 Measurement of absorption coefficients by the wedge method

The principle of the design of the wedge cuvette is shown in fig. 4.1. Two plan-parallel glass plates (length 7 cm) are arranged at a small but well-known angle of which the tangent (μ) is between 3.10^{-3} and 9.10^{-3}. A mechanical device scans the same light beam as applied in the oxygenation measurements across the wedge.

At a position x of the beam relative to a point of reference the length of the optical path within the wedge equals μx, and according
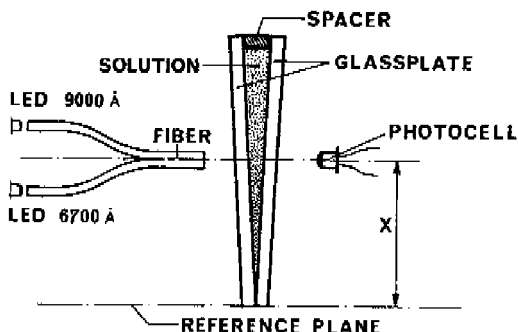
*Fig. 4.1. Outline of the wedge method for determining light absorption
coefficients at the two different wavelengths of the oximeter
(see section 4.1.4). The wedge cuvette is constructed of two plane-
parallel glass plates arranged at a small but well-known angle. The
light of two Light Emitting Diodes (LED) is conducted by fiber optics
to pass through the hemoglobin layer and is received by a photocell
(a light-sensing diode). A mechanical device scans the optical system
(fiber end and photocell) across the wedge. The light absorption
coefficient εb follows from eq. 1.8.*

to eq. 4.1 the light intensity as a function of x is given by

$$\log I(x) = \log I_a - \varepsilon b \mu x \qquad (4.6)$$

where $\log I_a$ = apparatus constant

    μ = tangent of the wedge angle

    x   = position of the beam relative to a point of reference

    εb   = absorption coefficient

Thus when plotting $\log I(x)$ versus μx the absorption coefficient can
be readily found.

Application of a "van Abbe" length measuring instrument, as
commonly used in metrology , allows measuring of μx with an accuracy
of approximately $\pm$ 1.0 μm on the outside of the wedge.

4.1.3 Description of the diffusion chamber and basic experimental procedure

Fig. 4.2a shows a cross-section of the diffusion chamber as well as
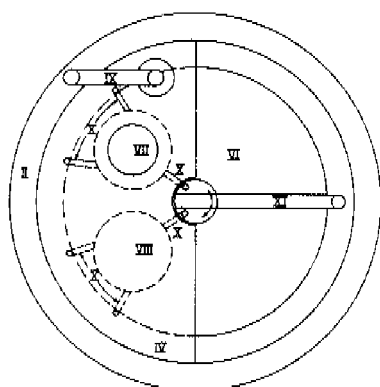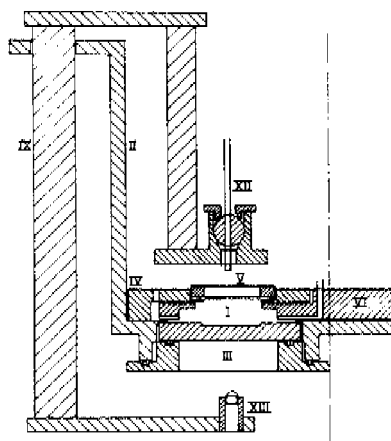
fig. 4.2 b   fig. 4.2 a

Fig. 4.2(a,b). Outline of the experimental apparatus. Fig. 4.2a shows
a cross-section and fig. 4.2b presents a view from the top. For an
overall view of the apparatus refer to picture 2.

    I diffusion chamber;

   II cylindrical housing of the diffusion chamber;

  III step-shaped glass plate to carry the hemoglobin layer (see
      also picture 1 and fig. 4.5);

   IV top plate, mounted rigidly on the bottom of the housing;

    V double glass upper window;

   VI teflon turntable provided with two chambers;

  VII nitrogen gas chamber;

VIII oxygen gas chamber;

   IX swivel arm on which both the optical fiber and the photocell
      are mounted;

    X inlet and outlet channels for the gases;

   XI arm for turning the teflon table;

  XII end of the fiber mounted in a ball-joint, allowing to adjust
      the direction of the lightbeam;

XIII photocell.

its housing and the relevant part of the optical system. Fig. 4.2b
presents a view from the top.

The diffusion chamber (I) is housed in a metal cylinder (II) of 14.5 cm diameter and basically consists of three parts:

1) a profiled glass plate (III) to carry the hemoglobin sample and being mounted at the bottom of the cylinder;

2) a top plate (IV) containing a double glass window (V) designed to be easily mountable after a hemoglobin layer has been spread;

3) a turntable (VI) made of teflon between the bottom of the cylinder and the top plate. This table is provided with two holes to act as gas chambers for nitrogen (VII) and oxygen (VIII) respectively.

By appropriate design and careful matching, leakage between gas spaces and outer atmosphere can be minimized. Inlet and outlet ports permit flushing with gas. By turning the table the hemoglobin film can be exposed either to nitrogen or to oxygen. The change from nitrogen to oxygen can thus be achieved virtually as a step function.

The optical system consisting of an optical fiber and a sensing diode is mounted on a swivel arm (IX) (see also picture 1), thus allowing either to spread the hemoglobin layer or to clean the glass plate.
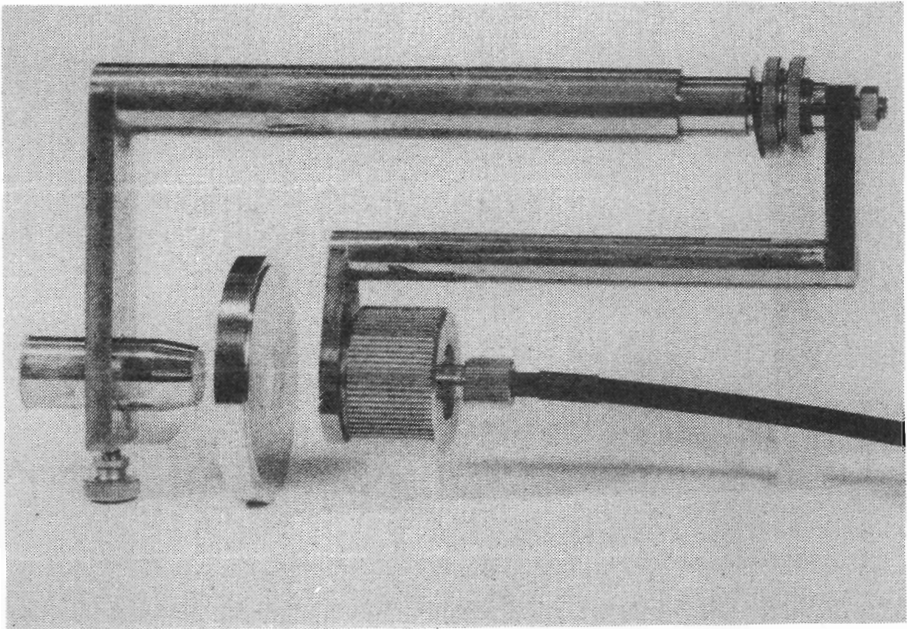
Picture 1. This picture shows the swivel arm on which both the optical fiber and the photocell are mounted, and the step-shaped sample holder. The outline of this picture is shown in fig. 4.2a.

Moreover, an angle-measuring device makes it possible to check the degree of uniformity of the layer thickness. This design provides an identical optical apparatus constant for both the "nitrogen" and "oxygen" situation of the device.

The gas mixtures are prepared from gas tanks, containing 5% CO_2 plus 95% nitrogen or 95% oxygen or air, by means of a gas mixing pump (Wösthoff). The accuracy of the mixing process is within 0.5% as tested
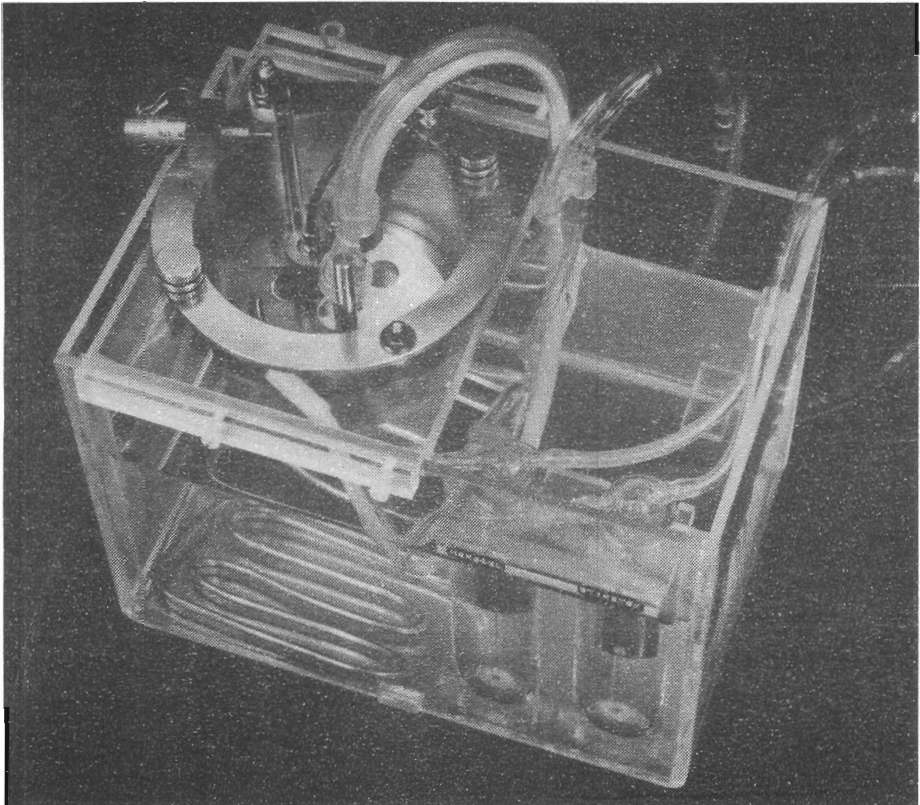
Picture 2. Overall view of the experimental set up. The outline of this picture in figs. 4.2a and 4.2b shows the most important elements of the diffusion apparatus. The housing of the diffusion chamber is immersed in a waterbath which also contains the wash flasks for humidifying the gases. The waterbath is temperature stabilized by a Homef thermostat (not shown in the picture). The gases are conducted from the wash flasks to the appropriate gas chamber through the inner tubes of coaxial tubing. Thermostating of the gas within the inner tube is achieved by pumping thermostated water through the outer tube.

with a gas chromatograph (Dept. of Instrumental Analysis T.H.E.). The gases are humidified by means of wash flasks containing thermostated water. The time needed for changing the PO_2 within the oxygen chamber from 700 to 0 mm Hg by readjusting the setting of the pump amounts to 10 minutes.

By means of a micro syringe (Hamilton) and a glass spatula a small amount of completely deoxygenated hemoglobin solution (between 20 and 50 μl depending on the desired layer thickness) is spread over the glass plate after removing the glass window. Prior to this operation the turntable is rotated over the glass plate in order to position the nitrogen chamber. After fixing the layer the window is replaced. Next the swivel arm is adjusted to direct the light beam to the center of the layer of hemoglobin solution (see also picture 2).

Subsequently the value of I_o is recorded. After a certain lapse of time the teflon turntable is moved to expose the hemoglobin layer to the oxygen-containing gas, whereafter the oxygenation process starts. The course of oxygenation is recorded by the change in the absorption coefficient of hemoglobin. After completion of the oxygenation the value of I_1 is recorded. In case the oxygen partial pressure of the gas is chosen to be $S_1 < 1$, the PO_2 is increased to determine I_1' at $S=1$.

The absorption coefficients at $S = 0$ and $S \approx 1$ are determined by means of the wedge method. The value I_1' has to be known for the calculation of both layer thickness and S_1.

4.1.4 Description of oximeter and accessory electronic equipment

When studying the oxygen uptake by non-moving hemoglobin layers, only one channel of a two-wavelength oximeter is used. Two light-emitting diodes (LED) are used as light sources. The first one has a peak intensity at a wavelength of 670 nm (Monsanto MV/10B) and the other one at 900 nm (Monsanto ME/4). The light intensity of both LED's alternates harmonically. The red one does so at a frequency of 1552 Hz whereas the infrared one operates at 5140 Hz.

The light of the LED's is conducted by fiber optics to pass through the hemoglobin layer, and some of it is received by a light-sensing diode (Monsanto MD 2). The signal generated by the diode is fed into a preamplifier. By appropriate filtering the output is split up into two signals of 5140 Hz and 1552 Hz respectively. Both outputs of the

oximeter consist of a superposition of a DC voltage and an AC voltage.
The DC component is proportional to the intensity of the light received,
the AC component is filtered out by a low-pass filter with a cut-off
frequency of 20 Hz.

In case of performing oxygenation experiments the output signals
(red and infrared) change as a function of time. In the case of a wedge
experiment or determination of uniformity of the thickness of the
hemoglobin layer the signals change as a function of the position of
the light beam.

A digital and analog recording system have been used simultaneously
(see fig. 4.3). The digital recording system uses a HP ten-channel
scanner. The scanner sequentially connects a number of signals to an
analog - digital converter. The digital numbers are punched in paper
tape. The information on paper tape is to be used for computer
calculations. When performing a wedge measurement or when determining
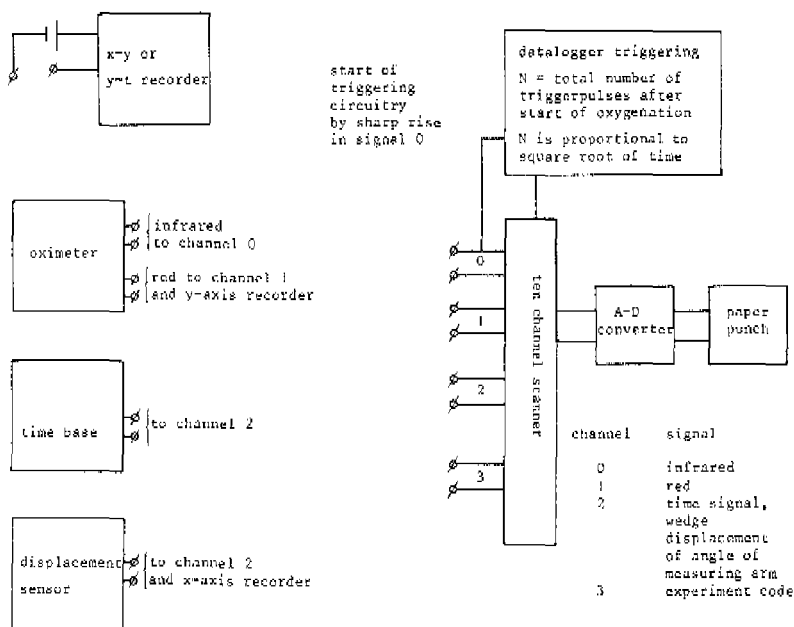
Fig. 4.3. Block diagram of data recording. A detailed description
of the instrumentation is given in section 4.1.4.

the layer uniformity the voltage proportional to the displacement of
the light beam is also connected to the scanner. In case of an
oxygenation experiment a circuit integrating a constant voltage is used
to provide the time base.

The integrator is started by a sharp rise in voltage of the infrared
channel of the oximeter. This corresponds to the moment when the oxygen
chamber in the teflon turntable is turned over the hemoglobin layer,
thus starting the oxygenation process. An electrical circuit to
trigger the data-logging has been designed in order to make the
interval time Δt between two measuring cycles proportional to the square
root of time. As far as the oxygen saturation also changes with the
square root of time, measurements are obtained at points of equal
increase in saturation. Sometimes a fourth channel is used to identify
each measuring cycle by supplying a known voltage to it.

A (x-y) or (y-t) recorder (Houston 2000) is used for the analog
recording of the wedge experiments and oxygenation experiments. From
the output signal of the oximeter connected to the recorder a constant
voltage is subtracted, thus small changes in intensity can be recorded
on full scale.

4.1.5 Preparation and handling of hemoglobin solutions. Description of various measurements

Fresh packed red blood cells (human blood group O^+) are rinsed three
times with saline (9% NaCl) and separated by centrifuging (6,000 g, 10
min). The cells are lyzed osmotically by adding 60 ml of distilled
water to 100 ml of packed cells. The red cell stroma is removed by
adding another 40 ml of toluene (C_6H_8) to the solution. After shaking
the mixture the toluene is separated from the hemoglobin solution by
centrifuging (6,000 g, 20 min). The hemoglobin solution is sucked off
from underneath the toluene ([Hb] between 16 and 19 g%) and poured into
specially designed tonometer bottles.

The tonometer bottles are turning continuously for a couple of hours
while being flushed with a humidified gas mixture of 95% N_2 and 5% CO_2.
The O_2 content of the solutions is checked with a Lex-O_2-Con. As soon
as the O_2 becomes undetectably small (less than 10^{-4} mol/l) the bottles
are pressurized (150 mm Hg), closed and stored at $4^{\circ}C$.

Hemoglobin concentration and percentage of methemoglobin are
determined by a single-beam spectrophotometer using the cyanide method

of Zijlstra and van Kampen and the method according to Evelyn and Malloy respectively, as described by van Assendelft (1970). By following this procedure of preparation and storage the methemoglobin content usually proved to be less than 1 percent of the total hemoglobin concentration.

The hemoglobin solutions are diluted by adding saline. High hemoglobin concentrations are obtained by ultra-filtration (Diaflow, Amicon Co.).

Oxygen binding capacity of the hemoglobin solutions is measured directly by using a Lex-O_2-Con or computed from the hemoglobin concentration. This computation is based on an oxygen binding capacity of 1.36 cc O_2 (STDP) per gram hemoglobin after correction for the presence of methemoglobin. This value was normally found ($\pm$ 1.5%) in experiments where both Hb was determined spectrophotometrically and the oxygen binding capacity was measured with the Lex-O_2-Con. For a further discussion the reader is referred to chapter 5.

4.2 Discussion of several elements of the measuring procedure

4.2.1 Influence of bandwidth of LED's on measurements of absorption

The bandwidth of the LED's is in the order of 40 nm. Particularly for the red emitter this is rather considerable when comparing it to the part of the absorption spectra relevant for the measurements. Within this part of the spectrum the extinction coefficient of hemoglobin changes by a factor of 8, that of deoxyhemoglobin by a factor of 2, and that of oxyhemoglobin by a factor of 0.7. Hence the influence of the bandwidth of the light sources used has to be taken into account.

Let $I_o(\lambda)$ be the intensity distribution function of the emitter and $g(\lambda)$ the sensitivity curve of the light sensor. When applying the law of Lambert-Beer to an infinitesimally small part $\Delta\lambda$ of the emission spectrum the current generated by the sensor can be described by

$$ i = \int_{\lambda=0}^{\lambda=\infty} g(\lambda) \ I_o(\lambda) e^{-\epsilon(\lambda)cd} \ d\lambda \qquad (4.7) $$

An approximation of the solution of eq. 4.7 can be obtained by introducing a function $\delta(\lambda)$ defined by the relationship

$$ \epsilon(\lambda) = \epsilon^* + \delta(\lambda) \qquad (4.8) $$

where ϵ^* is a constant of arbitrary value. Substitution of eq. 4.8 into eq. 4.7 results in

$$i = e^{-\varepsilon^* cd} \int_{\lambda=-\infty}^{\lambda=\infty} g(\lambda) \, I_o(\lambda) \, e^{-\delta(\lambda)cd} \, d\lambda \qquad (4.9)$$

Series expansion of the exponent in eq. 4.9 provides

$$i = e^{-\varepsilon^* cd} \int_{\lambda=-\infty}^{\lambda=\infty} g(\lambda) \, I_o(\lambda) d\lambda - \varepsilon^* cd \int_{\lambda=-\infty}^{\lambda=\infty} g(\lambda) \, I_o(\lambda) \, \frac{\delta(\lambda)}{\varepsilon^*} \, d\lambda$$

$$(4.10)$$

For small values of $\varepsilon^* cd$ eq. 4.8 can be approximated by

$$\frac{i}{i_o} = e^{-\varepsilon^* cd} \qquad (4.11)$$

where $i_o = \int_{\lambda=-\infty}^{\lambda=\infty} g(\lambda) \, I_o(\lambda) \, d\lambda$ is the "blank value" of the system.

In the red light $\delta(\lambda)$ is an even function of λ for most kinds of hemoglobin, and a value of ε^* may be chosen to make the first-order expansion term in eq. 4.10 equal to zero. Hence the law of Lambert-Beer may still be applied when introducing an adapted extinction coefficient (ε^*) which may differ essentially from the extinction coefficient at the peak wavelength of the emission spectrum. It may easily be seen that if different light-absorbing species are present in the solution the summation rule of absorbing species, thus in fact eq. 4.1, remains valid when using the adapted extinction coefficient.

Using the wedge method to calibrate the hemoglobin solution with respect to the $\varepsilon_1 b$ and $\varepsilon_o b$ values, the validity of relationship 4.11 has been shown to hold in the region of layer thicknesses as used in the oxygenation experiments. The summation rule has been tested by comparing the oxygen saturation as measured by the wedge method with measurements of the oxygen content of the same samples by the Lex-O_2-Con. Results are shown in fig. 4.4.

The value of ε^* depends on the bandwidth of the emission spectrum and, in turn, this bandwidth depends on the temperature of the LED. The dependency of ε^* on temperature at $\lambda = 670$ nm appeared to be 0.2% per
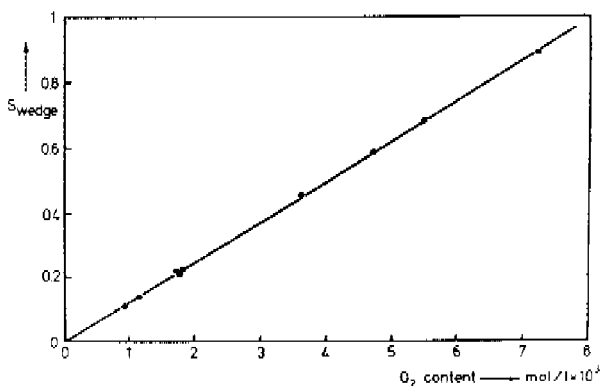
Fig. 4.4. Oxygen saturation as measured by the wedge method compared with the oxygen content of the same samples as determined by the Lex-O_2-Con. The hemoglobin concentration of the solution used is approximately 15 g%. The correlation between the two methods is within the experimental errors of both methods.

degree centigrade . For the elimination of this effect temperature stabilization to within 0.2°C at a level of 30°C has been provided.

4.2.2 Discussion of precautions taken with regard to the stability of the hemoglobin layer

According to the experimental model chosen, the geometry of the hemoglobin layer, at least at the point of incidence of the light beam, has to remain unchanged throughout the course of oxygenation. Apart from qualitative visual observation the behavior of the hemoglobin layer with time can only be judged quantitatively by means of light absorption recordings. Since the light absorption at S=0 is ten times larger than at S=1, the stability of the hemoglobin layer has to be checked when the diffusion chamber is flushed with nitrogen.

Changes in light absorption may be caused by several factors:
1) The hemoglobin layer has not been spread anaerobically so that the layer may have a small initial saturation. Due to this the light intensity recording shows a downward drift.
2) The nitrogen flow is not sufficient to compensate for oxygen leakage through the sealing into the chambers. The light intensity recording shows an upward drift.

3) The glass plate has not been leveled sufficiently which results in a
   convective flux due to gravity, commonly resulting in an upward drift.
4) The nitrogen flow is too high and disturbs the layer surface. This
   sometimes results in a stable though erroneous signal but also may
   cause a drift of the signal.
5) The layer is drying. This only results in a signal change if the
   drying process is not uniform all over the layer. This is due to the
   fact that the light absorption is proportional to the product of
   hemoglobin concentration and layer thickness.

This product remains essentially constant when the evaporation process
proceeds uniformly in a layer of uniform thickness. However, as a rule
the layer dries faster at the edges than it does in the center. Hence
differences of total hemoglobin concentration may occur within the layer
resulting in a convective flux of water. In this case the signal may
show a drift as a result of the drying effect. The drying effect is more
marked at high hemoglobin concentrations.

   By trial and error an experimental technique has been developed which
eliminates these possible sources of error. In this context the anaerobic
technique of spreading the hemoglobin layer is not only favourable as far
as it reduces the measuring time but is indispensable for permitting the
study of effects of changing sample geometry.

   When performing preliminary experiments the oxygenation process was
investigated using a film of hemoglobin solution not being attached to
the edges of the glass plate (fig. 4.5a). This system had been chosen
for its simplicity in making layers of different thicknesses. However,
the requirements in leveling the sample plate appeared to be too severe.
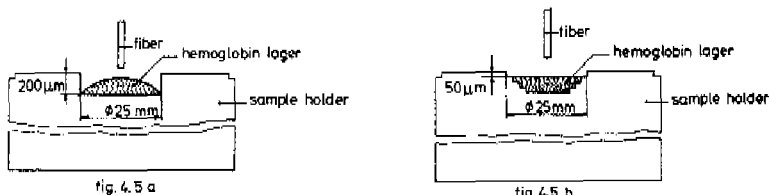
fig. 4.5 a   fig. 4.5 b

*Fig. 4.5a. Outline of the sample holder as used during the earlier
investigations. A hemoglobin layer is spread over the bottom of
this sample holder, not touching the edges of the well.
Fig. 4.5b. Outline of the sample holder as used in the final
experiments. The sample holder is provided with a step-shaped
well. The hemoglobin layer attaches to one of the well edges.*

Sample holders as designed later (fig. 4.5b and picture 1) are provided with a step-shaped well so that the hemoglobin layer can be attached to one of the well edges. When using this particular geometry of the sample plate it is still simple to obtain a different layer thickness but the leveling is much less critical. A tilting angle of up to 0.7 degrees does not affect the stability of the signal.

Although the oxygen uptake of the hemoglobin layer is minor compared to the total volume of the diffusion chamber, maintenance of flow is required to compensate for loss of gas due to leakage. The minimum adjustment of the gas flow was determined using the following procedure.

The nitrogen flow is stopped and the hemoglobin layer is allowed to take up some oxygen from the air leaked in. After having achieved an average saturation of 5% the nitrogen flux is reestablished to decrease the saturation again. According to the saturation curve this decrease is only possible if the PO_2 in the gaseous atmosphere over the hemoglobin layer does not exceed 2 mm Hg.

The lower limit of gas flow thus determined is 0.4 cc N_2/sec. The upper limit for the gas flow through the diffusion chamber should be 5 cc N_2/sec in order to avoid disturbance of the layer. Actually the nitrogen flow before starting the oxygenation process is chosen to be 2 cc N_2/sec and the gas flow during and after oxygenation is adjusted to 0.4 cc/sec.

Under these conditions of gas flow the measuring signals before and after oxygenation remain stable during a time longer than needed for even the longest oxygenation processes studied (30 min). When cleaning the sample plate after an oxygenation experiment, drying of the layer is not observed. Finally the experimental results prove to be independent of the time the layer had been exposed to the humidified nitrogen flow.

4.2.3 Time constants of the change in gas conditions and absorption measurements

The application of the theoretical models to the experimental results requires a sharp rise in oxygen partial pressure. The resulting sharp change in light absorption has to be recorded adequately. Therefore the transient behavior of the system in terms of time constants is important and requires some discussion.

As explained before, the step-like change is achieved by a teflon turntable . The time necessary to switch the oxygen chamber over the hemoglobin layer amounts to 0.04 sec. The dead space of the diffusing chamber inherent to the design of the device is about 0.06 cc. The total volume of the diffusing chamber is about 4 cc. Thus roughly 98.5% of the step is effected within 0.04 sec. The time constant of the remaining 1.5% is 10 sec when using a gas flow of 0.4 cc/sec. The time constant of the oximeter is mainly determined by the low-pass filters and amounts to 0.07 sec.

The most rapid oxygenation process studied was completed within 60 sec. Thus the time constants are sufficiently small for an accurate determination of t_1. The influence of the time constants on the recording of the course of oxygenation will be discussed in section 4.3.

4.3 Range of applicability of the instrumentation

4.3.1 Limitations due to experimental errors in the measurements of light absorption

The change in light absorption of a hemoglobin layer due to oxygenation depends on both the hemoglobin concentration and the layer thickness.

The oximeter is sensitive enough to detect a change of 0.075% in light absorption. Eq. 4.1 directly relates the absolute error ΔS in the measurement of oxygen saturation to both the error in light absorption measurement and the product $(\varepsilon_1 - \varepsilon_o)$ bd. Using a value of 0.394 1/cm/g% for $(\varepsilon_1 - \varepsilon_o)$ (see section 5.5.2) one finds that the lower limit of the product bd is $0.0019/\Delta S$ cm g%. Thus, if an absolute error $S = 0.01$ is aimed at and the minimum layer thickness applied is 100 μm, the hemoglobin concentration has to be more than 20 g%. With an error ΔS of 0.01 to 0.02 the lower limit of the hemoglobin concentration is 10 g% when applying a layer thickness ranging between 100 and 200 μm, whereas, when applying a thickness ranging between 200 and 400 μm, the lower limit of the concentration is 5 g%.

4.3.2 Limitations due to the error in determining the start of the oxygenation process

The high accuracy of the oximeter is partly due to the time constant (0.085 s) of the low-pass filter causing a delay in the start of the recording of the oxygenation process. Nevertheless, from the standpoint of measuring the course of oxygenation, this property of the instrument

introduces an experimental error. Another error in determining the start
of the oxygenation process is due to the time needed to rotate the teflon
turntable. The recording of the oxygenation starts as soon as the optical
system has returned to its operational position. However, the oxygenation
of the layer may have started slightly earlier because of the oxygen
trapped in the narrow gap between turntable and cylinder bottom. An
additional small error is due to some electrical noise on the signal of
the time base.

Assuming that all possible initial errors only contribute to an
uncertainty τ in the start of the oxygenation process one may write
according to the half-infinite layer model

$$S_m = \sqrt{\frac{t + \tau}{t_1}} = \sqrt{S_r^2 + \frac{\tau}{t_1}} \qquad (4.12)$$

where t = the actual lapse of time from the start of oxygenation,

τ = the uncertainty in the start of oxygenation,

t_1 = the actual oxygenation time,

S_m = the oxygen saturation determined at the apparent time $(t + \tau)$,

S_r = the oxygen saturation at the actual time t.

From eq. 4.12 it follows that

$$\frac{\tau}{t_1} = (S_m - S_r)(S_m + S_r) \qquad (4.13)$$

Requiring arbitrarily that at $S_r = 0.05$ the difference $(S_m - S_r)$ has to be
less than 0.01 the ratio $|\tau/t_1|$ must be smaller than 0.001. Since the
uncertainty τ is in the order of 0.05 s (somewhat less than the time
constant of the low-pass filters) the oxygenation time in the experiments
should not be less than 50 s. In practice this was so in most cases.

CHAPTER 5

REPORT ON THE EXPERIMENTAL INVESTIGATIONS AND DATA PROCESSING

5.1 Introduction to the experiments

The experiments may be classed into three groups according to the growing experimental skill and the development of the equipment. In the preliminary phase of the work (first group of experiments) the experimental set-up was not quite the same as described in chapter 4. The anaerobic technique was already used, but the teflon turntable was not yet available. The change in the gas atmosphere from nitrogen to oxygen was obtained by means of a three-way stopcock in the gas lead to the diffusion chamber. Only two different oxygen pressures where applied, i.e., $P_1 = 720$ and 120 mm Hg respectively. The hemoglobin solutions used in these preliminary experiments contained between 2 and 20% of methemoglobin, a rather large amount. As could be shown, the formation of methemoglobin was due to the non-anaerobic storage of the solutions and also to the contact with toluene for hours. The tendency to oxidation appeared to be stronger at high hemoglobin concentration than at low hemoglobin concentration. From an experimental point of view the presence of a high percentage of methemoglobin is not favorable since the absorption spectrum of methemoglobin depends on pH which is changing during oxygenation (see section 2.1) of the hemoglobin layer. The preliminary results of these diffusion measurements have been published previously (Spaan et al. 1974) and will not be discussed here (see section 6.2.1).

The experimental set-up used in both the earlier experiments (second group) and the final experiments (third group) is described in chapter 4. In the second group a flat glass plate was used as a sample holder (see fig. 4.5) and moreover the digital recording of the oximeter output was less accurate than in the final experiments. For this reason some oxygenation times were directly derived from the analog recordings. This second group of experiments still had the character of trial and error, and in fact the experimental technique was established during this experimental phase. Consequently the results of these earlier diffusion measurements show more scatter than those of the final group. As discussed in section 4.2.2 the experiments in the final (third) phase were performed using the sample holder provided with a step-like

well. By then the experimental technique was well established. This final group of experiments proved to be superior to the earlier group in terms of reproducibility. Hence, in the present chapter main attention will be paid to the experiments of this final phase, but the results of the second phase will also be mentioned. The results of the second phase confirm the conclusions from the experiments of the final phase although the values of oxygen permeability αD_C and D_H estimated from the former show a large scatter.

5.2 The experimentally determined course of oxygenation

The experimental method to measure the course of oxygenation in a completely deoxygenated layer of hemoglobin after a sudden change in oxygen partial pressure at the gas-liquid interface is described in sections 4.1.1 to 4.1.3. The data recording system was outlined in section 4.1.4.

Fig. 5.1 shows a computer plot obtained from the digital recording of a final series of oxygenation experiments performed with a hemoglobin solution of 29 g%. Both the layer thicknesses and the P_1 values applied are given in the figure. The values used for the extinctions of the deoxygenated and oxygenated hemoglobin solution will be discussed in section 5.2.1. The increase in fractional saturation is plotted on the ordinate whereas the square root of t/d^2 is plotted on the abscissa.

Fig. 5.1. Computer plot of the experimentally determined course of oxygenation as a function of the square root of normalized time $t_n (= t/d^2)$. $[Hb] = 29$ g%, $(\varepsilon_1 - \varepsilon_0) = 0.394$ $1/cm/g$%Hb, P_1 varies between 700 and 35 mm Hg. The straight lines in the figure were obtained by linear regression analysis on the linear part of the experimental curves (see section 3.5.2). The layer thickness and the P_1 value applied in each individual experiment are given in the table of the figure.

SATURATIE (SRD)

1.1
1
.9
.8
.7
.6
.5
.4
.3
.2
.1
0

$\sqrt{\dfrac{t}{d^2}}$ → s$^{1/2}$/cm

0   250   500   750   1000   1250   1500   1750   2000   2250   2500

1   2   3   4   5   6   7

curves	P_1 mm Hg	symbol	d µm
1	700	+ × ⊙	117 50 123
2	420	□ ◇	181 129
3	280	△ ▽	84 122
4	210	• ×	74 87
5	140	○ □	170 124
6	70	◇ △	124 125
7	35	▽ •	93 119

SQRT(T/(O×D))   9.E. 26-4-1976

18

Each point is defined by the simultaneously measured values of ψ and t/d^2. The points for different experiments at equal values of P_1 are characterized by different symbols. The straight lines in fig. 5.1 are obtained by linear regression analysis on data points from any one oxygenation experiment in the saturation range where the half-infinite model is assumed to be applicable. The determination of this range will be defined in section 5.3.2. Below we will refer to t/d^2 as the normalized time, t_n, so that

$$ t_n = t/d^2 \tag{5.1} $$

Obviously this normalized time is proportional to the dimensionless time t^* ($t^* = t \, D_O/d^2$).

A first glance at the results presented in fig. 5.1 confirms the basic assumptions and conclusions of both the finite layer model and the half-infinite layer model:

1) The curves measured at equal values of P_1 coincide when t/d^2 is used as an independent variable. This supports the assumption of chemical equilibrium (the difference between the curves measured at $P_1 = 280$ and at 210 mm Hg are due to oxygen leakage into the sample syringe).

2) The saturation increase is, up to a high degree of oxygenation, proportional to the square root of time as predicted by the half-infinite layer model.

3) The deviation of the oxygenation process from that predicted by the half-infinite layer model occurs at lower values of ψ if lower values of P_1 are used. At $P_1 = 700$ mm Hg, the oxygenation process is terminated abruptly, thus giving evidence of a sharp oxygenation front within the hemoglobin layer.

In chapter 3 the normalized oxygenation time ($t_{n,1} = t_1/d^2$) has been chosen to be the quantity characterizing the oxygenation process of a hemoglobin layer. This normalized oxygenation time can be calculated from the slope of the linear range of the ψ versus $\sqrt{t_n}$ curves according to

$$ \overline{\psi} = \sqrt{\frac{t_n}{t_{n,1}}} \tag{5.2} $$

The determination of normalized oxygenation times will be discussed in section 5.3.

5.3 The determination of normalized oxygenation time

5.3.1 Principle of determination of normalized oxygenation times

As mentioned in section 5.2 the normalized oxygenation time can be calculated from the slope of the curves of $\bar{\psi}$ versus $\sqrt{t}$ according to eq. 5.2. By means of eq. 4.5 for $S_1 = 1$ (as is the case for $P_1 > 100$ mm Hg; see fig. 5.6) eq. 5.2 changes to

$$\bar{\psi} = \sqrt{\left\{ \frac{t(\varepsilon_1 b - \varepsilon_o b)^2}{(\log(I_1/I_o))^2} \right\}} \frac{1}{\sqrt{t_{n,1}}} \tag{5.3}$$

This can be expressed in terms of the measured quantity $I(t)$ by using eqs. 4.4 and 5.3, which leads to

$$\log I(t) - \log I_o = \frac{\sqrt{t}}{\sqrt{t_{n,1}}} (\varepsilon_1 b - \varepsilon_o b) \tag{5.4}$$

where t = actual lapse of time from the start of the experiment. Consequently, the normalized oxygenation time can be determined from the slope of the $\log I(t)$ versus $\sqrt{t}$ curve without knowing the value of either I_o or I_1, the latter being eliminated when passing from eq. 5.2 to eq. 5.4.

5.3.2 Procedure followed in determining the normalized oxygenation time

From each oxygenation experiment a computer plot analogous to fig. 5.1 was made in terms of ψ versus $\sqrt{t/(\log(I_1/I_o))^2}$. From these plots it was judged by eye as to which degree of oxygenation this relationship is linear. Data points above this limit were not considered in determining the value of $t_{n,1}$. When the range of linearity appeared to exist only for $\psi < 0.6$ the experiment was discarded. Usually a number (between 1 and 4) of initial data were not considered either when they clearly deviated from the linear part of the curve as discussed in section 4.3.2. Moreover, now and then an individual point was not used in further analysis when it was obviously far from coinciding with the oxygenation curve which might be due to disturbances in the mains. On the remaining data a regression analysis was performed using the method of least squares according to

$$\overline{\psi} = x_2 + x_1 \sqrt{\left\{ \frac{t}{(\log(I_1/I_o))^2} \right\}} \tag{5.5}$$

where x_1 and x_2 are parameters to be estimated. The parameter x_1 is clearly of physical origin whereas x_2 introduces a degree of freedom to account for uncertainties in the experimental conditions. Comparison of eqs. 5.5 and 5.4 shows that

$$t_{n,1} = \frac{(\varepsilon_1 b - \varepsilon_o b)^2}{x_1^2} \tag{5.6}$$

Essentially the value of x_2 has to be zero. Exceptionally x_2 may have a small value due to, for instance, a small change in the apparatus constant $\log I_a$, as sometimes occurs when interchanging the gas chambers.

5.3.3 Discussion of the measured normalized oxygenation times

As has been explained in the introduction to this chapter (section 5.1), the results of two groups of experiments will be reported, referred to as earlier and final experiments respectively. As a rule the oxygenation experiments using one single hemoglobin concentration were performed in series of 10 to 15 runs. The P_1 values ranged between 700 and 140 mm Hg.

The final experiments were performed in four complete experimental series of 50 single oxygenation experiments in total and two incomplete series. As will be shown in section 5.4, the diffusion coefficient of hemoglobin D_H and the oxygen permeability αD_c may be estimated from a complete series. From an incomplete series either of these two quantities may be estimated assuming a fixed value of the other one.

Normalized oxygenation times as a function of reciprocal boundary PO_2 $(1/P_1)$ in three different final experimental runs are presented in fig. 5.2. The values used for $(\varepsilon_1 b - \varepsilon_o b)$ will be discussed in section 5.5. The solid lines in fig. 5.2 were obtained by fitting eq. 3.24 to the experimental results (see section 5.4). The figure next to each point refers to the thickness of the corresponding hemoglobin layer. The convex shape of the experimental curve clearly shows the presence of hemoglobin-mediated oxygen transfer within the hemoglobin solution. This phenomenon will be discussed quantitatively in section 5.4.1.
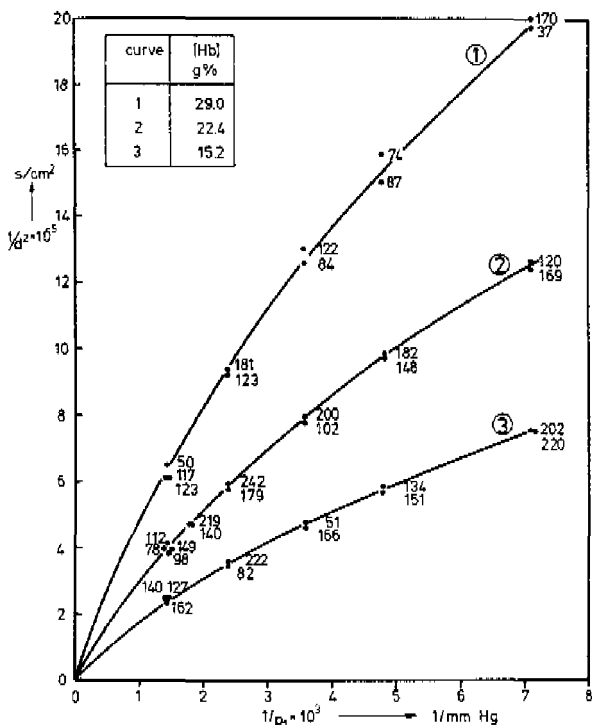
Fig. 5.2. *Experimentally determined normalized oxygenation time*
$t_{n,1} = \sqrt{t_1/d^2}$ *versus reciprocal boundary oxygen pressure* $(1/P_1)$.
The results of three final experimental series were obtained with
hemoglobin concentrations of 15.2, 22.4, and 29 g%. The number next
to each point represents the respective layer thickness. The curves
were obtained by fitting the polygonal model to the experimental
data on the basis of the method of least squares by varying the
parameters αD_C *and* D_H. *The parameter values found and the*
"95% confidence limit" for each experimental series are as follows:

[Hb] g%	$\alpha D_C \ 10^{11}$ $\dfrac{mol \ cm^2}{s \ l \ mm \ Hg}$	$D_H \ 10^7$ cm^2/s
15.2	2.38 ± 3.2%	4.51 ± 5.3%
22.4	2.04 ± 3.5%	2.73 ± 6.2%
29.0	1.64 ± 2 %	1.75 ± 8.6%

In the final experiments the values for $|x_2|$ were always less than 0.01 (except in 3 experiments), so obviously the apparatus constant log I_a (see section 4.1.1) remains virtually constant. Linear variance analysis resulted in a 95% confidence limit of x_1 of less than 0.01 x_1. Hence the linear relationship between ψ and $\sqrt{t}$ is confirmed (fig. 5.1). An estimate of the reproducibility of the experiments may be obtained from fig. 5.2. With the exception of 4 normalized oxygenation times at $|Hb|$ =29 g%,the reproducibility of the experimental results is better than 4%. The exceptions are due to oxygen leakage into the sample syringe as stated before. Using the Lex-O_2-Con this could be proven to be the cause when checking the remaining solution within the syringe after spreading the hemoglobin layers. No systematical difference could be observed as an effect of the layer thickness of each individual experiment though this thickness ranged between 50 and 220 μm.

The earlier experiments were performed in 10 complete series including a total of approximately 120 single oxygenation experiments. As stated in section 5.1 this earlier experimental phase had the character of trial and error, and several series could not be used for further analysis because of too much scatter (more than 20%) in the oxygenation times obtained. From some of the remaining complete series a small number (never more than 4) of single oxygenation experiments were excluded from analysis because the 95% confidence limit of x_1 was more than 4% or the drift in the signals I_0 and I_1 exceeded an equivalent value of 1% oxygen saturation change per minute. The reproducibility of the earlier measurements appeared to be between 5 and 10%, thus being roughly two to three times poorer than that of the final experiments.

The dimensionless oxygenation times obtained from both the earlier and final experiments will be considered to be independent measurements for the estimation of the oxygen permeability and diffusion coefficient of hemoglobin. A poor reproducibility of the normalized oxygenation times will find its expression in wide confidence limits of the parameter values estimated from them.

5.4 Parameter estimation from the experimental normalized oxygenation times

5.4.1 Estimated values of oxygen permeability, hemoglobin diffusion coefficient and related quantities

The experimental data of normalized oxygenation time versus reciprocal

boundary oxygen pressure (fig.5.2) were fitted to eq. 3.24 by using the polygonal approximation. The parameters to be estimated are αD_C and D_H. For $(\varepsilon_1 - \varepsilon_0)$ a value of 0.394 1cm/g% Hb, for P_c a value of 26 mm Hg,
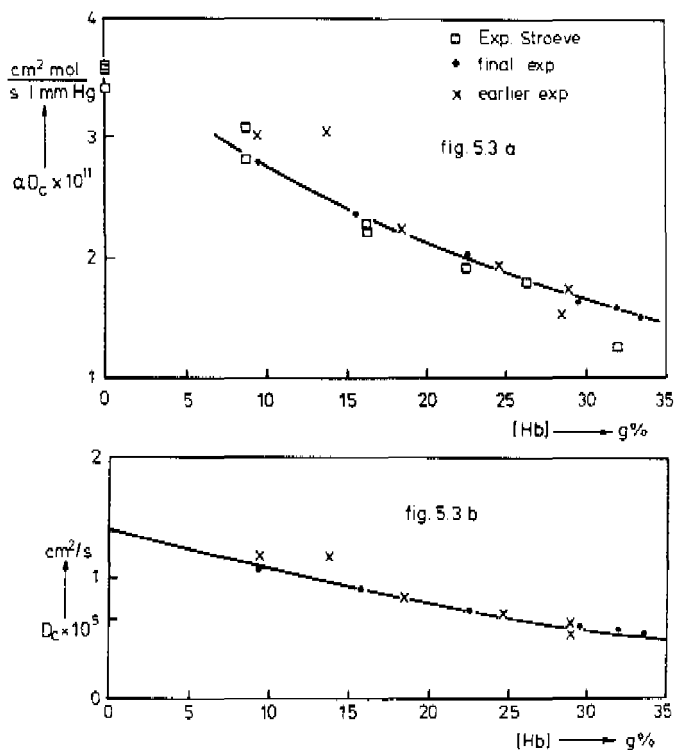
Fig. 5.3a. Values found for the permeability of oxygen αD_C as a function of hemoglobin concentration. The dots correspond to the final experiments, the crosses to the earlier experiments, and the open squares to the experimental data of Stroeve (1973). The final experiments have an accuracy of the order of 3%, the earlier experiments of the order of 8%. Fig. 5.3b. The diffusion coefficients of oxygen calculated from the experimentally found permeability by using values for the solubility as discussed in section 6.3, compared with the compromise curve suggested by Kreuzer (1970) for the values of D_C found in the literature (see section 6.4). The dots refer to the final experiments, the crosses to the earlier experiments. Temperature is 25 $^{\circ}C$.

and for h a value calculated from the hemoglobin concentration corrected for methemoglobin were used. These values will be discussed in section 5.5.

Fitting of theory to experiments was performed by using the criterion of least squares. Three results of this procedure were shown in fig. 5.2 above. Linear variance analysis was applied to get some idea of the reliability of the estimated parameters. This reliability will be given in terms of a confidence limit, in spite of the fact that the estimations of parameters are not expected to be normally distributed.

A whole experimental series includes 10 to 15 individual oxygenation experiments. This 95% confidence limit for αD_C is 3%, whereas for D_H it is 7% when estimated from the final experiments. The earlier
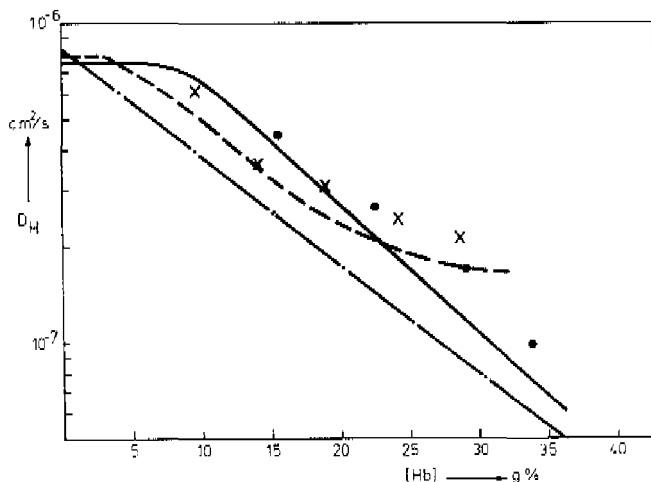
Fig. 5.4. Values found for the diffusion coefficient of hemoglobin D_H as a function of hemoglobin concentration. The dots refer to the final experiments, the crosses to the earlier experiments. The final experiments have an accuracy of the order of 8%, the earlier experiments of the order of 15%. Temperature is 25 °C.

—·—·— compromise curve of Kreuzer (1970),

— — — — experimental results of Keller et al. (1971),

——————— experimental results of Riveros-Moreno and
　　　　　Wittenberg (1972).

For a discussion of the published data of the diffusion coefficient of hemoglobin see section 6.5.

experiments, performed in the second stage, are less reliable as was discussed in sections 5.1 and 5.3. Variance analysis in this case shows 95% confidence limits of 6 – 10% for αD_C and approximately 15% for D_H.

Results for αD_C are shown in fig. 5.3 and are compared with results of Stroeve (1973). The dots refer to the final experiments, the crosses to the earlier experiments, and the squares to the experiments of Stroeve. Stroeve performed his experiments by measuring the oxygen flux through layers of methemoglobin solution at steady state. The agreement between these results obtained by two different techniques is quite satisfactory.

The estimated values of D_H are presented in fig. 5.4. D_H values as a function of $[Hb]$ as published by Keller et al. (1971) and Riveros-Moreno and Wittenberg (1972)(the latter after correction for temperature) are also presented. The present results will be compared with those of other studies in more detail in section 6.5.
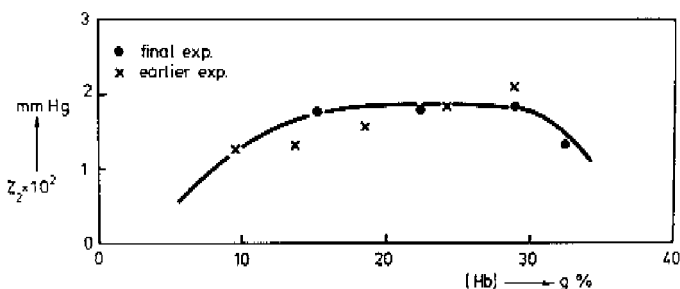
Fig. 5.5. Experimental values of $Z_2 = h\, D_H/\alpha D_C$ as a function of hemoglobin concentration. Z_2 is virtually constant in the range of $[Hb]$ from 15 to 29 g%. Outside this range the values of Z_2 decreases.

Fig. 5.5 shows the estimated values for $Z_2 = h\, D_H/\alpha D_C$ as a function of hemoglobin concentration. It can be shown that the confidence limit for Z_2 equals the confidence limit for D_H. Z_2, and hence the relative influence of facilitation at a fixed value of P_I proves to be virtually independent of hemoglobin concentration over a wide range of hemoglobin concentration.

5.4.2 Influence of errors in measurement of extinction on estimated parameter values

The difference in extinction between oxyhemoglobin and deoxyhemoglobin

is an important quantity in determining the normalized oxygenation time $t_{n,1}$. The value used will be discussed in section 5.5. Here only the influence of errors in the experimental data will be analyzed. The influence of a systematical error may be readily seen from eq. 5.8 as derived from eqs. 3.24 and 4.5

$$\frac{t}{(\log (I_1/I_o))^2} = f_1 \quad f_2 \quad (Z_2, \frac{1}{P_1}) \quad \frac{Z_1}{(\varepsilon_1 b - \varepsilon_o b)^2} \quad \frac{1}{P_1} \qquad (5.8)$$

The left-hand term of eq. 5.8 is independent of the values chosen for the extinctions. When fitting the experiments in terms of $t/(\log (I_1/I_o))^2$ versus $1/P_1$, the quantities Z_2 and $Z_1/(\varepsilon_1 b - \varepsilon_o b)^2$ are the main parameters to be estimated. Whereas the value of Z_1 is affected by an error in the extinction coefficients, the value of Z_2 is not. Consequently the estimated values of both αD_C and D_H are influenced but their ratio is not.

5.4.3 <u>Influence of the position of the saturation curve on estimated parameter values</u>

As discussed in chapter 3 the saturation curve has not to be known very precisely. However it is not easy to assess directly to what extent

P_c mm Hg	[Hb] = 22.4 g%		[Hb] = 15.2 g%	
	$\alpha D_C \ 10^{11}$ $\frac{cm^2 \ mol}{s \ l \ mm \ Hg}$	$D_H \ 10^7$ cm^2/s	$\alpha D_C \ 10^{11}$ $\frac{cm^2 \ mol}{s \ l \ mm \ Hg}$	$D_H \ 10^7$ cm^2/s
1	$2.08 \pm 3.4\%$	$2.43 \pm 6.9\%$	$2.40 \pm 3.3\%$	$3.99 \pm 6.5\%$
26	$2.05 \pm 3.5\%$	$2.73 \pm 6.2\%$	$2.35 \pm 3.2\%$	$4.51 \pm 5.3\%$
80	$1.98 \pm 3.4\%$	$3.47 \pm 4.3\%$	$2.27 \pm 2.7\%$	$5.79 \pm 3.4\%$

Table 5.1. Influence of an error in the position of the adopted saturation curve on the estimated values of αD_C and D_H. The value of 26 mm Hg for P_c used in the polygonal approximation is estimated from the saturation curve measurements shown in fig. 5.6. Obviously the position of the saturation curve is more important for the estimation of D_H than for the estimation of αD_C. The accuracies given in the table correspond to the 95% confidence limits for the estimated parameter values.

a shift of the saturation curve affects the estimated parameter values.
To study this effect a parameter analysis was performed on two
experimental series using different values of P_c. The results are shown
in table 5.1. The values obtained for the different P_c values deviate
considerably. In practice, however, P_{50} of the saturation curve and so
P_c are known within 20% (see section 5.5). This results in an uncertainty
of at most 2% in the estimated parameter values.

5.5 Values of constants used for the estimation of parameter values
from the experiments

5.5.1 Oxygen binding capacity

It was intended to directly determine the oxygen binding capacity of
each individual hemoglobin solution used. For this a Lex-O_2-Con apparatus
was available. Although the reproducibility of this instrument and its
linearity over a wide range of oxygen concentrations $(0 - 2 \ 10^{-2} \ \text{mol/l})$
appeared to be quite adequate (within $10^{-4} \ \text{mol/l}$) for hemoglobin
solutions, the calibration on atmospheric air, according to the
instructions, was often troublesome. These difficulties are mainly caused
by the poor gas-tightness of the sample syringe after using it for some
time. For this reason it was decided to routinely calculate the oxygen
binding capacity from the hemoglobin concentration. This procedure,
however, calls for some discussion.

Based on its molecular weight $(M = 64,500)$, the oxygen binding
capacity of hemoglobin should be $6.2 \ 10^{-5} \ \text{mol/g Hb}$ $(1.39 \ \text{cc } O_2\text{/g Hb})$.
However, the oxygen binding capacity of a hemoglobin solution (and blood)
may be affected by oxidation of Fe^{2+} in the hemes or by occupation by
other ligands (section 2.2). Hence it may be understood that Hüfner (1894)
(section 1.1) found a value of only $1.34 \ \text{cc } O_2\text{/g Hb}$ for the oxygen binding
capacity of whole blood. In order to estimate the oxygen binding capacity
of the hemoglobin solutions prepared according to the procedure described
in section 4.1.5, five independently prepared hemoglobin solutions were
carefully analyzed, using the Lex-O_2-Con for the determination of the
total oxygen concentration (chemically bound and physically dissolved)
and a spectrophotometer for the determination of total hemoglobin
concentration and of fraction of methemoglobin. In all these cases the
oxygen binding capacity was found to be $1 - 4\%$ less than the value
calculated from the hemoglobin concentration (corrected for the fraction

of methemoglobin present) as measured by a spectrophotometer (see
section 4.1.5). Recently very accurate measurements of the oxygen
binding capacity of hemoglobin were performed by Dijkhuizen et al.
(1975) which also showed an oxygen binding capacity lower than predicted
from the concentration of the supposedly active hemoglobin. It was
decided to use, in the present calculations, a binding capacity of
$6.07 \cdot 10^{-5}$ $(1-S_{Hi})$ mol O_2/g Hb, where S_{Hi} is the fraction of methemoglobin
present. This figure was checked to be accurate to within $\pm$ 1.5%.

The presence of HbCO has been neglected throughout these experiments.
Once a solution was checked spectrophotometrically (as described by van
Assendelft 1970) for HbCO which appeared to be present in an amount of
less than 0.5%. Another indication that the HbCO fraction was always
very minor is obtained from a comparison of oxygen binding capacity as
measured by the Lex-O_2-Con with the value as calculated from the
hemoglobin concentration. This low HbCO concentration is plausible since
during deoxygenation of the hemoglobin solution by flushing the tonometer
bottles with nitrogen some CO is also removed.

5.5.2 The difference in extinctions of oxygenated and deoxygenated hemoglobin solution

In order to calculate for an oxygenation experiment the thickness of
the hemoglobin layer and the normalized oxygenation time the difference
between the extinctions of oxyhemoglobin and deoxyhemoglobin has to be
known. This difference $(\varepsilon_o-\varepsilon_1)$ was calculated for each individual
hemoglobin solution from ε_{HbO2} and ε_{Hb}, the extinctions of pure
oxyhemoglobin and deoxyhemoglobin respectively, and the fraction of
methemoglobin present (note that the "extinction" refers to the "adapted
extinction" as defined for the red channel of the oximeter used; see
section 4.2.1).

As mentioned in section 5.1 the extinction of methemoglobin depends
on the pH of the hemoglobin solution and consequently on the degree of
oxygenation. For the extinctions ε_1 and ε_o we may write in analogy to
eqs. 4.2 and 4.3

$$\varepsilon_1 = \varepsilon_{HbO_2} (1-S_{Hi}) + \varepsilon_{Hi,1} S_{Hi} \qquad (5.9)$$

$$\varepsilon_o = \varepsilon_{Hb} (1-S_{Hi}) + \varepsilon_{Hi,0} S_{Hi} \qquad (5.10)$$

where $\varepsilon_{Hi,1}$ and $\varepsilon_{Hi,0}$ are the extinctions of methemoglobin of the

oxygenated and deoxygenated hemoglobin solution respectively. Eqs. 5.9
and 5.10 lead to

$$\frac{\varepsilon_o - \varepsilon_1}{\varepsilon_{Hb} - \varepsilon_{HbO_2}} = (1-S_{Hi}) + \frac{(\varepsilon_{Hi,0} - \varepsilon_{Hi,1})}{(\varepsilon_{Hb} - \varepsilon_{HbO_2})} \, S_{Hi} \qquad (5.11)$$

The extinction of methemoglobin is of the same order of magnitude as
$(\varepsilon_{Hb} - \varepsilon_{HbO_2})$ and varies by approximately 10% during oxygenation. Since
S_{Hi} never exceeded 3%, the error in $(\varepsilon_o - \varepsilon_1)$ when calculated by

$$\varepsilon_o - \varepsilon_1 = (\varepsilon_{Hb} - \varepsilon_{HbO_2}) \, (1-S_{Hi}) \qquad (5.12)$$

is of the order of 0.3%.

In the preliminary experimental phase (see section 5.1) the wedge
method for determining extinction coefficients was tested extensively
(v.d. Borne 1972) by using solutions of methemoglobin, malachite green,
Evans blue, oxyhemoglobin and deoxyhemoglobin. The last two solutions
showed a high methemoglobin fraction. Hence, although linearity,
reproducibility and accuracy were well established in this stage, no
reliable values of ε_{HbO_2} and ε_{Hb} could be obtained. During the second
phase emphasis was given to the oxygenation measurements and no due
attention was paid to the wedge measurements. From 9 independently
prepared hemoglobin solutions with [Hb] between 8 and 29 g% a value of
0.43 ± 6%, 1/cm/g% (95% confidence limit) was found for ε_{Hb}. In the final
experimental phase again special attention was paid to the wedge
experiment. When measuring the value of ε_{Hb} for three independently
prepared fresh hemoglobin solutions of 17.1, 18.5 and 29 g% hemoglobin
concentration, values of 0.433, 0.432, 0.438 1/cm/g% were found
respectively. From these values a mean value of ε_{Hb} = 0.434 was adopted.
For ε_{HbO_2} a value of 0.040 1/cm/g% was found. Thus a value of
$(\varepsilon_{Hb} - \varepsilon_{HbO_2})$ = 0.394 was used in all experiments.

5.5.3 The saturation curve

A saturation curve was measured over its entire range for two
different hemoglobin solutions. A Radiometer electrode was used for the
PO_2 determination and the Lex-O_2-Con for the estimation of oxygen
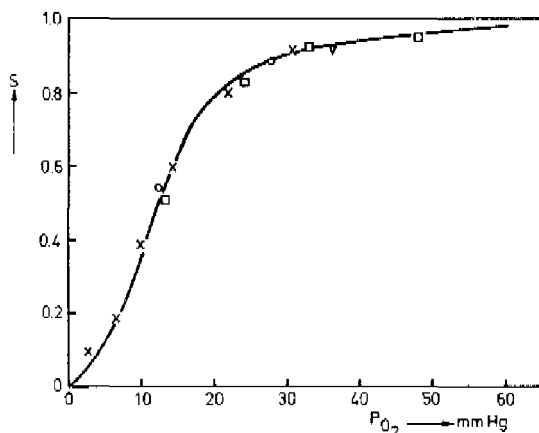saturation. Three times a few points of the saturation curve were obtained

Fig. 5.6. Experimental data for determining the value of P_{50} of the actual saturation curve holding in the present experiments. The solid line is the Standard Dissociation Curve (SDC) of fig. 3.3 with the PO_2 axis attenuated by a factor of 2.2. From this figure it is concluded that the actual $P_{50} = 12$ mm Hg (26.4/2.2).

using the diffusion apparatus. For this a layer of hemoglobin solution was equilibrated with gases of different but known PO_2. The saturation was measured optically. Results are shown in fig. 5.6. The solid line represents the Standard Dissociation Curve (SDC) with its PO_2 axis attentuated by a factor of 2.2. From fig. 5.6 it may be concluded that the saturation curve holding for the present investigation is shifted to the left with regard to the SDC and has a P_{50} of 12 mm Hg, and therefore P_c equals 26.4 mm Hg according to the findings of section 3.5.2.

5.6 Discussion of the experimental results

5.6.1 General interpretation of the experimental results

In chapter 3 the behavior of the oxygenation process of a fully deoxygenated layer of hemoglobin solution has been studied theoretically on the basis of the first and second law of Fick applied to the diffusion of both oxygen and hemoglobin. The conclusions of this study, in terms of average oxygen saturation increase in time, are confirmed by the results of the experimental investigation:

1) The quantity t/d^2 can be used as an independent variable to describe the oxygenation of a deoxygenated hemoglobin layer of arbitrary thickness.

2) The saturation increase is, up to a high degree of layer oxygenation, proportional to the square root of time.

3) This proportionality holds up to a higher saturation when increasing P_1. At $P_1 = 700$ mm Hg the oxygenation process terminates abruptly, thus giving evidence of a sharp oxygenation front within the hemoglobin layer.

4) Normalized oxygenation time (t_1/d^2) defined according to the half-infinite layer model, when plotted versus the reciprocal P_1 value, indeed shows a curvature indicating carrier facilitation of the oxygen uptake by hemoglobin.

A mathematical relationship between the normalized oxygenation time and reciprocal boundary condition (eq. 3.24) was fitted by the least-square procedure to the different data experimentally found by varying two parameters, the permeability αD_C and the hemoglobin diffusion coefficient D_H. The 95% confidence limits found for these parameters in the final experiments (3% for αD_C, 7% for D_H and Z_2) show the quantitative applicability of the theoretical model, at least within the range of hemoglobin concentrations and P_1 values studied. The difference in confidence limits of the parameters mentioned may be explained by the fact that at high P_1 values the influence of D_H on $t_{1,n}$ is small compared to the influence of αD_C, whereas the influences of D_H and αD_C on $t_{1,n}$ are comparable at the low P_1 values applied.

Basically the interpretation of a single oxygenation experiment, in terms of change in light absorption as a function of time, is simple since the relationship between $\log I$ and $\sqrt{t}$ is linear. Normalized oxygenation times can be determined when knowing the value of only one physical constant, being $(\varepsilon_i - \varepsilon_o)b$. However, in estimating the value of $Z_2 = h\, D_H/\alpha D_C$ the value of this constant is even not needed. Note that Z_2/P_1 may be interpreted as the ratio of "permeability for bound oxygen" and "permeability for physically dissolved oxygen". It is interesting to see (fig. 5.5) that Z_2 remains virtually constant over a wide range of hemoglobin concentration. But Z_2 strongly depends on hemoglobin concentration when this concentration gets near the hemoglobin concentration of the red cell.

5.6.2 Discussion of the reliability of the estimated parameter values

The accuracy of the numerical values estimated for αD_C and consequently for D_H holding for a certain hemoglobin solution strongly depends on the accuracy of the data for the oxygen binding capacity and the difference in the extinctions of deoxyhemoglobin and oxyhemoglobin respectively. Initially it was intended to determine, for each individual hemoglobin solution studied, the oxygen binding capacity by means of the Lex-O_2-Con, the hemoglobin and methemoglobin concentration by using a spectrophotomete and $(\varepsilon_l b - \varepsilon_o b)$ by applying the wedge method. However, all these determinations proved to be too time-consuming. Moreover the technique of the first and the third measurement mentioned was not fully established during all experiments so that the original plan had to be dropped. It should be kept in mind that a complete experimental run takes 4 to 9 hours, depending on the hemoglobin concentration of the solution examined. Nevertheless, the numerical values found for the permeability αD_C agree fairly well with the data reported by Stroeve (1973), though he used a completely different method. This supports the correctness of the value for $(\varepsilon_o - \varepsilon_l)$ applied, and thus also the correctness of the value for D_H.

CHAPTER 6

GENERAL DISCUSSION

6.1 Theoretical models of nonsteady-state oxygen uptake by hemoglobin layers

6.1.1 Moving boundary models with particular reference to the polygonal approximation

The polygonal approximation is part of a class of problems in nonsteady-state linear heat conduction or diffusion where two or more phases or regions separated by a moving plane interface are involved. Such a moving boundary always represents a local process discontinuity, as for example a discontinuous change in concentration, a discontinuity in the concentration gradient, or a phase change as in the case of progressive freezing of a liquid (e.g. Danckwerts 1950).

Mostly the moving boundary equations are derived using the time and place variables separately. This, however, impairs the understanding of the essential features of the method. The mathematical treatment of the problem is greatly simplified by combining the dimensionless variables of place x^* and time t^* into one single variable being $\eta = x^*/\sqrt{t^*}$. Then the transfer equation valid in each region appears in the form of eq. 3.25, which can be solved in terms of error functions (eq. 3.27). However, the introduction of the new independent variable η restricts the number of boundary conditions since they only can be defined at fixed values of η. Time and place corresponding to fixed values of η are $x^* = 0$, equivalent to $t^* = \infty$, and $t^* = 0$, equivalent to $|x^*| = \infty$, and moreover those interfaces which change position according to $x^*/\sqrt{t^*}$ = constant. The differences in the mathematical treatment of a particular physical problem obviously depend on the specific boundary conditions.

Hill (1928/1929) theoretically studied, using a moving boundary model, the recovery of a tissue as a result of the oxidation of lactid acid. This situation is similar to the oxygenation problem. A tissue initially containing lactic acid and no oxygen is suddenly exposed at its surface to a certain oxygen partial pressure. Oxygen diffuses into the tissue which recovers as a result of the oxidation of lactic acid. Hill's model assumes two regions within the tissue, i.e. a recovered "oxygen" region where all lactic acid has been oxidized, and a fatigued "lactic acid" region where no oxygen is present. Both regions are separated by an

interface where the oxidation reaction occurs. This interface moves into the tissue as recovery proceeds. The model allows for diffusion of oxygen within the recovered region and for diffusion of lactic acid within the fatigued region. Hill's model for the half-infinite layer (he studied cylindrical geometry as well) may be considered as a particular case of the polygonal model (discussed in section 3.1), when $\phi_c = 0$ and $\psi_c = 1$.

The solutions of Hill's model have been applied by Roughton (1959) to reinterpret the experimental results of Longmuir and Roughton (1952) on the uptake of CO by hemoglobin solution, and of Klug, Kreuzer and Roughton (1956) on the uptake of O_2 by hemoglobin solution (see also below).

6.1.2 Advancing front models

In the same paper as cited in section 6.1.1, Hill (1928/1929) also showed that, using the notation of the present study, if $D_H = 0$ the solution of his moving boundary equation leads to the following approximation of the dimensionless average saturation

$$\bar{\psi} = \sqrt{\frac{2\ t^*}{H}} \tag{6.1}$$

Eq. 6.1 is known as the advancing front equation and can easily be obtained directly by balancing the assumed steady-state oxygen flux through the oxygenated part of the layer to the amount of oxygen taken up by hemoglobin at the advancing oxygenation front

$$\frac{\alpha\ D_C(P_1 - P_i)}{x_f} = h\ (1 - S_i)\ \frac{d\ x_f}{dt} \tag{6.2}$$

where x_f = distance of the advancing front from the gas-liquid interface. Eq. 6.1 results from the integration of eq. 6.2 by using the boundary conditions given in fig. 6.1.

Eq. 6.1 was used by Klug, Kreuzer and Roughton (1956) for the interpretation of the oxygenation of hemoglobin layers (see also section 6.2), by Longmuir and Roughton (1952) for the interpretation of experiments on the CO uptake by hemoglobin layers, as well as by Marx et al. (1960) and Thews and Niesel (1959) to explain the oxygen uptake by layers of blood. Both Marx and Thews extended eq. 6.1 to account for the presence of an extra diffusion resistance at $x = 0$, i.e. a membrane (Marx) or a plasma layer (Thews). Spaan (1973) presented an extension of
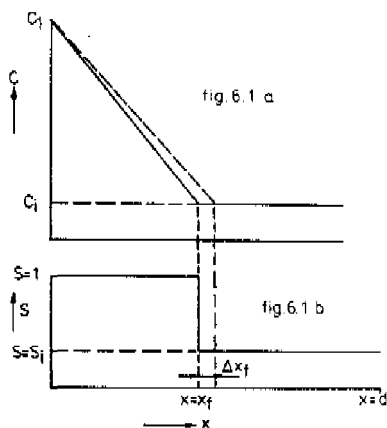
*Fig. 6.1. Profiles of oxygen concentration C (fig. 6.1a) and oxygen
saturation S (fig. 6.1b) within a layer of hemoglobin solution
according to the advancing front model. Boundary conditions are:
$t < 0$ for all x, $C = C_i$ and $S = S_i$; $t \geq 0$ and $x = 0$, $C = C_1$ and $S = 1$.
Steady-state oxygen transfer is assumed within the oxygenated part
of the layer. Δx_f indicates the progression of the advancing front
in a time interval Δt.*

formula 6.1, taking into account the increase of the amount of dissolved
oxygen during the inward movement of the oxygenation front, while still
assuming steady-state oxygen transport in the oxygenated layer. Eq. 6.1
then changes to

$$\bar{\psi} = \sqrt{\frac{2 \ t^*}{H + 0.5}} \tag{6.3}$$

where the correction term 0.5 arises from the physically dissolved
oxygen. The accuracy of the advancing front eqs. 6.1 and 6.3 can be
evaluated from the parameter analysis described in chapter 3. The
numerical results of the polygonal approximation with $\phi_c = D^* = 0$
may be given by the formula

$$t_1^{*,o} = t^* \ (\bar{\psi} = 1) = \frac{1}{2} \ (H + 0.326) \tag{6.4}$$

The advancing front eq. 6.1 underestimates the dimensionless oxygenation
time compared to eq. 6.4 whereas the extended advancing front eq. 6.3

overestimates it. However, eq. 6.4 underestimates the oxygenation time when the influence of the saturation curve is also considered. Generally speaking the extended advancing front eq. 6.3 will be a better approximation to the computer solutions for $D_H = 0$ than is the advancing front eq. 6.1. However, the suitability of the advancing front eqs. 6.1 and 6.3 for the interpretation of experimental data on oxygen transfer in blood or hemoglobin solution strongly depends on the influence of carrier facilitation where $D_H > 0$.

6.1.3 Computer solutions assuming chemical equilibrium

Marx et al. (1960) solved the problem of diffusion into an infinite layer of hemoglobin solution, using an analog computer and assuming the hemoglobin to be immobile. The saturation curve was approximated by a function generator. The computer solution showed a steep oxygenation front for $P_1 = 760$ mm Hg. From this qualitative observation the authors assumed the results of the advancing front eq. 6.1 to be correct. Dindorf, Lightfoot and Solem (1967) solved the same problem as Marx, but used a Runge-Kutta numerical integration technique. They only considered cases where $S_i \approx 0.4$, and so the Hill approximation (eq. 2.6a) of the saturation curve could be used. By varying P_1 between 70 and 700 mm Hg they showed the advancing front eq. 6.1 to give an upper limit for the oxygen uptake rate, whereas the linear approximation of the saturation curve as shown in fig. 3.10 and discussed in section 3.5.2 gave a lower limit. Applying the terminology of chapter 3 to their conclusions, the ratio $t_1^*/t_1^{*,0}$ never assumes values less than one, which is due to the virtually convex shape of the dimensionless saturation curve used.

Spaan (1973) presented some solutions for finite layers of hemoglobin solutions using the Adair equation (see eq. 2.8) for the saturation curve with $S_i = 0$ and moreover hemoglobin supposed to diffuse. Conclusions of this paper are mentioned in chapter 3.

6.1.4 Models assuming linear approximation of the saturation curve

A next special case of the moving-boundary model implies the assumption of a linear saturation curve. This model also was used by Hill (1928/1929) to show the possible influence of facilitation of CO_2 transfer by HCO_3^-. However, in section 3.5.2 a poor agreement between this model and the numerical solutions of the transfer equations using the sigmoid saturation curve was found. In fact the linear approximation leads to a definition of an apparent diffusion coefficient for oxygen

$$D_{app} = \frac{D_C}{1 + \frac{h}{\alpha} m} \qquad (6.5)$$

where α = gas solubility

m = slope of the linear saturation curve (1/mm Hg).

Thews (1957) used this notion of an apparent diffusion coefficient but quite arbitrarily replaced the slope $m = (S_1 - S_i)/(P_1 - P_i)$ in eq. 6.5 by $m(\bar{\psi}/(t))$. This method leads to an erroneous relationship between average saturation increase and time. As shown above $\bar{\psi}$ is proportional to $\sqrt{t}$ for a large range of ψ. This, however, does not hold if the apparent diffusion coefficient changes with time. Thews' method has also been severely critisized by Roughton (1959).

6.2 <u>Experimental investigations reported in the literature</u>

6.2.1 <u>Oxygenation of hemoglobin layers.</u>

Prior to the present study the Fribourg experiments were the only systematical experimental study of the oxygenation of hemoglobin layers. As has been mentioned in chapter 1, these experiments were performed according to the same principles as the present experiments.

In both cases deoxygenated layers of hemoglobin solutions are suddenly exposed to a gas mixture containing oxygen, and the oxygenation process is recorded by a change in light absorption. The present experiments and the Fribourg experiments mainly differ in the experimental procedure and naturally in the instrumentation as improved and developed over a period of a quarter of a century (Kreuzer and Betticher 1951). Some of these differences are:

1) In the Fribourg experiments the layer thickness was calculated from the amount of solution spread over a known area, in the present experiments the thickness is measured optically.

2) In the Fribourg experiments the layers, after having been spread, first had to be deoxygenated by nitrogen, whereas in the present study they are spread anaerobically.

3) In the present experiments the change in gas atmosphere is effected more rapidly than in the Fribourg experiments where the new gas mixture was sucked into the gas chamber.

4) In the Fribourg experiments the light intensity was recorded relative to the intensity at $S = 0$, thus in fact $(I-I_o)$, whereas in the present experiments the absolute light intensity (I) is measured.

In the publications reviewed by Kreuzer (1953) only the time for complete oxygenation was read and evaluated. The determination of this time from the recordings is subject to errors because the curves become very flat at their top. In a later publication Klug et al. (1956) reported the times needed for 1/3 and 1/2 of full deflection. However, these deflections were assumed to be equal to the rise in saturation which in fact they are not. Knowing the extinctions of oxyhemoglobin and deoxyhemoglobin at the wavelength of the light used, the saturation belonging to 1/2 and 1/3 deflection can be calculated (see Appendix D). Assuming a linear relationship between S and $\sqrt{t}$, the real time needed to reach $S = 1/2$ and $S = 1/3$ can be estimated. The difference between the values estimated and the original data depends on the hemoglobin concentration as shown in figs. 6.2a and 6.2b. The influence of the
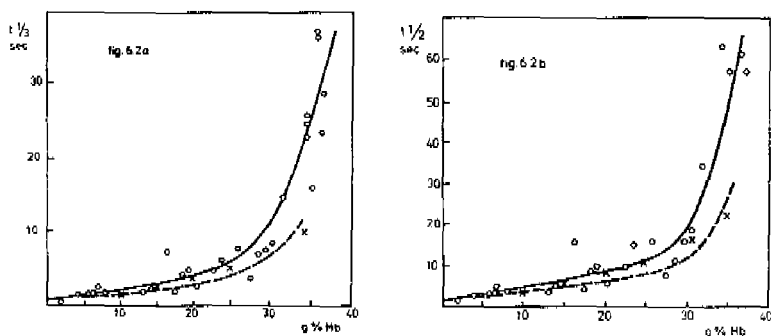

Fig. 6.2. Experimental results of Klug et al. (1956) for 100 μm layers of hemoglobin solution using pure oxygen as oxygenating gas ($P_1 = 700$ mm Hg under their conditions). Fig. 6.2a. Time needed to reach one third saturation as a function of hemoglobin concentration. Fig. 6.2b. Time needed to reach half saturation. Open circles are data points obtained by assuming the deflection of the oximeter to be proportional to the saturation increase. Solid line is the regression curve fitting the data points according to Klug et al. (1956). Broken line is the regression curve corrected for the non-linear relationship between oxygen saturation and light intensity (see text) and therefore presents a better estimate of the values of t 1/2 and t 1/3. Crosses are data calculated from the values of αD_C and D_H found in the present study.

correction is considerable in particular at high hemoglobin concentrations. In fig. 6.2 the crosses represent calculations of $t_{1/3}$ and $t_{1/2}$ based on the numerical values of αD_C and D_H estimated from the experimental results of the present investigation. They fall within the data range reported by Klug et al. From recordings of other incomplete series of oxygenation experiments performed by Kreuzer, using air instead of pure oxygen, the normalized oxygenation time has been determined by plotting log S versus log t and extrapolating the "straight part" of the curves to S = 1. The results are compared in fig. 6.3 with a calculated curve using the data for αD_C and D_H according to the present investigation. These data also scatter considerably but are of the same order of magnitude as the present results.
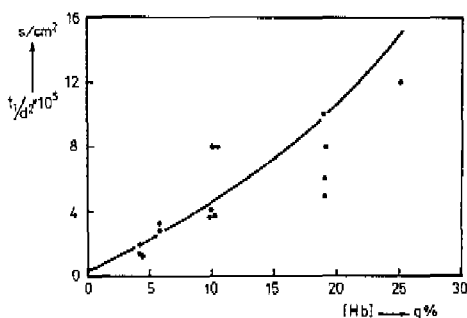

Fig. 6.3. Normalized oxygenation times determined from recordings of other incomplete series of oxygenation experiments performed by Kreuzer (1953), using air as oxygenating gas ($P_1 = 140$ mm Hg under his conditions). The solid line is drawn based on the results of αD_C and D_H found in the present study. Temperature is 25 °C.

In fig. 6.4 the results of the preliminary experiments of the present investigation are compared with curves calculated on the basis of data for αD_C and D_H obtained from the earlier and final experiments. These normalized oxygenation times are also obtained from log S versus log t plots. The values of the extinctions used are those obtained from the wedge experiments performed in the preliminary phase. The gases used in the preliminary experiments contained 5% CO_2. Fig. 6.4a shows results for $P_1 = 700$ mm Hg and fig. 6.4b for $P_1 = 140$ mm Hg. Next to the curves the percentage of hemiglobin is given as measured for the different
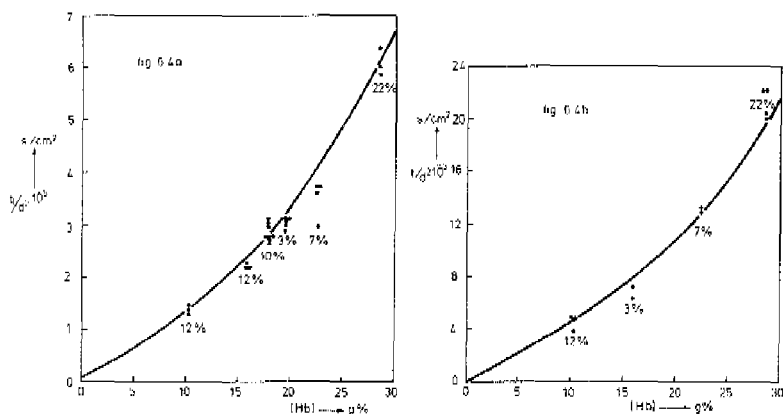
Fig. 6.4. Results of the preliminary experiments of the present study (dots) compared with curves calculated on the basis of the experiments of the 2nd and 3rd group. Fig. 6.4a presents results for $P_1 = 700$ mm Hg, fig. 6.4b presents results for $P_1 = 140$ mm Hg. The numbers next to the group of points show the percentage of methemoglobin present in the respective experiments. Although S_{Hi} is quite high the agreement between the preliminary experiments and the experiments performed later is fairly good.

solutions used. It is remarkable that good agreement between the calculated curves (which are based on $S_{Hi} = 0$) and the experimental values exists. Previously (Spaan et al. 1974) the normalized oxygenation time had been presented as a function of the oxygen binding capacity h, leading to a much larger deviation between the preliminary and later experiments. The relatively good agreement between data points and calculated curves of fig. 6.4 may be explained by compensating effects; increasing S_{Hi} decreases the oxygen binding capacity and thus decreases $t_{1,n}$, whereas D_C and hD_H are lower than when using a hemoglobin solution of the same value of h but $S_{Hi} = 0$; this consequently leads to increased values of $t_{1,n}$.

6.2.2 Oxygenation of single cells

Thews (1959) studied the oxygen uptake of mono-erythrocytic layers. The deoxygenated layer was suddenly exposed to a gas of known PO_2 corresponding to P_1 values ranging from 8 to 150 mm Hg. The smallest dimension of the human red cell is about 1.6 µm, the largest about 7 µm. Assuming that the cells lie flat in a monolayer, they have a plasma

104

boundary layer of approximately 1.5 μm thickness on both sides. When applying a PO_2 of 100 mm Hg, 80% oxygen saturation was obtained within 80 msec, whereas Kutchai (1970) and Moll (1968) calculated a time of approximately 34 ms   for a cell without boundary layer. Thews (1959) applied the advancing front equation extended for the diffusion resistance of the plasma layer to this experiment (P_{50} of the blood was 8 mm Hg). The agreement between calculation and experiment was satisfactory.

Other experiments on the oxygen uptake by red cells were performed using the rapid-reaction technique. The interpretation of the experimental results is quite complex and hence is often oversimplified, certainly in the case of the "stopped-flow" technique (Holland and Forster 1966, Holland 1970). In these experiments two liquids, one containing a small amount of deoxygenated red cells and the other equilibrated with a known PO_2, are rapidly (within 1 msec) mixed in a mixing chamber. Subsequently the liquid is stopped in an observation tube, and the oxygenation of the red cells is recorded colorimetrically. The models used to describe these experiments, however, are far from adequate. For example it is assumed that the oxygen concentration of the cell-liquid interface is constant and equal to the bulk oxygen concentration without accounting for the oxygen binding to hemoglobin. However, assuming the red cell to be a sphere, the total amount of oxygen taken up by one red cell during a 10% saturation increase equals the total amount of oxygen (P_1 = 100 mm Hg) present in a shell around the cell with a thickness of 1 to 2 times the radius of the cell. Hence these experiments might be explained by a "sink" model applied to absorption from an infinite medium rather than by a red cell oxygenation model.

Mochizuki (1970) performed similar experiments with a rapid reaction apparatus. Here the liquid remains in motion during the observation. These experiments clearly demonstrated an effect of the flow on the oxygenation rate of the red cells. The author refers to Mochizuki and Fukuoka (1958) to explain the flow dependency of the oxygen uptake by the presence of a plasma boundary layer around the cell, the thickness of the layer depending on flow rate. Comparison of their results (their fig. 1) with the oxygenation models of Kutchai (1970) and Moll (1968) is not possible because of the differences in the boundary conditions applied.

6.3 The solubility of oxygen in hemoglobin solutions

As shown in chapter 3 the solubility need not be known accurately
for the determination of αD_C and D_H . However, for the determination
of D_C the solubility obviously has to be known with an accuracy at least
comparable to the determination of the permeability αD_C. As shown by
Sendroy, Dillon and van Slyke (1934), the solubility of oxygen in water
(α_{H_2O}) is decreased by the presence of dissolved salts but increased
by dissolved proteins. The same authors showed that the law of Henry
is valid for blood within the range of O_2 pressures of interest. There
are some uncertainties in the literature concerning the value of the
oxygen solubility of hemoglobin solutions (α_{Hb}). Sendroy et al, (1934)
are the only authors reporting on the oxygen solubility of hemoglobin
solutions. They found no difference in solubility increase per g Hb
between stroma-free hemoglobin solutions and suspensions of red cells
in saline at $38^{\circ}C$. However, the oxygen solubility of blood (α_B) found
by Sendroy et al. is 4% higher at $37^{\circ}C$ and 20% higher at $20^{\circ}C$ than that
found more recently by Christoforides and Hedley-Whyte (1969) .
Hedley-Whyle and Laver (1964) measured the temperature coefficient of
the oxygen solubility and showed that the ratio α_B/α_{H_2O} is independent
of temperature. Although this ratio does not linearly depend on
hemoglobin concentration their results can be approximated to within
1,5% by

$$\alpha_B/\alpha_{H_2O} = 0.9 + 0.00312 \; |Hb| \tag{6.6}$$

where $|Hb|$ is in units of g%.
The oxygen solubility of the hemoglobin solutions used in the present
study was calculated from α_{H_2O} given by the Handbook of Physics and
Chemistry (1952) ($\alpha_{H_2O} = 1.69 \; 10^{-6}$ at $25^{\circ}C$), taking into account the
decrease of solubility due to dissolved salts by the factors given by
Sendroy et al. ($\Delta\alpha = 4.3 \; 10^{-7}$ per mol NaCl, $|NaCl|$ approximately equals
0.07 mol/l) and the increase of solubility due to hemoglobin as found
from formula 6.6 leading to

$$\alpha_{Hb} = \alpha_{H_2O} \; (1 + 0.00312 \, |Hb|) - \Delta\alpha \, |NaCl| \tag{6.7}$$

6.4 The diffusion coefficient of oxygen in hemoglobin solutions

The diffusion coefficient of oxygen in hemoglobin solutions was

studied experimentally by several authors. Comparison of their results
is meaningful only in terms of the ratio of D_C in hemoglobin solution to
that in saline as reported by the same author. Commonly a value of
$2.07 \ 10^{-5} \ cm^2/s$, as published by Goldstick and Fatt (1970) is accepted
as a standard value for D_C in saline (= $D_{C,s}$). A compilation of the
available data on D_C, corrected to $D_{C,s} = 2.07 \ 10^{-5} \ cm^2/s$, was provided
by Kreuzer (1970). This compilation is presented in fig. 6.5. In fig.
5.3 diffusion coefficients as calculated from the permeabilities (αD_C)
found in the present investigation are compared with the regression
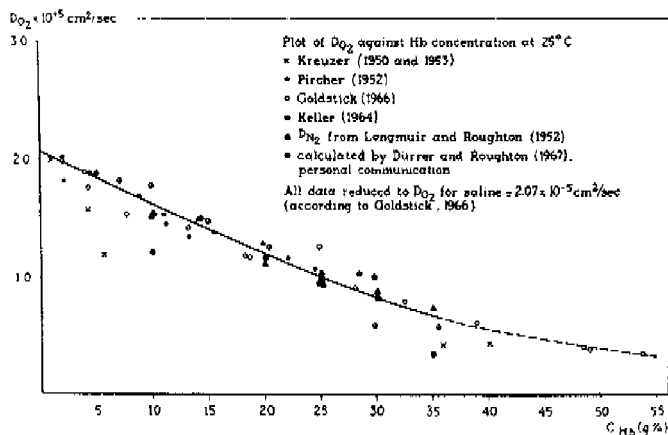

*Fig. 6.5. Compilation by Kreuzer (1970) of the data available for the
diffusion coefficient of oxygen in hemoglobin solution, normalized to
a value of D_C in saline (= $D_{C,s}$) of $2.07 \ 10^{-5} \ cm^2/s$ according to
Goldstick (1966). C_{Hb} = hemoglobin concentration.*

curve of fig. 6.5. The present values of D_C fit quite well within the
range of experimental error. A small deviation may be explained by an
error in $D_{C,s}$ as found by Goldstick and Fatt (1970) or by an error in
the values of the solubility used here.

Goldstick and Fatt (1970) compiled the data available in the
literature on the diffusion coefficient of oxygen in water. These values
scatter between $1.87 \ 10^{-5}$ and $2.44 \ 10^{-5} \ cm^2/s$. In the opinion of
Goldstick and Fatt (1970) the large scatter of these values is due to
differences in the methods used, most of them requiring specific
"empirical constants, fluid flow characterization and/or chemical
analysis".

The diffusion coefficient of oxygen at the red cell hemoglobin concentration (35 g%) is about one third of the value in saline. This decrease can be explained by reduction of the diffusion area available for the oxygen molecules. Stroeve (1974) compared the results of Goldstick and Fatt (1970) on D_C for bovine serum albumine and hemoglobin solution with a Maxwell model for stationary diffusion in a heterogeneous medium, assuming the protein molecules to be immobile with respect to the oxygen molecules. This comparison appeared to be quite satisfactory when assuming a bimolecular water layer surrounding the protein molecule.

6.5 The diffusion coefficient of hemoglobin

6.5.1 Agreement between mutual and tracer diffusion coefficients of hemoglobin

The diffusion coefficient of hemoglobin has been measured by applying a known gradient in the hemoglobin concentration or by applying a known gradient of labeled hemoglobin with no gradient in the total (labeled plus unlabeled) hemoglobin concentration. The diffusion coefficient estimated by the first method is commonly referred to as "mutual diffusion coefficient" whereas that estimated by the latter method as "tracer diffusion coefficient". Theoretically the values of the two diffusion coefficients may be different as a result of the interaction between labeled and unlabeled solute. Keller et al. (1971) studied experimentally both the tracer and mutual diffusion coefficient of hemoglobin and found no significant difference. This result is of practical importance for the present study where in fact the oxyhemoglobin molecules are considered as labeled hemoglobin molecules. For a more detailed theoretical consideration of the diffusion coefficient of hemoglobin the reader is referred to Keller et al. (1971), and for several definitions of the diffusion coefficient to Crank (1975).

6.5.2 Compilation of the published values of the diffusion coefficient of hemoglobin

In 1970 Kreuzer compiled the published values of D_H at temperatures between 20 and 25°C as a function of hemoglobin concentration. This compilation is shown in fig. 6.6 together with the curve chosen by Kreuzer to be a compromise.

As already shown in fig. 5.4 our data presently found are high above this compromise curve. Moreover, the values of D_H as reported by Keller
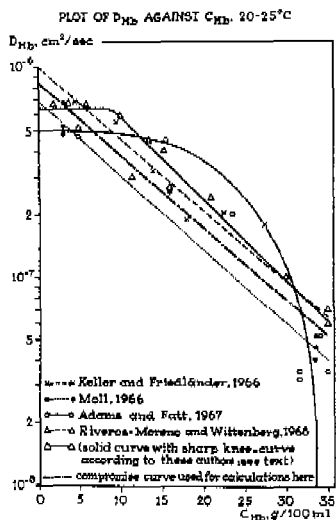
Fig. 6.6. Compilation by Kreuzer (1970) of the data available for the diffusion coefficient of hemoglobin in the temperature range of 20 to 25 °C as a function of hemoglobin concentration (C_{Hb}).

et al. (1971) were not yet available to Kreuzer. Because of the large scatter in the data, the publications dealing with the diffusion coefficient of hemoglobin have been reconsidered, correcting and completing the original data as follows (for details see section 6.5.3):

1) All D_H values found at temperatures between 20 and 25°C were recalculated for 25°C.

2) The values of D_H found by Adams and Fatt (1967) are not shown since, as will be discussed below, they deviate too much from those reported by the other authors.

3) The results of Moll (1966) were corrected for tortuosity.

4) The results of Keller et al. (1971) replace the results of Keller and Friedlander (1966).

5) The results of the present study are added.

These revised data are plotted in fig. 6.7. Here also the original compromise curve of Kreuzer (1970) from fig. 6.6 is included to demonstrate the effect of these corrections. However, this compromise curve now should also be adjusted accordingly since it had been constructed from the original data of the literature.
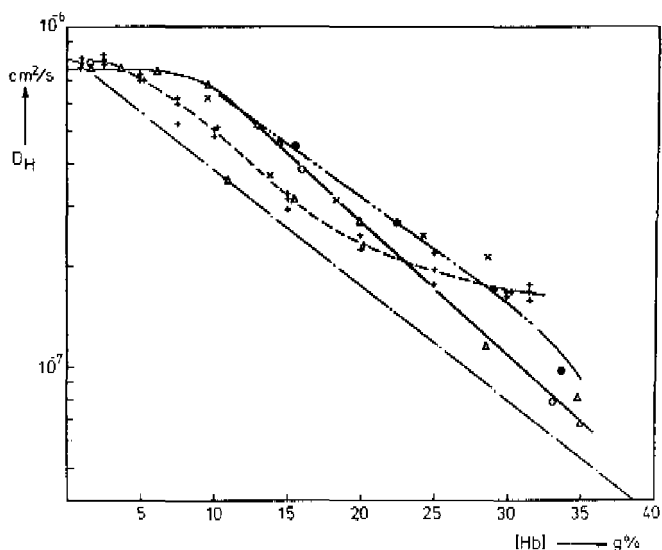
Fig. 6.7. New compilation of data available for the diffusion coefficient of hemoglobin. Now the data of Moll (1966) and Riveros-Moreno and Wittenberg (1972) are corrected for temperature (25 °C), and for the filters applied (Moll).

- • *final experiments*
- × *earlier experiments*
- + *Keller et al. (1971)*
- Δ *Riveros-Moreno and Wittenberg (1972)*
- ○ *Moll (1966)*

6.5.3 Discussion of the corrections applied to the results of different authors

The effect of temperature on D_H was studied by Keller et al. (1971). They reported a temperature coefficient between 3.2 and 3.4%/°C for Hb concentrations between 1 and 35 g% and temperatures between 25 and 37°C, but a value of 2.3%/°C for a $[Hb]$ = 2.5 g% and temperatures between 15 to 25°C. Hence quite arbitrarily a value of 3%/°C has been used in the present study to correct the data reported by Riveros-Moreno et al. (1972) and by Moll (1966). At low hemoglobin concentrations the values of D_H at 25°C found by Riveros-Moreno et al. (1972) and Keller et al. (1971) coincide.

Moll (1966) determined D_H (tracer method) for hemoglobin solutions free of stroma or containing stroma. Only the values found for stroma-free hemoglobin solutions are considered here. Moll used two different methods for measuring D_H although both followed the same principle. Hemoglobin solutions were arranged in four layers of equal thickness. The hemoglobin of one layer, which had been labeled, diffused into the other layers. After a suitable time the layers were separated. The distribution of the labeled hemoglobin was determined and yielded a value of the diffusion coefficient of hemoglobin. The difference of the two methods lies in the manner the layers were produced:

1) by a set of chambers formed by boreholes (diameter 1 cm) in discs (thickness 1 or 2 mm) piled up around a central bar, or

2) by millipore filters (HAWPO 4 74 SO, thickness when wet 160 μm).

The first method only was applied by Moll to stroma-free hemoglobin solutions with a hemoglobin concentration of 3 g%. The second method was applied to solutions having a hemoglobin concentration of 2 to 4 g%, 16 g% and 33 g%. As is well known (see also below) the pores within these filters are not quite straight and parallel as Moll also recognized. However, a correction factor for the filter may be found by assuming that D_H determined by both methods at $[Hb] = 3$ g% has to be the same. This assumption results in a virtual increase of the diffusion path length by 17%. Hence, the values for D_H found by Moll at hemoglobin concentrations of 16 g% and 33 g% have to be multiplied by a factor of 1.37. So, after temperature correction and filter correction (tortuosity), the results of Moll are in fair agreement with those of Riveros-Moreno et al. (1972).

6.5.4 Review of the experimental methods using stirred reservoirs

Porous materials for maintaining a well-defined layer of hemoglobin solution were applied by Adams and Fatt (1966) (sintered glass 22 mm thick, 2 cm diameter, Pyrex Grade Fine, 5 μm pore spaces), Keller and Friedlander (1966) (RA Millipore filter, 150 μm thick, porosity 82%), Keller et al. (1971) (WS Millipore filter, 150 μm thick, porosity 45%, pore diameter 3 μm) and Riveros-Moreno and Wittenberg (1971) (HA Millipore filter, 150 and 300 μm thick, porosity 79%, pore size 0.45 μm).

Adams and Fatt studied the hemoglobin release from the hemoglobin solution contained within the sintered glass disc into a well-stirred reservoir containing a protein solution of equal concentration. The

protein had a molecular weight and dimensions within five percent of
those of hemoglobin. In fact this study is of quasitracer nature.

The other authors applied the principle of the diaphragm cell method.
Basically the apparatus consists of two well-stirred reservoirs separated
by a porous diaphragm. The concentration of the diffusing species (Hb or
labeled Hb) differs in the two reservoirs and the diffusion coefficient
is determined by measuring the respective concentration changes with
time.

The experiments described above may be criticized since notwithstanding
the application of stirring a diffusion boundary layer may arise at the
boundaries of the disc. The thickness of this boundary layer depends on
the one hand on the flow pattern at the disc surfaces, and on the other
hand on the diffusion coefficient of the diffusing species. Certainly
this effect is important because the diffusion apparatus mostly are
calibrated with a NaCl or KCl solution having diffusion coefficients
approximately 20 to 200 times larger than those at hemoglobin
concentrations of 3 and 35 g% respectively. It is not clear from the
cited papers, whether the effect of stirring was thoroughly studied for
solutions of different hemoglobin concentration.

6.5.5 Discussion of the published data on the diffusion coefficient
of hemoglobin

At a hemoglobin concentration of 2.5 g% and lower there is good
agreement between four experimental studies, the three shown in fig. 6.7
and the study of Lamm and Polson (1936) providing a value of $6.8 \ 10^{-7} \ cm^2/$
at $20^{\circ}C$ or, after temperature correction, $7.8 \ 10^{-7} \ cm^2/s$ at $25^{\circ}C$. The
value of D_H found by Adams and Fatt (1967) at low hemoglobin concentration
($5 \ 10^{-7} \ cm^2/s$) is significantly lower than that found by the other
authors ($7.8 \ 10^{-7} \ cm^2/s$). At a hemoglobin concentration of 31 to 35 g%
the values of D_H found by Adams and Fatt again are much lower than those
found by 3 other authors. Hence, it seems justified to not longer
consider the values of D_H found by Adams and Fatt (1967). Rejecting the
measurements of Adams and Fatt (1967), reconsidering the measurements
of Moll (1966), and adding the recent results of Keller et al. (1971)
and those of the present study provide a picture completely different
from that reported by Kreuzer (1970) (fig. 6.6). Nevertheless, essential
features of the various measurements still differ. The shape of the
curve drawn through the data points of Keller et al. (1971) is quite

different from the curve drawn through the data points of Riveros-
Moreno and Wittenberg (1972); the data of Moll (1966) are similar to
those of the latter. It should be noted here that Moll's data are based
on 8 or 9 single observations showing a standard deviation of
approximately 10%. An explanation of the divergent results has to be
sought in the different experimental techniques applied, in the
difference in temperature at which the experiments were performed, or
in a combination of both. The D_H values from the present investigation
differ significantly from the results of Keller et al. (1971) around
10% $\lvert Hb \rvert$ but agree at 30 g% Hb . The reverse is true with the results
of Riveros-Moreno and Wittenberg (1972). An explanation of these
differences would be purely speculative and will therefore not be
attempted here.

6.6 Concluding discussion

In the present investigation the nonsteady-state oxygen uptake of
layers of hemoglobin solution has been studied theoretically and
experimentally. The theoretical models are based on the application
of Fick's first and second law to the diffusion of oxygen as well as
of hemoglobin. An extended parameter analysis has been performed to
obtain general insight into the problem of facilitated diffusion and
to define the range of parameter values experimentally applicable in
order to estimate values of the permeability of oxygen and of the effect
of hemoglobin-mediated oxygen transfer. An experimental method has been
developed and instrumentation has been designed and developed to measure
normalized oxygenation times (t_i/d^2) as a function of the reciprocal
boundary oxygen partial pressure. The experimental technique appeared
to be applicable to hemoglobin solutions with hemoglobin concentrations
between 10 and 34 g%, layer thicknesses between 50 and 220 µm, and
boundary PO_2 values (P_I) between 700 and 140 mm Hg. The experimental
data of the normalized oxygenation time versus the reciprocal boundary
oxygen pressure were fitted to the theoretical diffusion model using
the polygonal approximation. The estimated parameters were αD_C and D_H,
the first parameter with an accuracy between 3.5% and 10%, the second
parameter with an accuracy between 7 and 15%. The final experiments
proved to be more accurate than the earlier experiments. The values
found for αD_C as a function of hemoglobin concentration agree fairly
well with those found by Stroeve (1973) using a completely different

method. Reliable data for the oxygen solubility in hemoglobin solutions are not available in the literature. However, values of this solubility were estimated from solubility measurements in water, saline and whole blood. The values of the diffusion coefficient of oxygen calculated from the measured permeabilities by using the estimated values of the solubility agree quite well with the data from the literature as compiled by Kreuzer (1970).

Considerable discrepancy exists between the diffusion coefficients of hemoglobin as obtained in different studies. The dependence of D_H on hemoglobin concentration found here is similar to that found by Riveros-Moreno and Wittenberg (1972). The results of Keller et al. (1971), show a completely different picture. The present study fails to present sufficient and accurate data of D_H at very high hemoglobin concentration. However, it is quite difficult to obtain accurate data at a high hemoglobin concentration. The hemoglobin concentration of a highly concentrated solution easily changes due to crystallization of Hb. The same must hold for the experiments performed by other authors. Moreover, when highly concentrated hemoglobin solutions are not very stable even in bulk solution, how the stability will be within a filter during experiments lasting many hours (30 hours in the Riveros-Moreno and Wittenberg experiments)?

With regard to the facilitated diffusion within the red cell the shape of the curve in fig. 3.8 is of particular importance. The relative influence of a reduction in oxygenation time due to facilitated diffusion is highest at low values of D^*. Applying the following data to the interior of the red cells, $[Hb] = 34.5$ g%, $D_H = 7.5 \ 10^{-8} \ cm^2/s$, $D_C = 0.8 \ 10^{-5} \ cm^2/s = 1.7 \ 10^{-6}$ mol/l/mm Hg, $(S_1-S_i)/(P_1-P_i) = 0.015$ 1/mm Hg, provides a value of 1.74 for D^*. Consequently under normal physiological circumstances the oxygenation time according to the half-infinite equilibrium model is reduced by more than 50% as a result of hemoglobin-mediated diffusion. The influence of carrier facilitation may become even larger when the oxygen is exchanged in the steeper part of the saturation curve.

Numerical method applied to the finite layer diffusion model

The numerical method applied is based on the finite difference scheme of Crank-Nicholson as dealt with in several textbooks, e.g. Lapidus (1962) and Crank (1975). The differential equation (eq. 3.11) which has to be solved can be written as

$$\frac{\partial F}{\partial t} = \frac{\partial^2 G}{\partial x^2} \tag{A.1}$$

where $F = \phi + H\psi$ \hfill (A.2)

$G = \phi + D\psi$ \hfill (A.3)

For simplicity the dimensionless time and dimensionless space variables now will not be marked by an asterisk. Approximate values of F and G are calculated at n+1 equidistant points at time intervals of Δt as illustrated in fig. A.1. The Crank-Nicholson method essentially is
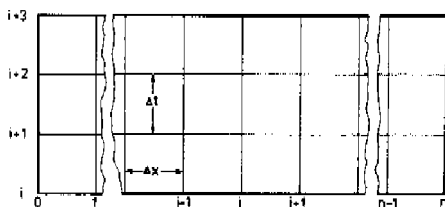
Fig. A.1. Illustration of the Crank-Nicholson method. The hemoglobin layer is divided into n + 1 equidistant points numbered by $0 \leqslant j \leqslant n$; at these points approximations of a continuous function are calculated at time intervals Δt numbered by i.

based on series expansion of F and G around the points $i+\frac{1}{2}$, j and results in the following difference equation

$$\frac{F_{i+1,j} - F_{i,j}}{\Delta t} = \frac{1}{2} \left\{ \frac{G_{i+1,j-1} - 2\,G_{i+1,j} + G_{i+1,j+1}}{\Delta x^2} \right. +$$

$$\left. \frac{G_{i,j-1} - 2\,G_{i,j} + G_{i,j+1}}{\Delta x^2} \right\} \tag{A.4}$$

Eq. A.4 holds in the points where $1 \leqslant j \leqslant n-1$. For $2 \leqslant j \leqslant n-1$ all values of F and G with index i are known whereas with index i+1 are unknown. For j=1 the values of $G_{i,0}$ as known from the boundary condition at x=0 are used in eq. A.4. For j=n the value $G_{i,n+1}$ appears in eq. A.4. However, since the boundary condition at x=1 requires $\frac{\partial G}{\partial x} = 0$ and moreover the problem may be considered symmetrical around x=1 one may write

$$G_{i,n+1} = G_{i,n-1} \tag{A.6}$$

Hence n equations are obtained having 2 n unknowns being $G_{i+1,j}$ and $F_{i+1,j}$ with $1 \leqslant j \leqslant n$. The terms $G_{i+1,j}$ and $F_{i+1,j}$ are connected by the dimensionless saturation curve and thus also 2 n equations become available, though not being linear. To overcome this difficulty only ϕ is considered to be unknown at the points i+1, and an estimate is made for $\psi_{i+1,j}$ according to

$$\psi_{i+1,j} - \psi_{i,j} = (\frac{d\psi}{d\phi})_{i,j} \ (\phi_{i+1,j} - \phi_{i,j}) \tag{A.7}$$

The difference equation to be applied now can be deduced from eq. A.4 to be

$$\frac{1}{\Delta t} \left| \ (1+H(\frac{d\psi}{d\phi})_{i,j}) \ \phi_{i+1,j} - (1+H(\frac{d\psi}{d\phi})_{i,j}) \ \phi_{i,j} - H \ \psi_{i,j} \ \right| =$$

$$\frac{1}{2(\Delta x)^2} \left| \ (1+D^*(\frac{d\psi}{d\phi})_{i,j-1}) \ \phi_{i+1,j-1} + (1-D^*(\frac{d\psi}{d\phi})_{i,j-1}) \ \phi_{i,j-1} + D^*\phi_{i,} \right.$$

$$- \ 2(1+D^*(\frac{d\psi}{d\phi})_{i,j}) \ \phi_{i+1,j} - 2(1-D^*(\frac{d\psi}{d\phi})_{i,j}) \ \phi_{i,j} - 2 \ D^*\psi_{i,j}$$

$$+ \ (1+D^*(\frac{d\psi}{d\phi})_{i,j+1}) \ \phi_{i+1,j+1} + (1-D^*(\frac{d\psi}{d\phi})_{i,j}) \ \phi_{i,j+1} + D^* \ \psi_{i,j+1} \left. \right|$$

$$\tag{A.8}$$

In this way a number of n linear equations are obtained with n unknowns which are easily solved by the method of elimination.

In deriving the finite difference equations the higher-order terms in the series expansions are neglected, resulting in a truncation error.

This truncation error depends on the one hand on the values chosen for Δx and Δt, and on the other hand on the higher-order derivatives. The higher-order derivatives become smaller when time increases and hence Δt may be chosen to increase whilst the truncation error remains of the same order of magnitude at every time step. The quantity of main interest is $\bar{\psi}$ which increases with $\sqrt{t}$ over a wide range. Hence it was decided to change Δt according to

$$\Delta t_i = \sqrt{\Delta t_1} \quad \sqrt{t_i}$$

where Δt_i = time interval at step i

Δt_1 = time interval chosen for the first step

$t_i = \sum\limits_{j=1}^{i} t_j$ = the actual time after step i.

Convergence of the numerical procedure was studied by doubling the number of intervals and halving Δt_1. The order of convergence appeared to be approximately 1.6.

Appendix B

Numerical method applied to the half-infinite layer model</u>

As mentioned in section 3.3.1 the equation to be solved numerically is

$$\frac{d^2\phi}{d\eta^2} = -\frac{1}{A}\frac{d\phi}{d\eta}\left\{\frac{1}{2}\ \eta B + D^*\frac{d^2\psi}{d\phi^2}\ \frac{d\phi}{d\eta}\right\}\tag{B.1}$$

where $A = 1 + D^*(\frac{d\psi}{d\phi})$ (B.2)

$B = 1 + H(\frac{d\psi}{d\phi})$ (B.3)

with the physical boundary conditions

$$\eta = 0\ ;\ \phi = 1\tag{B.4}$$

$$\eta \to \infty\ ;\ \phi \to 0\tag{B.5}$$

In the computer library a numerical integration routine is at disposal requiring two boundary conditions at $\eta = 0$. Hence boundary condition eq. B.5 has to be replaced by:

$$\eta = 0\ ;\ \frac{\partial\phi}{\partial\eta} = \chi_0\tag{B.6}$$

where the value of χ_0 has to be found such that $\phi = 0$ for $\eta \to \infty$. In case $d\psi/d\phi$ remains positive and χ_0 is given a negative value the relationship between ϕ and η will follow a curve like the one shown in fig. B.1: ϕ decreases as a function of η and approaches to a limit value ϕ^∞ for $\eta \to \infty$. Consequently a criterion is needed to decide that the upper integration boundary η_ℓ is large enough to make $\phi_\ell (= \phi$ at $\eta = \eta_\ell)$ sufficiently close to ϕ^∞.

The quantity of interest is the dimensionless oxygenation time t_1^*, hence according to eq. 3.23
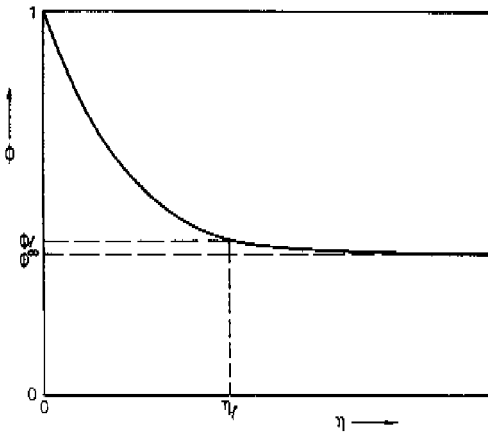
$$\int_0^\infty \psi_\infty(\eta)d\eta\tag{B.7}$$

118

Fig. B.1. Typical shape of a ϕ versus η curve as calculated by the Runge-Kutta method with an arbitrary value of $(d\phi/d\eta)_{\eta=0}$. ϕ_{ℓ} is the approximation of ϕ^{∞} when truncating the integration at $\eta = \eta_{\ell}$. ϕ = dimensionless oxygen concentration; $\eta = x^{*}/\sqrt{t^{*}}$.

When truncating the integration at $\eta = \eta_{\ell}$ and in case $\phi^{\infty} = 0$ the relative error in $\sqrt{t_{1}^{*}}$ can be written as

$$\beta = \frac{\displaystyle\int_{\eta_{\ell}}^{\infty} \psi_{\infty}(\eta)\,d\eta}{\displaystyle\int_{0}^{\infty} \psi_{\infty}(\eta)\,d\eta} \tag{B.8}$$

An approximation of the numerator in eq. B.8 may be found by assuming that η_{ℓ} is so large that ϕ_{ℓ} is already close to ϕ^{∞}. In this case the relationship between ψ and ϕ will be linear for $\eta > \eta_{\ell}$ and thus in this region eq. B.1 reduces to eq. 3.25 with the general solution

$$\phi = E \ \mathrm{erf}\left(\frac{\eta}{2}\sqrt{\frac{B}{A}}\right) + K \tag{B.9}$$

where $A = 1 + D^{*}\left(\dfrac{d\psi}{d\phi}\right)_{\eta=\eta_{\ell}}$; $B = 1 + H\left(\dfrac{d\psi}{d\phi}\right)_{\eta=\eta_{\ell}}$ (B.10)

Eq. B.9 equals eq. 3.27, however, the boundary conditions differ:

$$\eta \rightarrow \infty \; ; \; \phi \rightarrow 0 \tag{B.11}$$

$$\eta = \eta_\ell \; ; \; (\frac{d\phi}{d\eta}) = \chi_\ell \tag{B.12}$$

Using these boundary conditions and applying some mathematical properties holding for the error functions (see Appendix C) it can be shown that

$$\int_{\eta_\ell}^{\infty} \psi d\eta \approx (\frac{d\psi}{d\phi})_{\eta_\ell} \chi_\ell \qquad \frac{A^2}{B^2 \; \eta_\ell^2} \tag{B.13}$$

An expression for the denominator of eq. B.8 can be found by writing

$$\int_{x=0}^{\infty} h \; (S(x,t) - S_i) dx = \int_0^t (D_C (\frac{\partial C}{\partial x})_{x=0} + h \; D_H (\frac{\partial S}{\partial x})_{x=0}) dt \tag{B.14}$$

Eq. B.14 forms a mass balance between the oxygen taken up by the hemoglobin layer at time t (when neglecting the physically dissolved oxygen) and all the oxygen that has passed the layer surface at time t. Eq. B.14 may be rewritten to

$$H \int_{\eta=0}^{\infty} \psi d\eta = (\frac{d\phi}{d\eta})_{\eta=0} + D^* (\frac{d\psi}{d\eta})_{\eta=0} \tag{B.15}$$

and thus

$$\beta = \frac{\chi_\ell}{\chi_o} \; (\frac{A}{B^2} \; \frac{H}{\eta_\ell^2} \; (\frac{d\psi}{d\phi})_{\eta=\eta_\ell}) \tag{B.16}$$

Within the range of parameters as mentioned in chapter 3 the term between parentheses in eq. B.16 is in the order of magnitude of 0.1. The ratio $\chi_\ell/\chi_o = 5 \; 10^{-5}$ was taken as the truncation criterion for the integration process. Although derived in case $\phi^\infty = 0$ the truncation criterion of eq. B.16 also holds if $\phi^\infty \neq 0$.
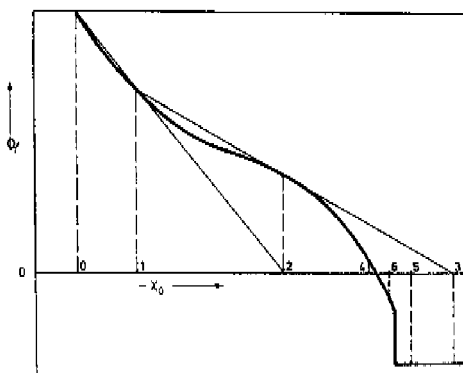
Fig. B.2. Illustration of the shape of the ϕ_l versus χ_o curve and the procedure to find the root of this relationship. The inversion point of this curve is a result of the sigmoid shape of the saturation curve. The discontinuity in this curve for negative values of ϕ_l, is artificial and has to be introduced because the Adair equation shows a minimum for the saturation S at a "P_{O_2}" $\approx$ - 4 mm Hg. The values of χ_o at points 0 and 1 form the starting points of the root-search procedure. Points 2 and 3 are both found by the interpolation method of Aitken and define the interval in which the root is present. Points 4, 5 and 6 are found by halving the interval. Points 4 and 6 define an interval in which the root is present and the relationship between ϕ_l and χ_o is continuous. Finally the root is found by applying the procedure Regula Falsi.

The truncation criterion being known, ϕ_l can be calculated as a function of χ_o. In principle, from a mathematical point of view, there is no objection against negative values of ϕ_l as long as $d\psi/d\phi$ remains positive. When using the Adair scheme for describing the saturation curve $d\psi/d\phi$ changes in sign at a "PO_2" $\approx$ - 4 mm Hg. Hence the integration always was stopped at this point and ϕ_l was given the value of - $8/P_1$. The relationship between ϕ_l and χ_o has the shape shown in fig. B.2. Because of the bending point in this curve and the discontinuity of the curve at $\phi = -4/P_1$, a combination of three different techniques was applied to find the value of χ_o where $\phi_l = 0$:

1) The extrapolation method according to Aitken on condition that ϕ_l is in the range where its second derivative to χ_o is positive. Because of

the bending point in the curve of B.2 an interval will be found in which the point searched for is present. However, then the upper interval limit for χ_o will be on the horizontal part of the ϕ_ℓ versus χ_o curve.

2) Next the method of halving the interval was applied to find an interval containing the root of the ϕ_ℓ versus χ_o relationship and in which this relationship is continuous.

3) Finally the method "Regula falsi" was applied for estimating the value of χ_o where $|\phi_\ell| < 10^{-4}$.

With this strategy the root of the ϕ_ℓ versus χ_o relationship was found after 4 to 10 iterations .

Mathematical equations relevant to the polygonal approximation

Properties of the error function are

$$\text{erf}(x) = \frac{2}{\sqrt{\pi}} \int_0^x \exp(-y^2)dy \tag{C.1}$$

$$\frac{d\ \text{erf}(x)}{dx} = \frac{2}{\sqrt{\pi}} \exp(-x^2) \tag{C.2}$$

$$\int_0^x \text{erf}(y)dy = x\ \text{erf}(x) + \frac{1}{\sqrt{\pi}}(\exp(-x^2)-1) \tag{C.3}$$

$$\int_x^\infty (1-\text{erf}(y))dy = x(\text{erf}(x)-1) + \frac{1}{\sqrt{\pi}} \exp(-x^2) \tag{C.4}$$

$$\int_0^\eta \exp(-\frac{B}{4A} y^2)\ dy = \sqrt{\frac{\pi A}{B}}\ \text{erf}(\eta\sqrt{\frac{B}{4A}}) \tag{C.5}$$

$$\int_0^{\eta_c} \text{erf}(\eta\sqrt{\frac{B}{4A}})d\eta = \eta_c\ \text{erf}(\eta_c\sqrt{\frac{B}{4A}}) + \sqrt{\frac{4A}{\pi B}}(\exp(-\frac{B}{4A} \eta_c^2) - 1) \tag{C.6}$$

$$\int_{\eta_c}^\infty (1-\text{erf}(\eta\sqrt{\frac{B}{4A}}))d\eta = \eta_c(\text{erf}(\eta_c\sqrt{\frac{B}{4A}}) - 1) + \sqrt{\frac{4A}{\pi B}}\ \exp(-\frac{B}{4A} \eta_c^2) \tag{C.7}$$

The following approximations are relevant to the polygonal approximation as well as to the contents of Appendix B (for large x)

$$1 - \text{erf}(x) \approx \frac{2}{\sqrt{\pi}}\ \frac{\exp(-x^2)}{2x}\ \left\{ 1 - \frac{1}{2x^2} \right\} \tag{C.8}$$

$$\int_x^\infty (1-\mathrm{erf}(y))dy \approx \frac{\exp(-x^2)}{2\,x^2\,\sqrt{\pi}} \tag{C.9}$$

$$1 - \mathrm{erf}(\eta\sqrt{\tfrac{B}{2A}}) \approx \sqrt{\frac{4A}{\pi B}}\ \ \frac{\exp(-\eta^2\frac{B}{4A})}{\eta}\ \left|1 - \frac{A}{2\eta B}\right| \tag{C.10}$$

$$\int_{\eta_\ell}^\infty (1-\mathrm{erf}(\eta\sqrt{\tfrac{B}{4A}}))d\eta \approx \sqrt{\frac{A}{\pi B}}\ \left(\frac{A}{B\eta_\ell^2}\right) \tag{C.11}$$

In calculating the dimensionless oxygenation time an expression for $\int_0^\infty \psi d\eta$ is needed. According to the polygonal approximation it holds

$$\int_0^\infty \psi d\eta = (1-\psi_c)\sqrt{\left|\frac{4\,A_1}{\pi\,B_1}\right|}\ \ \frac{1 - \exp\left(-\frac{B_1}{4A_1}\eta_c^2\right)}{\mathrm{erf}\left(\eta_c\sqrt{\frac{B_1}{4A_1}}\right)}$$

$$+ \psi_c\sqrt{\left|\frac{4\,A_2}{\pi\,B_2}\right|}\ \ \frac{\exp\left(-\frac{B_2}{4A_2}\eta_c^2\right)}{(1-\mathrm{erf}(\eta_c\sqrt{\frac{B_2}{4A_2}}))} \tag{C.12}$$

Next only these cases will be considered where $\psi_c = 1$. Hence, the first term on the right-hand side of eq. C.12 is ruled out whilst $B_1 = A_1 = 1$ as a result of $d\psi/d\phi = 0$ in region I.

A special case arises if $\phi_c \to 0$ because then in region II $d\psi/d\phi = \psi_c/\phi_c \to \infty$. This problem can be solved by writing

$$\frac{B_2}{A_2} = \frac{\phi_c + H\psi_c}{\phi_c + D^*\psi_c} \tag{C.13}$$

and

$$\frac{\phi_c}{1-\phi_c}\sqrt{\left|\frac{A_2\,B_2}{A_1\,B_1}\right|} = \sqrt{(\phi_c + H\psi_c)(\phi_c + D\,\psi_c)} \tag{C.14}$$

The latter equation is a condition for eq. 3.31 to remain real.

124

A more specific problem appears when both ϕ_c and D approach zero, since in this case the ratio B_2/A_2 approaches infinity. To solve this problem we consider

$$\lim_{D^*, \phi_c \to 0} \frac{1 - \mathrm{erf}(\eta_c \sqrt{\frac{B_2}{4A}})}{\sqrt{\phi_c + D^*} \ \exp(-\eta_c^2 \ \frac{B_2}{4A})} \ = \frac{2}{\eta_c \sqrt{\pi} \sqrt{H}} \tag{C.15}$$

Because of eq. C.15 eq. 3.31 changes to

$$H \frac{\eta_c}{2} \sqrt{\pi} = \frac{\exp(-\eta_c^2/4)}{\mathrm{erf}(\eta_c/2)} \tag{C.16}$$

and eq. C.12 changes to

$$\int_0^\infty \psi d\eta = \eta_c \tag{C.17}$$

Derivation of the correction equation applied to the regression curves of Klug et al. (1956)

As dealt with in section 6.2.1, in the Fribourg experiments the light intensity was recorded relative to the intensity at $S = 0$. In order to calculate the value S corresponding to the reading of the oximeter it is defined that

$$\text{at } S = 0 \; ; \; I = I_o \tag{D.1}$$

$$\text{at } S = 1 \; ; \; I = I_1 \tag{D.2}$$

and

$$\Delta I = I_o - I_1 \tag{D.3}$$

so

$$\text{at any } S : I = I_o + \gamma \Delta I \tag{D.4}$$

where γ changes with time and is related to the change in oxygen saturation. According to eq. 4.1 one may write

$$I_o = I_A \, 10^{-\varepsilon_o \, bd} \tag{D.5}$$

and

$$I = I_o + \gamma \Delta I = I_A \, 10^{-(\varepsilon_o + (\varepsilon_1 - \varepsilon_o)S)bd} \tag{D.6}$$

Substituting I_A according to eq. D.5 into eq. D.6 results in

$$I_o + \gamma \Delta I = I_o \, 10^{-(\varepsilon_1 - \varepsilon_o)S \, bd} \tag{D.7}$$

and consequently

$$S = \frac{{}^{10}\log\ (1+\gamma\frac{\Delta I}{I_o})}{(\epsilon_o - \epsilon_1)bd} \tag{D.8}$$

Substitution of $\Delta I/I_o$ according to eq. D.7 in case $S = 1$ into eq. D.8 results in

$$S = \frac{(1-\gamma(1-10^{(\epsilon_o - \epsilon_1)bd}))}{(\epsilon_o - \epsilon_1)bd} \tag{D.9}$$

Eq. D.9 relates S to γ when the values of ϵ_o, ϵ_1, b and d are known.

References

Adair, G.S.: The hemoglobin system. VI. The oxygen dissociation curve of hemoglobin. J. Biol. Chem. 63, 529-545 (1925)

Adams, L.R., and Fatt, I.: The diffusion coefficient of human hemoglobin at high concentrations. Respir. Physiol. 2, 293-301 (1967)

Assendelft, O.W. van: Spectrophotometry of haemoglobin derivatives. Van Gorcum, Ltd., Assen, The Netherlands (1970)

Barnikol, W.K.R., and Thews, G.: Zur Interpretation der O_2-Bindungskurve des Human-Hämoglobins. Pflügers Arch. 309, 232-249 (1969)

Barnikol, W.K.R., and Thews, G.: Zur Dissociation des Human-Hämoglobins. Pflügers Archiv. 309, 224-231 (1969)

Benesch, R., and Benesch, R.E.: The effect of organic phosphates from the human erythrocyte on the allosteric properties of hemoglobin. Biochem. Biophys. Res. Commun. 26, 162 - 167 (1967).

Bert, Paul: Recherches expérimentales sur l'influence que les changements dans la pression barométrique exercent sur les phénomènes de la vie. Compt. Rend. Acad. Sci. Paris 75, 88-92, and 543-547 (1872)

Bird, R.B., Steward, W.E., and Lightfoot, E.N.: Transport Phenomena. Wiley, New York (1966)

Briehl, R.W.: Relation between aggregation and oxygen equilibrium in human and lamprey hemoglobin. In: Structure and Activity of Enzymes, Academic Press, New York, 171-178 (1964)

Briehl, R.W.: Relation between aggregation of subunits and the oxygen equilibrium of human hemoglobin. J. Biol. Chem. 245, 538-543 (1970)

Borne, P. van de: Inleidende zuurstofverzadigingsmetingen aan stromende hemoglobineoplossingfilmen. Afstudeerverslag, Eindhoven University of Technology (1972)

Buckles, R.G.: An analysis of gas exchange in a membrane oxygenator. Ph.D. Thesis. M.I.T., Cambridge (1966)

Christoforides, C., and Hedley-Whyte, J.: Effect of temperature and hemoglobin concentration on solubility of O_2 in blood. J. Appl. Physiol. 27, 592-596 (1969)

Crank, J.: The Mathematics of Diffusion. 2nd edition, Clarendon Press, Oxford (1975)

Curl, R.L., and Schultz, J.S.: A polygonal approximation for unsteady state diffusion of oxygen into hemoglobin solutions. In: Oxygen Transport to Tissue. Pharmacology, Mathematical Studies, and

Neonatology. Eds. D.F. Bruley and H.I. Bicher. Advances in
Experimental Medicine and Biology Vol. 37B, Plenum Press,
New York, 929-935 (1973)

Damköhler, G.: Einfluss von Diffusion, Strömung und Wärmetransport
auf die Ausbeute bei chemisch-technischen Reaktionen. Der Chemie-
Ingenieur Bd. III, 359-485 (1937)

Danckwerts, P.V.: Unsteady-state diffusion or heat conduction with
moving boundary. Trans. Faraday Soc. 46, 701-712 (1950)

Dindorf, J.A., Lightfoot, E.N., and Solen, K.A.: Prediction of blood
oxygenation rates. Chem. Eng. Symp. Ser. 67, 75-87 (1971)

Dijkhuizen, P., Buursma, A., Fongers, T., Oeseburg, B., and Zijlstra, W.G.:
Oxygen binding capacity of haemoglobin. Digest 16th Dutch Fed. Meeting,
121 (1975)

Forbes, W.H., and Roughton, F.J.W.: The equilibrium between oxygen and
haemoglobin. I. The oxygen dissociation curve of dilute blood
solutions. J. Physiol. 71, 229-260 (1931)

Garred, L.J.: Aspects of mass transport in biological systems. Ph.D. Thesis
University of Minnesota (1975)

Gibbon, Jr.,J.H.: Extracorporeal maintenance of cardiopulmonary function.
Harvey Lectures 53, 186-224 (1959)

Goldstick, T.K., and Fatt, I.: Diffusion of oxygen in solutions of blood
proteins. Chem. Eng. Symp. Ser. 66, 101-113 (1970)

Hartridge, H., and Roughton, F.J.W.: The kinetics of haemoglobin. III. The
velocity with which oxygen combines with reduced haemoglobin. Proc.
Roy. Soc. A 107, 654-683 (1925)

Hedley-Whyte, J., and Laver, M.B.: O_2 solubility in blood and temperature
correction factors for PO_2. J. Appl. Physiol. 19, 901-906 (1964)

Hill, A.V.: The diffusion of oxygen and lactic acid through tissues.
Proc. Roy. Soc. B 104, 39-96 (1928/1929)

Holland, R.A.B., and Forster, R.E.: The effect of size of red cells on
the kinetics of their oxygen uptake. J. Gen. Physiol. 49, 727-742 (1966)

Holland, R.A.B.: Factors determining the velocity of gas uptake by
intracellular hemoglobin. In: Blood Oxygenation. Ed. D. Hershey,
Plenum Press, New York, 1-23 (1970)

Hüfner, G.: Neue Versuche zur Bestimmung der Sauerstoffcapacität des
Blutfarbstoffes. Arch. Anat. Physiol., Physiol. Abt.,130 (1894)

Keller, K.H., and Friedlander, S.K.: Diffusivity measurements of human
methemoglobin. J. Gen. Physiol. 49, 681-687 (1966)

Keller, K.H., Canales, E.R., and Yum, S.I.: Tracer and mutual diffusion coefficients of proteins. J. Phys. Chem. 75, 379-387 (1971)

Keller, K.H.: Effect of fluid shear on mass transport in flowing blood. Fed. Proc. 30, 1591-1599 (1971)

Kellett, G.L., and Schachman, H.K.: Dissociation of hemoglobin into subunits. J. Mol. Biol. 59, 387-399 (1971)

Klug, A., Kreuzer, F., and Roughton, F.J.W.: Simultaneous diffusion and chemical reaction in thin layers of haemoglobin solution. Proc. Roy. Soc. B 145, 452-472 (1956a)

Klug, A., Kreuzer, F., and Roughton, F.J.W.: The diffusion of oxygen in concentrated haemoglobin solutions. Helv. Physiol. Pharm. Acta 14, 121-128 (1956b)

Koshland, D.E., Némethy, G., and Filmer, D.: Comparison of experimental and theoretical models in proteins containing subunits. Biochemistry 5, 363-385 (1966)

Kreuzer, F.: Über die Gültigkeit des Fickschen Gesetzes bei der Diffusion des Sauerstoffs in dünne Schichten hochkonzentrierter Hämoglobinlösungen. Thesis,Zürich-Fribourg (1950)

Kreuzer, F., and Betticher, A.: Eine Apparatur hoher Empfindlichkeit und Stabilität zur Messung der Oxydationszeiten des Hämoglobins. Helv. Physiol. Pharm. Acta 9, 224-253 (1951)

Kreuzer, F.: Modellversuche zum Problem der Sauerstoffdiffusion in den Lungen. Helv. Physiol. Pharm. Acta 11, Suppl 9.(1953)

Kreuzer, F.: Facilitated diffusion of oxygen and its possible significance; a review. Respir. Physiol. 9, 1-30 (1970)

Kreuzer, F., and Hoofd, L.J.C.: Facilitated diffusion of oxygen in the presence of hemoglobin. Respir. Physiol. 8, 280-302 (1970)

Kutchai, H.: Numerical study of oxygen uptake by layers of hemoglobin solution. Respir. Physiol. 10, 273-284 (1970)

Kutchai, H.: O_2 uptake by 100 μ layers of hemoglobin solution: theory vs experiment. Respir. Physiol. 11, 378-383 (1971)

Laidler, K.G.: Chemical Kinetics. 2nd edition. McGraw-Hill, New York (1965)

Lamm, O., and Polson, A.: The determination of diffusion constants of proteins by a refractometric method. Biochem. J. 30, 528-541 (1936)

Lapidus, L.: Digital computation for chemical engineers. McGraw-Hill, New York (1962)

Laszt, L.: Modelversuche mit Hämoglobinlösungen zur Frage des Gasaus-

tauches in den Lungen. Helv. Physiol. Pharm. Acta 3, 291–328 (1945)

Leeuw, R.J.M., de: De glycolyse in menselijk bloed. Thesis, R.U. Utrecht (1971)

Longmuir, I.S., and Roughton, F.J.W.: The diffusion coefficients of carbon monoxide and nitrogen in haemoglobin solutions. J. Physiol. 118, 264–275 (1952)

Margaria, R.A.: A mathematical treatment of the blood dissociation curve for oxygen. Clin. Chem. 9, 745–761 (1963)

Marx, T.I., Snijder, W.E., John, A.D.ST., and Moeller, C.E.: Diffusion of oxygen into a film of whole blood. J. Appl. Physiol. 15, 1123–1129 (1960)

Mochizuki, M., and Fukuoka, J.: The diffusion of oxygen inside the red cell. Jap. J. Physiol. 8, 206–223 (1958)

Mochizuki, M.: Oxygenation velocity of the red cell and pulmonary diffusing capacity. In: Blood oxygenation. Ed. D. Hershey, Plenum Press, New York, 24–61 (1970)

Monod, J., Wyman, J., and Changeux, J.P.: On the nature of allosteric transitions: a plausible model. J. Mol. Biol. 12, 88–118 (1965)

Moll, W.: The influence of hemoglobin diffusion on oxygen uptake and release by red cells. Respir. Physiol. 6, 1–34 (1968)

Müller, A.: Bemerkungen zum Gasaustausch in den Lungen. Helv. Physiol. Pharm. Acta 3, 203–213 (1945)

Nicholson, P., and Roughton, F.J.W.: A theoretical study of the influence of diffusion and chemical reaction velocity on the rate of exchange of carbon monoxide and oxygen between the red blood corpusele and the surrounding fluid. Proc. Roy. Soc. B 138, 241–264 (1951)

Oomens, J.M.M., Spaan, J.A.E., and Donders, A.F.F.: Annular membrane oxygenator with tangential flow/Oxygen transfer analysis and scaling rules. In: Physiological and Clinical Aspects of Oxygenator Design Eds. S. Dawids and H.C. Engell ASP. Biological and Medical Press, Amsterdam (in press).

Overcash, M.R.: Couette Oxygenator. Ph.D. Thesis, University of Minnesota (1972)

Pauling, L.: The oxygen equilibrium of hemoglobin and its structural interpretation. Proc. Nat. Acad. Sci. 21, 186–191 (1935)

Perutz, M.F.: The haemoglobin molecule. Proc. Roy. Soc. B 173, 113–140 (1969)

Perutz, M.F.: Haemoglobin: The molecular lung. New Scientist and

Science Journal 17, 676-679 (1971)

Pircher, L.: Über die Diffusion des Sauerstoffs in dünne Schichten von Wasser und Hämoglobinlösungen. Thesis, Fribourg (1951)

Riveros-Moreno, V., and Wittenberg, J.B.: The self-diffusion coefficients of myoglobin and hemoglobin in concentrated solutions. J. Biol. Chem. 247, 895-901 (1972)

Roughton, F.J.W.: Diffusion and chemical reaction velocity as joint factors in determining the rate of uptake of oxygen and carbon monoxide by the red blood corpuscle. Proc. Roy. Soc. B 111, 1-36 (1932)

Roughton, F.J.W.: Diffusion and chemical reaction velocity in cylindrical and spherical systems of physiological interest. Proc. Roy. Soc. B 140, 203-229 (1952)

Roughton, F.J.W.: Diffusion and simultaneous chemical reaction velocity in haemoglobin solutions and red cell suspensions. Progr. in Biophysics and Biophysical Chemistry 9, 55-104 (1959)

Roughton, F.J.W.: Transport of oxygen and carbon dioxide. Handbook of Physiology, Section 3: Respiration, vol. 1, 767-825 (1964)

Roughton, F.J.W.: The oxygen equilibrium of mammalian hemoglobin. J. Gen. Physiol. 49, 1, Part 2, 105-124 (1965)

Roughton, F.J.W., DeLand, E.C., Kernohan, I.C., and Severinghaus, J.W.: Some recent studies of the oxyhaemoglobin dissociation curve of human blood under physiological conditions and the fitting of the Adair equation to the standard curve. In: Alfred Benzon Symposium IV: Oxygen Affinity of Hemoglobin and Red Cell Acid Base Status. Eds. M. Rorth and P. Astrup, Munksgaard, Copenhagen, 73-83 (1972)

Schachman, H.K., and Edelstein, S.J.: Ultracentrifuge studies with absorption optics. IV. Molecular weight determinations at microgram level. Biochemistry 5, 2681 (1966)

Sendroy, J., Dillon, R.T., and van Slyke, D.D.: Studies of gas and electrolyte equilibria in blood. J. Biol. Chem. 105, 591-632 (1934)

Spaan, J.A.E.: Transfer of oxygen into haemoglobin solution. Pflügers Arch. 342, 289-306 (1973)

Spaan, J.A.E., Hoofd, L.J.C., and Kreuzer, F.: The facilitation of nonstationary transfer of oxygen into thin layers of hemoglobin solution. Digest 15th Dutch Fed. Meeting, 337 (1974)

Stroeve, P.: Diffusion with reversible chemical reaction in heterogenous media. Thesis, M.I.T., Cambridge, Mass. (1973)

Stroeve, P.: On the diffusion of gases in protein solutions. I. and EC.
    Fundamentals 14, 140–141 (1975)

Thews, G.: Ein Verfahren zur Berechnung des O_2-Diffusionskoefficienten
    aus Messungen der Sauerstoffdiffusion in Hämoglobin- and Myoglobin-
    Lösungen. Pflügers Arch. 265, 138–153 (1957)

Thews, G., and Niesel, W.: Zur Theorie der Sauerstoffdiffusion im
    Erythrocyten. Pflügers Arch. 268, 318–333 (1959)

Thews, G.: Untersuchung der Sauerstoffaufnahme und -abgabe sehr dünner
    Blutlamellen. Pflügers Arch. 268, 308–317 (1959)

Thiele, E.W.: Relation between catalytic activity and size of particle.
    Industrial and Engineering Chemistry 31, 916–920 (1939)

Thompson, C.J.: Models for hemoglobin and allosteric enzymes. Biopolymers
    6, 1101–1118 (1968)

Turek, Z., Kreuzer, F., and Hoofd, L.J.C.: Advantage of disadvantage of
    a decrease of blood oxygen affinity for tissue oxygen supply at
    hypoxia. A theoretical study comparing man and rat. Pflügers Arch.
    342, 185–197 (1973)

Weigelt, C.: Mikrokryophotometrische Messungen zur Untersuchung des
    erleichterten Sauerstofftransports in Gegenwart von Hämoglobin.
    Thesis, Bochum, Germany (1975)

Zilversmit, D.B.: Oxygen-hemoglobin systems: a model for facilitated
    membranous transport. Science 149, 874–876 (1965)

Summary

This thesis deals with theoretical and experimental aspects of the nonsteady-state uptake of oxygen by completely deoxygenated layers of hemoglobin solutions spread on a glass plate. At its free boundary the layer of hemoglobin solution is exposed to a gas atmosphere which initially does not contain any oxygen. Then a sudden change in oxygen partial pressure from zero to a certain value P_1 is induced. Oxygen diffuses from the gas phase into the hemoglobin solution and reacts with hemoglobin to form oxyhemoglobin. Oxygen transfer within the hemoglobin solution occurs as a result of the diffusion of both dissolved oxygen and oxyhemoglobin.

Theoretically this process has been studied by solving the diffusion-reaction equation based on Fick's law for the diffusion of both oxygen and hemoglobin and on the assumption of chemical equilibrium between oxygen and hemoglobin. A dimensionless analysis has been performed: the dependent variable is $\bar{\psi} = \bar{S}/\bar{S}_1$ where $\bar{S}$ is the average oxygen saturation of the layer and $\tilde{S}_1$ is the saturation of the layer in equilibrium with P_1; the independent variable is $t^* = t\, D_C/d^2$ where t is the lapse of time after the start of oxygenation, D_C is the diffusion coefficient of oxygen and d is the layer thickness; the dimensionless parameters applied are:

1) $H = h\, S_1/\alpha P_1$ where h is the oxygen binding capacity of the solution and α is the oxygen solubility,

2) $D^* = H\, D_H/D_C$ where D_H is the diffusion coefficient of hemoglobin,

3) $\phi_{50} = P_{50}/P_1$ where $P_{50} = PO_2$ at which $S = 0.5$ according to the saturation curve.

The results of a finite layer model are compared with the results of a half-infinite layer model in terms of the relationship between $\bar{\psi}$ and t^*. According to the half-infinite layer model $\bar{\psi}$ is proportional to $\sqrt{t^*}$ until $\bar{\psi}$ equals unity. The course of oxygenation predicted by the finite layer model initially coincides with the predictions of the half-infinite layer model, but later $\bar{\psi}$ approaches unity asymptotically. The range of coincidence depends on the values of ϕ_{50} and D^*. For low values of ϕ_{50} (< 0.02) and $D^* (< 0.2)$ the range of coincidence extends $\bar{\psi}$ almost to $\bar{\psi} = 1$. According to the half-infinite model, $\bar{\psi} = \sqrt{t^*/t_1^*}$ where t_1^* is a constant referred to as dimensionless oxygenation time. The influence of H, D^* and ϕ_{50} on t_1^* has been studied in terms of $t_1^*/t_1^{*,0}$ where $t_1^{*,0}$ is the dimensionless oxygenation time obtained when $\phi_{50} = 0$. The ratio

$t_1^*/t_1^{*,0}$ appears to linearly depend on H with a proportionality factor f_2, being approximately a hyperbolic function of $D^*(f_2 \approx 0.74/(1.48+D^*))$. The influence of ϕ_{50} on t_1^* depends on the values of H and D^*.

The reaction of oxygen with hemoglobin causes a change in the light absorption of the solution and hence provides a tool for studying the oxygenation of hemoglobin layers. Applying this method the relationship between $\bar{\psi}$ and t/d^2 was measured colorimetrically at a wavelength of 670 nm.

The conclusions from the theoretical comparison of the finite layer model and half-infinite layer model were confirmed. For several solutions having a hemoglobin concentration between 10 and 34 g%, t_1/d^2 (t_1 is defined analogous to t_1^*) was determined as a function of $1/P_1$ (with P_1 between 140 and 700 mm Hg). These experiments were fitted to the half-infinite layer model using the method of least squares. The oxygen permeability αD_C and the diffusion coefficient of hemoglobin D_H could be estimated from this procedure. The values found for αD_C agree quite well with those found in the literature, but the values found for D_H are higher than those found by authors using tracer techniques for the estimation of D_H.

Samenvatting

Dit proefschrift behandelt theoretische en experimentele aspecten van de instationaire zuurstofopname van volledig gedeoxygeneerde lagen hemoglobine oplossingen, uitgestreken over een glazen plaat. Aan het oppervlak is de hemoglobine laag in contact met een gasatmosfeer die aanvankelijk geen zuurstof bevat. Plotseling wordt de partiële zuurstof druk in het gas op de waarde P_1 gebracht. Zuurstof diffundeert dan vanuit de gasfase de hemoglobine laag in en reageert met hemoglobine tot oxyhemoglobine. In de hemoglobine oplossing wordt zuurstof getransporteerd zowel door diffusie van opgeloste zuurstof als door diffusie van oxyhemoglobine.

Dit proces is theoretisch bestudeerd door uitgaande van de diffusie wet van Fick, toegepast op de diffusie van zuurstof en hemoglobine, en onder aanname van chemisch evenwicht tussen zuurstof en hemoglobine, de diffusie-reaktievergelijking te formuleren en op te lossen. Daartoe is een dimensieloze analyse uitgevoerd. Hierbij is de afhankelijke variabele $\bar{\psi} = \bar{S}/\bar{S}_1$, waarin S_1 de gemiddelde zuurstof verzadiging van de laag is en $\bar{S}_1$ de verzadiging in de laag wanneer die in evenwicht is met P_1; de onafhankelijke variabele is $t^* = t\, D_C/d^2$ waarin t de tijd is die is verstreken vanaf het begin van oxygenatie, D_C de diffusie coëfficiënt van zuurstof en d de laagdikte.

De dimensieloze parameters zijn:

1) $H = h\, S_1/\alpha P_1$ met h = de zuurstofbindingscapaciteit van de oplossingen en α = de oplosbaarheid van O_2,

2) $D^* = H\, D_H/D_C$ met D_H = de diffusie coëfficiënt van hemoglobine,

3) $\phi_{50} = P_{50}/P_1$ met $P_{50} = PO_2$ waarvoor $S = 0.5$ overeenkomstig de saturatieve curve.

De resultaten van het model waarin een eindige laag wordt aangenomen zijn vergeleken met de resultaten van een model dat uitgaat van een half-oneindige laag. Volgens het tweede model is $\bar{\psi}$ evenredig met $\sqrt{t^*}$, totdat $\psi = 1$. Het eerste model resulteert in een oxygenatieverloop dat aanvankelijk gelijk is aan dat voorspeld door het tweede model, maar nu nadert $\bar{\psi}$ asymptotisch naar één. De grootte van het gebied waarin beide curves samenvallen hangt af van de waarden van ϕ_{50} en D^*. Voor lage waarden van ϕ_{50} (< 0.02) en D^* (< 0.02) vallen de curves vrijwel geheel samen tot aan $\psi = 1$. Volgens het half-oneindige laag model geldt dat $\bar{\psi} = \sqrt{t^*/t_1^*}$ waarin t_1^* een constante is. Deze grootheid wordt aangeduid als de

dimensieloze oxygenatietijd. De invloed van H, D^* en ϕ_{50} op t_1^* is nagegaan door variatie van $t_1^*/t_1^{*,0}$, waarin $t_1^{*,0}$ de dimensieloze oxygenatietijd is berekend voor $\phi_{50} = 0$. Het quotiënt $t_1^*/t_1^{*,0}$ blijkt lineair afhankelijk te zijn van H met een evenredigheidsconstante f_2, die zelf een hyperbolische funktie is van D^* ($f_2 \approx 0.74/(1.48+D^*)$). De invloed van ϕ_{50} op t_1^* is afhankelijk van de waarden van H en D^*.

Als gevolg van de reaktie van zuurstof met hemoglobine verandert de lichtabsorptie van de oplossing, hetgeen een mogelijkheid biedt om de oxygenatie van hemoglobine lagen te bestuderen. Met deze methode is de relatie tussen $\bar{\psi}$ en t/d^2 colorimetrisch gemeten bij een golflengte van 670 nm.

De conclusie van de theoretische vergelijking van het eindige laag model en het half-oneindige laag model werd experimenteel bevestigd. Voor verschillende oplossingen met een hemoglobine concentratie tussen 10 en 34 g% werd t_1/d^2 (t_1 is analoog aan t_1^* gedefinieerd) als functie van $1/P_1$ gemeten (met P_1 tussen 140 en 700 mm Hg). Volgens het criterium van de kleinste kwadraten werd een half-oneindig laag model aangepast aan de experimenteel gevonden relatie tussen t_1/d^2 en $1/P_1$. Op deze manier konden waarden worden geschat voor de zuurstof permeabiliteit αD_C en de diffusie coëfficiënt van hemoglobin D_H. De waarden die werden gevonden voor αD_C komen goed overeen met die in de literatuur; de waarden voor D_H echter zijn hoger dan die bepaald door andere auteurs met behulp van tracer technieken.

Acknowledgements

Levensbericht

20-2-1945   : Geboren te Breda.

1957-1963   : HBS-b gevolgd aan het Mgr. Frencken College
te Oosterhout (N.Br.).

1963-1970   : Technische Natuurkunde gestudeerd aan de
Technische Hogeschool te Eindhoven.

1-4-1970   : In dienst getreden als wetenschappelijk
medewerker van de afdeling der Werktuig-
bouwkunde, Technische Hogeschool Eindhoven.

1-9-1976   : In dienst getreden als wetenschappelijk
medewerker, bij het het laboratorium voor
Fysiologie van de Rijksuniversiteit te Leiden.

Stellingen

1. De toepassing van de plasticiteitsmechanica in de analyse van de mechanische produktieprocessen heeft zijn grootste waarde in de uitspraken die daarop kunnen worden gedaan ten aanzien van ontwerp en constructie van de gereedschappen waarmee die processen worden uitgevoerd.

2. Wanneer de prognoses ontleend aan een theoretisch model overeenstemmen met de resultaten van een experiment houdt dit noch een bevestiging in van het model noch van de juistheid van de uitvoering van het experiment.

3. The rapidity of diffusion attainable in systems of small dimensions is the basis of the capillary circulation, and herewith of the whole design of the larger animals.
   A.V. Hill: The diffusion of oxygen and lactic acid through tissues.
   Proc. Roy. Soc. B 104, 39-96 (1928/1929).

4. De trage O_2-opname van gedeoxygeneerde rode cellen na plotselinge menging met een zuurstofhoudende waterige oplossing moet worden verklaard vanuit de lage oplosbaarheid van O_2 in de oplossing vergeleken met de hoge O_2 bindingscapaciteit van de rode celinhoud . Roughton's stelling dat deze trage O_2 opname wordt veroorzaakt door de diffusie weerstand van het rode celmembraam is dan ook niet juist.
   F.J.W. Roughton: Diffusion and simultaneous chemical reaction velocity in haemoglobin solutions and red cell suspensions.
   Progr. in Biophysics and Biophys. Chem. 9, 55-106 (1959).

5. Na de ontdekking van de invloed van 2,3 DPG op de ligging van de zuurstof-dissociatie curve, moet in feite aan de standaard condities voor de bepaling van deze dissociatie curve de 2,3 DPG concentratie worden toegevoegd.

6. Het succes van gecompliceerde operatieve ingrepen is voor een belangrijk deel te danken aan het adapterend vermogen van het fysiologisch regelsysteem.

7. De verklaring voor het verschijnsel dat de aortaklep sluit gedurende de vertragingsfase van de systole, is in de eerste plaats gelegen in de aanwezigheid van holtes achter de klepvliezen.

   A.A. van Steenhoven: Een hydrodynamische analyse als basis voor de constructie van vliesklepprothesen.

   Afstudeerverslag T.H.E. (1975).

8. De typische mannelijke en vrouwelijke rolpatronen in onze cultuur verhinderen een volledige en gelijkwaardige ontwikkeling van algemeen menselijke eigenschappen door beide sexen.

   Ann Oakley: Op gelijke voet; Vermeende verschillen tussen man en vrouw.

   H. Nelissen B.V., Bloemendaal (1975).

9. Het instellen van een vakgroep heeft geen zin indien bij de betrokkenen aanleg en bereidheid tot samenwerking niet aanwezig is.

10. Het door wetenschapbeoefenaars vaak gebruikte argument dat internationale studiereizen het inzicht in het vakgebied verdiepen en daarom budgetair verantwoord zijn, heeft kortgeleden nog een extra accent gekregen door de studiereis van de staatssecretaris van volksgezondheid naar de Verenigde Staten van Noord-Amerika in verband met de situatie van de hartchirurgie in Nederland.

2 november 1976.   J.A.E. Spaan